Synthesis of Micrometer-sized Polymer Particles by Microsuspension Iodine Transfer Polymerization using Hydrophilic Monomers

黄，楚娟

(Degree)
博士（学術）

(Date of Degree)
2023-03-25

(Date of Publication)
2024-03-01

(Resource Type)
doctoral thesis

(Report Number)
甲第8651号

(URL)
https://hdl.handle.net/20.500.14094/0100482399

博士論文

Synthesis of Micrometer-sized Polymer Particles by Microsuspension Iodine Transfer Polymerization using Hydrophilic Monomers

親水性モノマーを用いたマイクロ懸濁ヨウ素移動重合によるマイクロメーターサイズの高分子微粒子の合成

令和 5 年 1 月

神戸大学大学院工学研究科

黄　楚娟

Huang　Chujuan

Acknowledgment

First and foremost, I want to express my great gratitude and thanks to my supervisor, Prof., Dr. Hideto Minami, for believing in me, and for his precious guidance, valuable discussion, and useful suggestion throughout this study. Additionally, I would like to thank him for his support and understanding over these three and half years.

I am also grateful to Research Assistant, Dr. Toyoko Suzuki for her repeated help, precious assignment, and useful suggestion throughout this study. Her warm words encourage me a lot during this research.

I wish to express my tremendous gratitude and respect to Prof. Dr. Masayoshi Okubo. Without his introduction, I would not have had a cherished opportunity to study at Soft Matter Interface Laboratory (SMIL:-) and experience a lot of happiness both in research and daily life.

I want to express my appreciation to Dr. Taro Omura and Dr. Ryohei Morimoto for their generous support and valuable discussions in the academic study. Without their considerate assistance, I would not have gone smoothly in the research process.

More than academic support, I want to show my thanks to the members of Soft Matter Interface Laboratory. Ms. Miku Onishi, Ms. Mana Fujii, Mr. Yuya Takeuchi, Mr. Katsuhiro Onita, Mr. Koki Shimogomi, Mr. Shunji Kimura, Mr. Mitsuru. Konishi, and Mr. Fumiya Takahashi assisted me a lot to adapt to the new environment. Mr. Takeru Michiura, Mr. Hayate Ikeda, and Mr. Kota Takemura provided their enthusiastic personal support in my university

life. Mr. Nao Minoshima, Mr. Shitaro Ishitate, Mr. Kodai Yamano, Ms. Ikuko Maitani, Ms. Hinano Morimoto, Ms. Haruka Yamamoto, Ms. Maytawee Malineerat and other fellows showed their friendliness and made my stay in this laboratory full of happiness and laughter. Owing to them, I could not only learn a lot from their serious attitude toward their studies but also enjoy the good time that we shared.

Finally, I would like to express my deepest appreciation to my family. They gave me the utmost freedom and support to chase my dream. During the tough time of coronavirus epidemic, although we could not meet with each other for three and half years, we have a tacit mutual understanding of each other's situation and your beliefs motivate me to work hard. Love you forever.

January, 2023

Chujuan Huang

Contents

General introduction

In manufacturing, conventional radical polymerization (CRP) is a widely used process from the viewpoint of industrial production and application. This technique is relatively easy to perform since it does not require stringent purification of the reagents and strict polymerization conditions. It generally leads to high molecular weight polymers under relatively mild conditions.[1] Many different processes can be applied such as bulk, solution, suspension, microsuspension, or emulsion polymerizations.[1]

Among these techniques, the polymerization carried out in an aqueous media is receiving more and more attention. On the one hand, the polymerization proceeding on an industrial scale is commonly performed in an aqueous dispersed system, ascribed to the affordable and readily available source of water. On the other hand, the increased environmental concern and sharp growth of pharmaceutical and medical applications for hydrophilic polymers, which fits the arising trend, make an aqueous phase attractive. Moreover, in contrast to the numerous polymerization methods employed in a homogenous system, which are typified by bulk or solution polymerization, aqueous polymerizations treated as a heterogenous system also provide many invaluable practical advantages over them, such as the absence of volatile organic compounds, better control of heat transfer, and the possibility to reach high molecular weight polymers with high conversion and a faster rate of polymerization. And the final water suspension of stable polymer particles is easy to handle even at high solid content, owing to the

alluring properties of water: a generally low viscosity, non-toxicity, and relatively low boiling point. As a consequence, the polymer suspended in water can be used directly for coating applications or as a dried polymer after the removal of water.

Nevertheless, the mostly used polymerization performed in an aqueous phase is emulsion polymerization,[2] which method is comparatively perfect, focusing on the preparation of submicrometer-sized particles. Therefore, we gave an eye to the preparation of micrometer-sized particles in an aqueous phase.

In addition, by utilizing a radical mechanism, a wide range of functional monomers could be polymerized and a great variety of random copolymers could be obtained by copolymerizations.[1] However, as mentioned above, conventional radical polymerization possesses intrinsic limitations: the lack of control over the molecular weight and molecular weight distribution, the lack of the end functionalities, and the difficulty to build a macromolecular architecture. Therefore, to achieve well-designed polymers, nowadays, tremendous progress has been achieved in reversible-deactivation radical polymerization (RDRP). Different techniques benefiting from RDRP enable control over architecture, composition, and chain length distributions in the construction of advanced materials with unique and enhanced properties. [1, 3-5]

Hence, in this work, the effort has been made to produce micrometer-sized particles in an aqueous phase with well-designed molecular weight (M_n) and molecular weight distribution (M_w/M_n), which could further satisfy the demands in particle morphology.

1. Process of reversible-deactivation radical polymerization (RDRP)

RDRP currently attracts much attention for providing a simple and versatile technique for the synthesis of well-defined, low polydispersity polymers and copolymers, which could provide control over the polymer architecture.[1, 3-5] More recently, the preparation of block copolymer with incompatible segments by RDRP has been intensively studied, which is not only attractive in maintaining the opposite physical and chemical properties simultaneously but also introducing different morphologies by self-assembly.[6-8] The familiar RDRP processes are atom transfer radical polymerization (ATRP),[9, 10] nitroxide mediated polymerization (NMP),[11] reversible addition-fragmentation chain-transfer (RAFT) polymerization,[12] iodine transfer polymerization (ITP),[13, 14] and some metallic mediated living radical polymerization.[15, 16]

All RDRP methods are based on establishing a rapid dynamic equilibration between a minority amount of growing free radicals and a large majority of the dormant species.[1, 3, 17] The dormant chains may be alkyl halides, as in partial ATRP or ITP; thioesters, as in RAFT; alkoxyamines, as in NMP; organometallic species, as in metallic mediated living radical polymerization. Based on the typical mechanism, the RDRP methods could be divided into three categories: deactivation by spontaneously reversible coupling, deactivation by catalyzed reversible coupling, and deactivation by degenerative transfer (DT), which could be represented by NMP, ATRP, and RAFT, respectively, as the mechanism shown in Figure 1.

As NMP has significate drawbacks that cannot proceed within good control due to the thermal degradation of an alkoxyamine structure requires a high temperature,[18] while the

methacrylate cannot be polymerized due to the inherent problems in NMP of methacrylates.[19]

Meanwhile, ATRP has an obvious limitation that gives an inevitable amount of metal catalyst

concentration in the system, which would further pollute the environment.[20]

Therefore, the strategy based on the mechanism of DT is emphasized in this work. As a

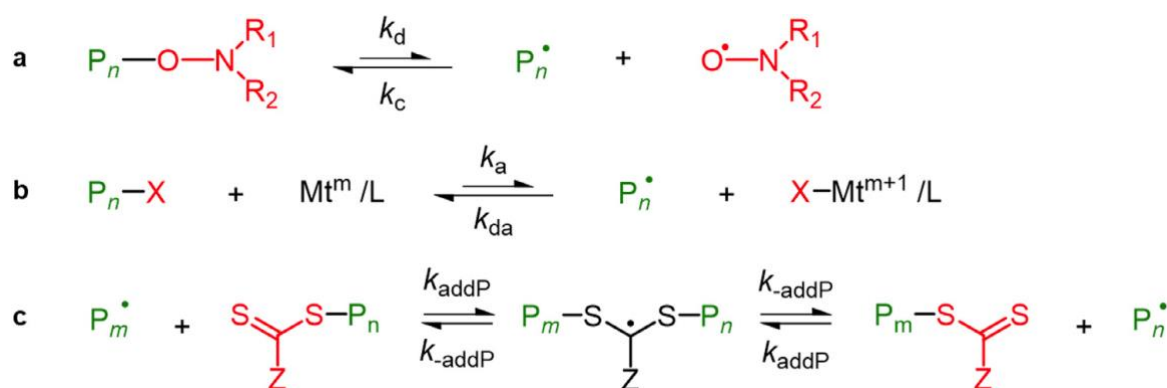simple and well-developed method, RAFT and ITP were explained specifically below.

Figure 1. Simplified mechanisms of activation-deactivation equilibria in RDRP. a) Nitroxide mediated polymerization; b) ATRP; c) RAFT polymerization.[5]

(i) Reversible addition-fragmentation chain-transfer (RAFT) polymerization

RAFT polymerization uses thiocarbonylthio compounds to regulate the degenerative

exchange of propagating radical species generated via general radical initiators in the early

stage of polymerization. As shown in Figure 1c, an intermediate specie is formed first by the

attachment between a propagating radical specie and a thiocarbonylthio group. Next, the

fragment at the weak C-S bond side would leave from the intermediate specie to form a dormant

thiocarbonylthio-capped chain and a new propagating radical.[21] Commonly used RAFT

polymerizations have been extensively studied, in which a range of thiocarbonylthio

compounds was attempted, including many derivatives of dithioesters,[22] trithiocarbonates,[23]

dithiocarbamates,[24, 25] and xanthate (especially suitable for less-activated monomers, such as vinyl acetate).[26] It also shows wide application on various monomers.[27]

However, as announced in D'Agosto's work,[28-30] during the RAFT polymerization of high reactivity monomers, besides the R substituent radical, the intermediate radical can give the additional radical R^z, which dropped from the stabilizing group (Figure 2). And due to the high activity of polymer radicals, the polymer radical transfers to the R^z group and works as the general propagating chain without the behavior of control/livingness. For the formed carboxyl group is much less reactive than carbon-sulfur double bond, the polymer chain was almost dead.
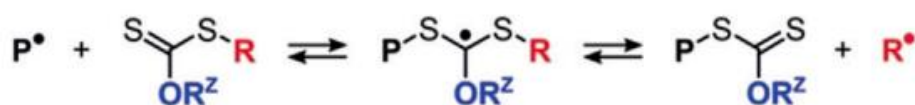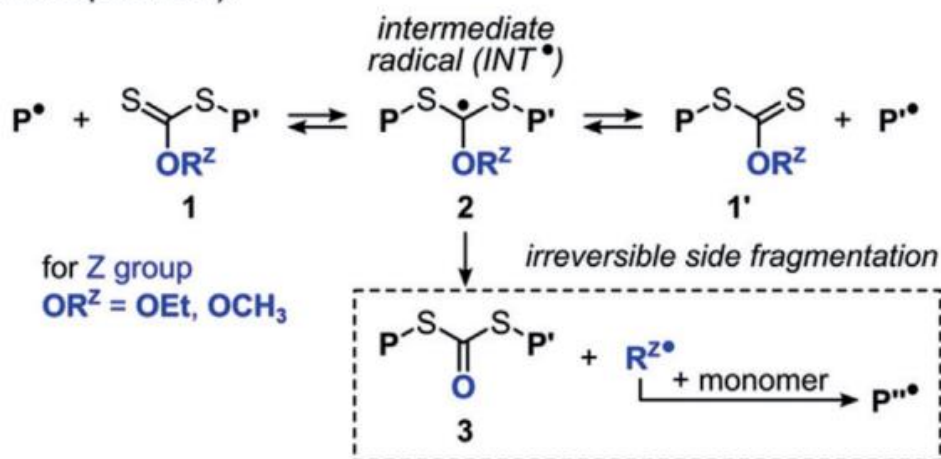

Figure 2. Pre-equilibrium and main equilibrium in RAFT with the observed side fragmentation for ethylene polymerizations.[29]

In the case of high reactivity monomers undergoing the RAFT polymerization, this kind of side thiocarbonylthio derivatives generated not only continuously decreased the livingness of the chains, but also impede the use of chain end functionalities. It goes against the achievement of RDRP, in which the intermediate radical species should fragment rapidly which allows all chains in the mixture to grow at approximately the same rate and obtain narrow polymer chain length distributions. Therefore, the polymerization under the rule of ITP displays an alluring property in that there are no additional radicals appeared during the polymerization. To understand the mechanism of ITP, a brief introduction will be declared in the following part.

(ii) Iodine transfer polymerization (ITP)

As an ancient method of RDRP, Tatemoto and coworkers first put forward the concept of ITP, in which iodocompound was utilized to regulate polymerization via a degenerative transfer polymerization mechanism.[31] This process relies on an exchange of an iodine end group between dormant alkyl iodide polymer chains and propagating radicals,[32] as the main-equilibrium shown in Figure 3. From the mechanism, there are no other side radicals to meet the termination with the propagation radicals, but only the iodine capping group takes part in the degenerative chain transfer. By using the method of ITP, some commercialized products could be synthesized, and further applied to many areas such as catalysts, medical devices, electronics, etc.[33-36] As a close to industrial production polymerization method, it has additional merits of low-cost and easy acquisition.

Significantly, the performance of iodide chain transfer agents depends a lot on the

structure of alkyl iodide compounds and the type of monomers.[34] Comparing with the results

in the synthesis of styrene, it has difficulty in polymerizing acrylates and vinyl acetate (VAc),

due to the high propagation rates of monomers.[37, 38] Moreover, to enhance the tolerance toward

unprotected functional groups,[39, 40] the most employed techniques of ITP are in a bulk or

solution system, which is a homogenous system. Consequently, it remains a challenge to

achieve ITP for high reactivity monomers in a heterogeneous system.

Reversible chain transfer in ITP (pre-equilibrium)

$$P_m\bullet \; + \; R\text{-}I \; \underset{k_{tr\text{-}1}}{\overset{k_{tr}}{\rightleftharpoons}} \; P_m\text{-}I \; + \; R\bullet$$
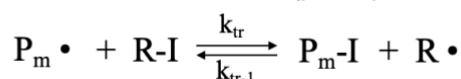
Degenerative chain transfer in ITP (main-equilibrium)

$$P_n\bullet \; + \; P_m\text{-}I \; \underset{k_{ex\text{-}1}}{\overset{k_{ex}}{\rightleftharpoons}} \; P_n\text{-}I \; + \; P_m\bullet$$
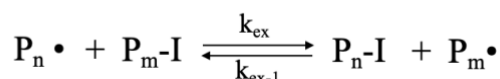
Figure 3. General pre-equilibriumand and main equilibrium in ITP.

2. Synthesis of micrometer-sized particles by ITP in an aqueous heterogeneous system

As mentioned above, besides meeting the low cost from the request of industrial production,

an aqueous phase of polymerization satisfies the needs for environmental-friendly and energy

conservation. Since the mostly sophisticated polymerization in an aqueous heterogeneous

system in manufacturing is emulsion polymerization,[2] leads to the lack of focus on the

preparation of micrometer-sized particles. These micrometer-sized particles have many

important applications, such as molecular imprinting,[41, 42] capsules for phase change

materials,[43-48] and cosmetics,[49] etc., we endeavor to realize the synthesis of micrometer-sized

particles in an aqueous heterogeneous system. As the universal methods to synthesize

micrometer-sized particles, several works have been done in dispersion polymerization, suspension polymerization, and microsuspension polymerization in an aqueous heterogeneous system with the strategy of ITP.

(i) Dispersion polymerization

Dispersion polymerization is a special heterogeneous system that originates from the homogeneous reaction mixture of the monomer, solvent, initiator, and stabilizer.[50] Ascribed to this characteristic, it is impossible to apply iodocompound, which is highly hydrophobic, in a pure aqueous phase. Moreover, after employing a monomer whose water solubility is finite, mere water is not enough to dissolve all materials. Therefore, a hydrophobic phase or a high amount of additional solvent in the water phase is needed.

In Okubo's work,[51] the iodine transfer dispersion polymerization was first applied to styrene in the media of supercritical carbon dioxide (scCO$_2$) using CHI$_3$ as a chain transfer agent (CTA). The polystyrene (PS) particles were successfully synthesized about 1 μm, however, with the defective linear M_n, comparatively narrow M_w/M_n (1.5-1.7), and low degree of livingness estimated at 56%.

In Winnik's work,[52] a two-stage ITP of styrene was carried out in an ethanol-water mixture using perfluorohexyl iodide (C$_6$F$_{13}$I) as CTA. This work focuses on the condition in controlling the dispersity of particle size. It was found that after adding C$_6$F$_{13}$I into the dispersion system before polymerization, the particle size wasn't as much monodispersed as in

the case of conventional dispersion polymerization, especially in the early stage of polymerization. This phenomenon resulted from the induction period of CTA. The improvement could be realized by adding $C_6F_{13}I$ into the system after the nucleation stage of free radical polymerization, which led to the higher M_n and broad M_w/M_n.

For this method is divergent from our vision of using a mere water media, the suspension and microsuspension are taken into consideration.

(ii) Suspension polymerization

Less work of ITP in the suspension process was studied. Only one work was found which was done by S. Choe and her coworkers.[53] The reverse ITP (RITP) was employed in a suspension system, which gives a more complex mechanism than ITP as shown in Figure 4. The main different mechanism of RITP is that iodine molecule (I_2) can react with initiator radical (A•), which arouses the appearance of the intermediate transfer agent A-I and behave as the ITP afterward.

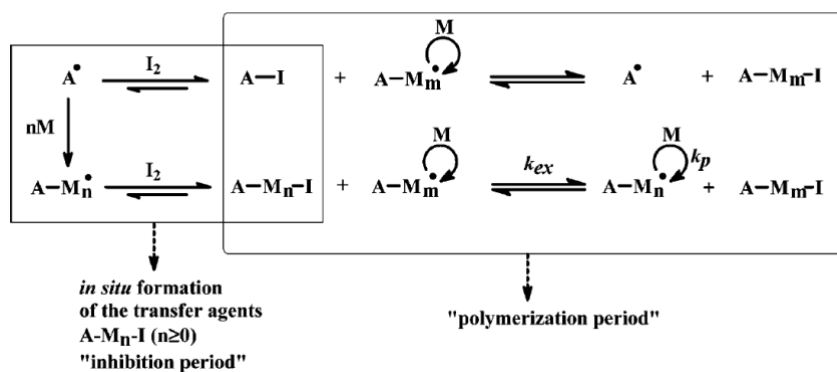**Figure 4.** Simplified Mechanism of RITP. (A•, radical from the initiator; I_2, molecular iodine; M, monomer unit; n, mean number degree of polymerization, k_{ex}, degenerative chain transfer rate constant; and k_p, propagation rate constant)[34]

In their work, the effect of iodine and styrene contents on the molecular characteristics was investigated. With the increase in the concentration of I_2, the M_n of the resultant polymer was effectively decreased. Meanwhile, they revealed that two different polymerizations, the emulsion and suspension, occurred in the RITP-suspension polymerization simultaneously, resulting in a big gap between the particle size as shown in Figure 5. With the increase in the concentration of I_2, the fraction of submicrometer-sized particles reduced, which were generated based on the mechanism of emulsion polymerization. This was arisen from the higher polymerization rate in the monomer droplet than in the micelle in the emulsion phase, due to the enhanced hydrophobicity of the monomer droplet upon the increased I_2. In other words, suspension polymerization dominated the two mechanisms.

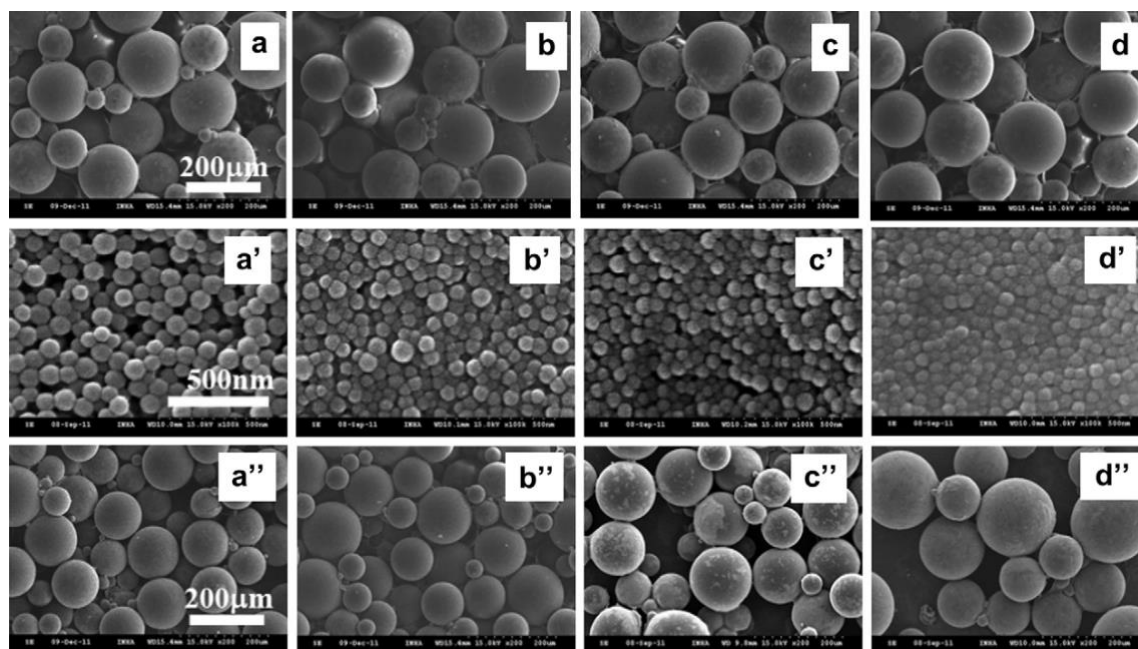**Figure 5.** The SEM photographs of the PS particles formed using various iodine concentrations in the RITP in a suspension system of styrene at 70°C for 10 h a, b, c, d: right after the suspension polymerization in the presence of 0.0, 0.05, 0.15, and 0.25 mmol of I_2; a',b',c',d': the PS particles obtained from the emulsion fraction and a", b", c", d": the PS particles obtained from the suspension fraction after centrifugation.[53]

So far, most works were performed on styrene because of the aforementioned reason for the stability of styrene in an RDRP. In addition, the high hydrophobicity of styrene makes it easier to synthesize micrometer-sized particles in an aqueous heterogeneous system. Nevertheless, the suspension-polymerized particles are in hundreds of micrometers, which is not that charming in the application.

Trying to apply ITP to the other monomers which fulfill the particle size in tens of micrometers, more work has been done in a microsuspension system.

(iii) Microsuspension polymerization

Microsuspension conventional radical polymerization (*ms* CRP) in an aqueous dispersed system is one of the most well-known techniques for the synthesis of micrometer-sized and capsule particles such as microspheres,[54-56] molecular imprinting particles,[41, 42] microcapsules encapsulated phase change materials[43-48] and cosmetic,[49] magnetic particles[57, 58] and hollow particles.[59] It is simple and environmentally friendly by utilization of water as a medium.[60-62]

Commonly, when hydrophilic monomer or high content of hydrophilic monomer in monomers is applied to *ms* CRP, a large number of submicrometer-sized polymer particles are often formed as a byproduct in the aqueous media in addition to the micrometer-sized ones, basing on the mechanism of emulsion polymerization.[63, 64] To depress the unexpected emulsion polymerization, a water-soluble inhibitor was often added therein.[65-68] However, it is not easy to get the optimum condition because it is a

very narrow region. As elaborated in Choe's work, the submicrometer-sized particles could be decreased after increasing the amount of iodine, which was used as a CTA. To clarify the mechanism of this behavior of iodocompounds in the aqueous heterogeneous phase of a relatively hydrophilic monomer, Okubo and his coworker attempted the microsuspension iodine transfer polymerization (*ms* ITP) at methyl methacrylate (MMA, solubility in water: 1.5 g/100 mL at 20°C [69]) using CHI_3 as the CTA with the high concentration of initiator to meet the demand of the industry.[70]
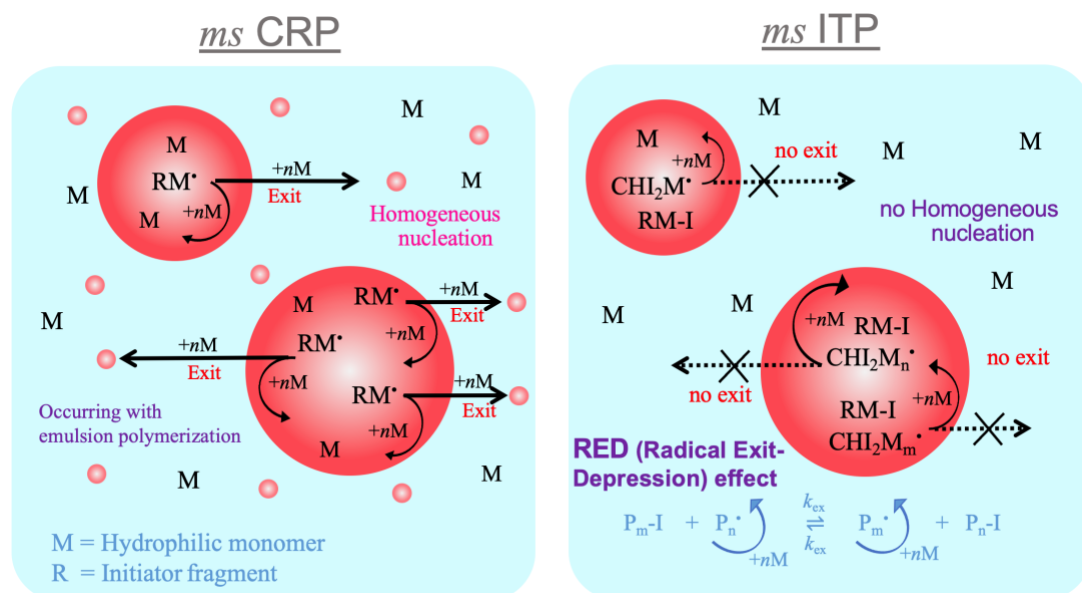
Figure 6. Schematic mechanism of microsuspension convention radical polymerization and the radical exit depression (RED) effect in microsuspension iodine transfer polymerization.[70]

In this case, Iodoform was used not only as the chain transfer agent but also worked as a kind of hydrophobe. That is the preliminary radicals having iodide group(s), must scarcely exit from the monomer droplet, because of the high insolubility of these iodine-captured radicals, which they named as radical exit depression (RED) effect.[71]

Specifically, CHI_3 could capture monomer or oligomer radicals within monomer droplets, as the mechanism displayed in Figure 6. After applying the same conditions as MMA to more hydrophilic monomers (e.g., ethyl acrylate (EA, solubility in water: 8.3 g/100 mL at 20°C [72]) and methyl acrylate (MA, solubility in water: 6.0 g/100mL at 20°C [73])), it becomes difficult to prevent the submicrometer-sized particles. Especially, in the case of MA, all particles are submicrometer-sized particles

To challenge the synthesis of micrometer-sized particles without submicrometer-sized poly(methyl acrylate) (PMA), Okubo and his coworkers did additional work on MA theoretically and experimentally.[74] By comparing the simulation plots of MA under different amounts of initiator with the plot of *ms* ITP of MMA, the assumptive condition for the synthesis of micrometer-sized particles without submicrometer-sized particles could be estimated. After processing polymerization under different amounts of initiators, it was figured out that the percentage of the byproduct particles decreased with a decrease in the BPO concentration, resulting in zero practically at 0.8 wt% BPO consistent with the simulation result, where polymer was maintained the control/livingness.

3. Outline of this dissertation

Attributing to the difficulty of applying ITP to hydrophilic monomers, which could partially dissolve in water, in an aqueous heterogeneous system, a few works devoted to preparing micrometer-sized particles of hydrophilic monomers by using ITP in an aqueous heterogenerous phase.

As mentioned among the above three systems, the nascent radicals in the preliminary stage of ITP influenced both particle size and control/livingness of the synthesized polymer. Hence, regulating the nascent radicals in the early stage should be a breakthrough in applying ITP to hydrophilic monomers in an aqueous heterogeneous phase to obtain micrometer-sized particles.

Consequently, hinted from Okubo's works, the optimal conditions to synthesize micrometer-sized homopolymer particles of hydrophilic monomers by utilizing *ms* ITP was studied theoretically and experimentally in this work. Moreover, the synthesis of micrometer-sized block copolymer particles and the morphology transition of these synthesized particles were also studied.

This dissertation consists of 5 Chapters to cover the content.

In **Chapter 1**, the simulation model was put forward to understand the kinetic of *ms* ITP of homopolymer, in which the chain transfer constant of CHI_3 under different polymerization conditions was further improved.

In **Chapter 2**, based on the kinetic simulation, the condition to synthesize micrometer-sized PMA particles with acceptable control/livingness by *ms* ITP was studied.

In **Chapter 3**, the condition to synthesize the micrometer-sized poly(vinyl acetate) (PVAc) with good control/livingness by *ms* ITP was studied. The influence from iodide species was discussed.

In **Chapter 4**, the synthesis of micrometer-sized poly(methyl methacrylate)-*block*-poly(vinyl acetate) (PMMA-*b*-PVAc) was discussed, meanwhile, the inner morphology of

PMMA-*b*-PVAc was studied.

In **Chapter 5**, a series of *ms* ITP-obtained PMMA-*b*-PVAc underwent the hydrolysis to fulfill the aim of morphology transition. The morphology evolution of these hydrolyzed PMMA-*b*-PVAc was discussed.

References

1. K. Matyjaszewski, T. P. Davis, *Handbook of Radical Polymerization*. Wiley-Interscience: New York, 2002.

2. R. G. Gilbert, *Emulsion Polymerization: A Mechanistic Approach*. Academic Press: London, 1995.

3. K. Matyjaszewski, *Controlled/Living Radical Polymerization: Progress in ATRP, NMP, and RAFT*. American Chemical Society: Washington, DC, 2000.

4. K. Matyjaszewski, *Advances in Controlled/Living Radical Polymerization*. American Chemical Society: Washington, DC, 2003.

5. N. Corrigan, K. Jung, G. Moad, C. J. Hawker, K. Matyjaszewski, C. Boyer, *Prog. Polym. Sci.*, **111**, (2020)

6. Z. Guo, G. Zhang, F. Qiu, H. Zhang, Y. Yang, A.-C. Shi, *Phys. Rev. Lett.*, **101** (2), 028301 (2008)

7. S. Lee, J. J. Shin, K. H. Ku, Y. J. Lee, S. G. Jang, H. Yun, B. J. Kim, *Macromolecules*, **53** (16), 7198-7206 (2020)

8. S. L. Canning, G. N. Smith, S. P. Armes, *Macromolecules*, **49** (6), 1985-2001 (2016)

9. K. Matyjaszewski, J. Xia, *Chem. Rev.*, **101**, 2921-2990 (2001)

10. M. Kamigaito, T. Ando, M. Sawamoto, *Chem. Rev.*, **101**, 3689-3745 (2001)

11. C. J. Hawker, A. W. Bosman, E. Harth, *Chem. Rev.*, **101**, 3661-3688 (2001)

12. G. Moad, E. Rizzardo, S. H. Thang, *Aust. J. Chem.*, **58**, 379-410 (2005)

13. Y. Ni, L. Zhang, Z. Cheng, X. Zhu, *Polym. Chem.*, **10** (20), 2504-2515 (2019)

14. C. B. Ghislain David, Jeff Tonnar, Bruno Ameduri, Patrick Lacroix-Desmazes, and Bernard Boutevin, *Chem. Rev.*, **106**, 3936−3962 (2006)

15. A. Goto, Y. Kwak, T. Fukuda, S. Yamago, K. Iida, M. Nakajima, J. I. Yoshida, *J. Am. Chem. Soc.*, **125** (29), 8720-8721 (2003)

16. Y. Gao, T. Zhao, D. Zhou, U. Greiser, W. Wang, *Chem. Commun.*, **51** (77), 14435-14438 (2015)

17. A. Goto, T. Fukuda, *Prog. Polym. Sci.*, **29**, 329-385 (2004)

18. K. A. Payne, P. Nesvadba, J. Debling, M. F. Cunningham, R. A. Hutchinson, *ACS Macro Lett.*, **4** (3), 280-283 (2015)

19. J. M. Schumers, C. A. Fustin, A. Can, R. Hoogenboom, U. S. Schubert, J. F. Gohy, *J. Polym. Sci., Part A: Polym. Chem.*, **47** (23), 6504-6513 (2009)

20. Q. Lou, D. A. Shipp, *Chem. Phys. Chem*, **13** (14), 3257-3261 (2012)

21. S. Perrier, *Macromolecules*, **50** (19), 7433-7447 (2017)

22. C. Barner-Kowollik, M. Buback, B. Charleux, M. L. Coote, M. Drache, T. Fukuda, A. Goto, B. Klumperman, A. B. Lowe, J. B. Mcleary, G. Moad, M. J. Monteiro, R. D. Sanderson, M. P. Tonge, P. Vana, *J. Polym. Sci., Part A: Polym. Chem.*, **44** (20), 5809-5831 (2006)

23. R. T. A. Mayadunne, E. Rizzardo, J. Chiefari, J. Krstina, G. Moad, A. Postma, S. H. Thang, *Macromolecules*, **33** (2), 243-245 (2000)

24. M. Destarac, D. Charmot, X. Franck, S. Z. Zard, *Macromol. Rapid Commun.*, **21** (15), 1035-1039 (2000)

25. G. Moad, *J. Polym. Sci. Part A: Polym. Chem.*, **57** (3), 216-227 (2019)

26. S. Perrier, P. Takolpuckdee, *J. Polym. Sci. Part A: Polym. Chem.*, **43** (22), 5347-5393 (2005)

27. G. Moad, E. Rizzardo, S. H. Thang, *Chem. Asian J.*, **8** (8), 1634-1644 (2013)

28. P. Galanopoulo, M. Lansalot, F. D'Agosto, *Polym. Chem.*, **11** (23), 3922-3930 (2020)

29. A. Wolpers, F. Baffie, L. Verrieux, L. Perrin, V. Monteil, F. D'Agosto, *Angew. Chem., Int. Ed.*, **59** (43), 19304-19310 (2020)

30. A. Wolpers, C. Bergerbit, B. Ebeling, F. D'Agosto, V. Monteil, *Angew. Chem. Int. Ed.*, **58** (40), 14295-14302 (2019)

31. M. Tatemoto, *Kobunshi Ronbunshu*, **49** (10), 765-783 (1992)

32. A. Goto, K. Ohno, T. Fukuda, *Macromolecules*, **31** (9), 2809-2814 (1998)

33. C. Boyer, D. Valade, P. Lacroix-Desmazes, B. Ameduri, B. Boutevin, *J. Polym. Sci., Part A: Polym. Chem.*, **44** (19), 5763-5777 (2006)

34. G. David, C. Boyer, J. Tonnar, B. Ameduri, P. Lacroix-Desmazes, B. Boutevin, *Chem. Rev. (Washington, DC, U. S.)*, **106** (9), 3936-3962 (2006)

35. C. Chen, L. Xiao, A. Goto, *Macromolecules*, **49** (24), 9425-9440 (2016)

36. C. G. Wang, A. Goto, *J. Am. Chem. Soc.*, **139** (30), 10551-10560 (2017)

37. S. G. Gaynor, J. S. Wang, K. Matyjaszewski, *Macromolecules*, **28** (24), 8051-8056 (1995)

38. G. Moad, D. H. Solomon, *The chemistry of radical polymerization*. Elsevier: 2006.

39. D. Boschmann, P. Vana, *Polym. Bull. (Heidelberg, Ger.)*, **53** (4), 231-242 (2005)

40. S. Sugihara, R. Kawakami, S. Irie, Y. Maeda, *Polym. J. (Tokyo, Jpn.)*, **53** (2), 309-321 (2021)

41. P. Li, T. Wang, F. Lei, X. Peng, H. Wang, L. Qin, J. Jiang, *J. Chromatogr. A*, **1502**, 30-37

(2017)

42. K. Takimoto, E. Takano, Y. Kitayama, T. Takeuchi, *Langmuir*, **31** (17), 4981-4987 (2015)

43. P. Chaiyasat, M. Z. Islam, A. Chaiyasat, *RSC Adv.*, **3**, 10202-10207 (2013)

44. P. Chaiyasat, S. Noppalit, M. Okubo, A. Chaiyasat, *Phys. Chem. Chem. Phys.*, **17**, 1053-1059 (2015)

45. W. Li, G. Song, G. Tang, X. Chu, S. Ma, C. Liu, *Energy*, **36** (2), 785-791 (2011)

46. P. Sangjun, A. Chaiyasat, *Fibers Polym.*, **21** (5), 935-943 (2020)

47. T. Suzuki, T. Mizowaki, M. Okubo, *Polymer*, **106**, 182-188 (2016)

48. A. Jamekhorshid, S. M. Sadrameli, M. Farid, *Renewable Sustainable Energy Rev.*, **31**, 531-542 (2014)

49. S. Nakai, M. Akiyoshi, M. Okubo, *J. Appl. Polym. Sci.*, **127** (4), 2407-2413 (2013)

50.   S. Majumdar, B. Goswami, D. Mahanta, Chapter 1. In *Green Sustainable Process for Chemical and Environmental Engineering and Science.*, Elsevier: 2020; pp 1-29.

51. Y. Kitayama, M. Yorizane, H. Minami, M. Okubo, *Macromolecules*, **45** (5), 2286-2291 (2012)

52. J. S. Song, M. A. Winnik, *Macromolecules*, **39** (24), 8318-8325 (2006)

53. K. Kim, N. R. Ko, S. E. Rhee, B. H. Lee, S. Choe, *Polymer*, **53** (19), 4054-4059 (2012)

54. J. Glasing, P. G. Jessop, P. Champagne, W. Y. Hamad, M. F. Cunningham, *Langmuir*, **36** (3), 796-809 (2020)

55. N. Ballard, M. Aguirre, A. Simula, J. M. Asua, *Chem. Eng. J.*, **316**, 655-662 (2017)

56. Y. Hata, T. Suzuki, H. Minami, M. Okubo, *Colloid Polym. Sci.*, **286** (13), 1561-1567 (2008)

57. Z. Li, Z. Wang, C. Wang, S. Ding, F. Li, H. Lin, *Appl. Surf. Sci.*, **496**, 143708 (2019)

58. H. Zhang, J. Deng, Y. Wu, *ACS Sustainable Chem. Eng.*, **5** (1), 658-666 (2017)

59. Y. Konishi, M. Okubo, H. Minami, *Colloid Polym. Sci.*, **281** (2), 123-129 (2003)

60. R. Arshady, *Colloid Polym. Sci.* , **270** (8), 717-732 (1992)

61. H. G. Yuan, G. Kalfas, W. H. Ray, *J. Macromol. Sci. Rev. Macromol. Chem Phys.*, **31** (2-3), 215-299 (1991)

62. P. Gurnani, S. Perrier, *Prog. Polym. Sci.*, **102**, 101209 (2020)

63. B. S. Casey, B. R. Morrison, R. G. Gilbert, *Prog. Polym. Sci.*, **18**, 1041-1096 (1993)

64. I. A. Maxwell, B. R. Morrison, R. G. Gilbert, *Macromolecules*, **24** (7), 1629-1640 (1991)

65. J. M. M. Simons, J. T. F. Keurentjes, J. Meuldijk, *Macromol. Symp.*, **333**, 102-112 (2013)

66. M. Okubo, H. Yonehara, T. Kurino, *Colloid. Polym Sci.*, **281** (10), 1002-1005 (2003)

67. G. H. Ma, H. Sone, S. Omi, *Macromolecules*, **37**, 2954-2964 (2004)

68. Z. Wang, R. Hong, *J. Polym. Res.*, **23**, 1-10 (2015)

69. J. K. Guillory, *J. Med. Chem.*, **46** (19), 4213-4213 (2003)

70. P. Chaiyasat, S. Namwong, M. Okubo, A. Chaiyasat, *RSC Adv.*, **6** (97), 95062-95066 (2016)

71. P. Chaiyasat, S. Noppalit, M. Okubo, A. Chaiyasat, *Sol. Energy Mater. Sol. Cells*, **157**, 996-1003 (2016)

72. A. P. Altshuller, H. E. Everson, *J. Am. Chem. Soc.*, **75** (7), 1727-1727 (1953)

73. D. Richon, A. Viallard, *Fluid Phase Equilib.*, **21** (3), 279-293 (1985)

74. C. Huang, N. Yamashita, A. Chaiyasat, X. Liu, M. Okubo, *Polymer*, **154**, 128-134 (2018

<div style="text-align:center">

Chapter 1

The kinetic simulation model for the synthesis of micrometer-sized particles

by microsuspension iodine transfer polymerization

</div>

1.1 Introduction

Commonly, when hydrophilic monomer or high content of hydrophilic monomer in monomers is applied to microsuspension conventional radical polymerization (*ms* CRP), a large number of submicrometer-sized polymer particles are often formed as a byproduct in the aqueous media in addition to the micrometer-sized ones. The byproduct formation is based on that some of the initiator and oligomeric radicals generated inside the droplets exit to an aqueous medium,[1, 2] resulting from the water solubility of these relative hydrophilic radicals, and then react with the hydrophilic monomer, which is partially dissolving in the aqueous medium. When the oligomer molecules reach their critical chain lengths, at which they precipitate in the aqueous medium, they gather and result in primary particles. The particles are more likely to absorb monomers from the monomer droplets via the aqueous medium and act as the polymerization loci of emulsion polymerization. As a result, all product is not micrometer-sized particles, but submicrometer-sized ones. To depress the emulsion polymerization in an aqueous

medium, a water-soluble inhibitor was often added therein.[3-6] However, it is not easy to get the optimum condition because it is a very narrow region.

From Chaiyasat's work,[7] we got a hint to overcome this drawback, in which microsuspension iodine transfer polymerization (*ms* ITP) of methyl methacrylate (MMA, solubility in water: 1.5 g/100 mL at 20°C),[8] was carried out to prepare micrometer-sized poly(methyl methacrylate). In this case, Iodoform was used not only as the chain transfer agent, but also worked as a kind of hydrophobe because of the high water-insolubility of iodoform (CHI_3), iodine group ($I\bullet$), and diiodomethyl group ($CHI_2\bullet$). That is, CHI_3 could capture monomer or oligomer radicals within monomer droplets. This function of CHI_3 has been named as the *r*adical *e*xit *d*epression (RED) effect.[9] However, with the more hydrophilic monomers (e.g., ethyl acrylate (EA, solubility in water: 8.3 g/100 mL at 20°C)[10] and methyl acrylate (MA, solubility in water: 6.0 g/100mL at 20°C)[11]), it becomes difficult to prevent the submicrometer-sized byproduct particles after applying same conditions to these monomers.

As mentioned above, the nascent radicals generated in the aqueous phase is the key to the synthesis of micrometer-sized particles. The kinetic simulation of the exited radicals generated in the preliminary stage in the case of *ms* ITP of MMA was performed using PREDICI software from CiTGmbH, and was regarded as the reference for the synthesis of micrometer-sized particles without submicrometer-sized particles.[12] By comparing the simulation plots of different monomers under the different hypothetical polymerization conditions with the plot of *ms* ITP of MMA, the assumptive condition

for the synthesis of micrometer-sized particles without submicrometer-sized particles could be estimated. Therefore, the feasibility of a certain condition to synthesize 100% micrometer-sized particles could be predicted under the instruction of this simulation. The specific scenarios would be discussed in the following chapters.

To understand the simulation well, the kinetic simulation model would be demonstrated in this chapter.

1.2 Experimental

1.2.1 Materials

MA (Nacalai Tesque, Inc. Kyoto, Japan; stabilizer: hydroquinone 5 ppm) and Vinyl acetate (VAc, Nacalai Tesque, Inc., Kyoto, Japan) were purified by passing it through a column packed with basic aluminum oxide (Alumina Activated 200, Nacalai Tesque, Inc. Kyoto, Japan). CHI_3 of analytical grade (Nacalai Tesque, Inc., Kyoto, Japan; purity, 99%), 2,2′-azobis(2-methylpropionitrile) (AIBN; Nacalai Tesque, Inc., Kyoto, Japan; purity $\geq$ 98.0%), 2,2'-azobis(4-methoxy-2,4-dimethylvaleronitrile) (V-70; Fujifilm Wako Pure Chemical Co., Osaka, Japan; purity $\geq$ 95.0%), Xylene (Nacalai Tesque, Inc., Kyoto, Japan), and *N,N*-dimethylformamide (DMF; Nacalai Tesque, Inc., Kyoto, Japan; purity $\geq$ 99.0%) were used as received. Benzyl peroxide (BPO, Nacalai Tesque, Inc., Kyoto, Japan; containing water $\leq$ 98.0%) was used after reprecipitation.

1.2.2 Synthesis of polymers in a *bulk* ITP system

Poly(methyl acrylate) (PMA) and Poly(vinyl acetate) (PVAc) were synthesized using *bulk* ITP. BPO (0.12 g) and CHI_3 (0.144 g, only for ITP) were dissolved in MA (12 g) in a molar ratio of $[MA]:[BPO]:[CHI_3] = 381:1.35:1$, While V-70 or AIBN (0.12 g) and CHI_3 (0.144 g) were dissolved in VAc (12 g) in a molar ratio of $[VAc]:[V-70]:[CHI_3] = 381:1.06:1$ and $[VAc]:[AIBN]:[CHI_3] = 381:2.00:1$, respectively. Subsequently, the solution was evenly divided into 6 glass tubes, which were sealed off after being degassed five times with vacuum/N_2 gas cycles. Finally, the polymerizations of different monomers were conducted at various temperatures for 1 h. In all the polymerizations, the sealed tubes were placed in a water bath with a horizontal shaking rate of 120 rpm.

1.2.3 Characterization

The solution was sampled every 10 min for conversion by taking one tube from the water bath. The monomer and CHI_3 conversions were measured by gas chromatography (GC-18A, SHIMADZU, Japan). Simulation of the ITP of monomers was conducted using the PREDICI software from CiT GmbH (Rasfede, Germany).

1.3 Results and discussion

1.3.1 The model used for simulation

Scheme 1 shows the model of the desorption of the free radical used for simulation. In the model, we suppose that the exiting free radical is tend to re-enter another particle without re-

exiting but remain. In another word, the model used in the simulation is under the supposition that a desorbed free radical has the only fate to re-enter another particle, and have a possibility of re-exit unless the radical terminates with another free radical in the last entered particle.[1]
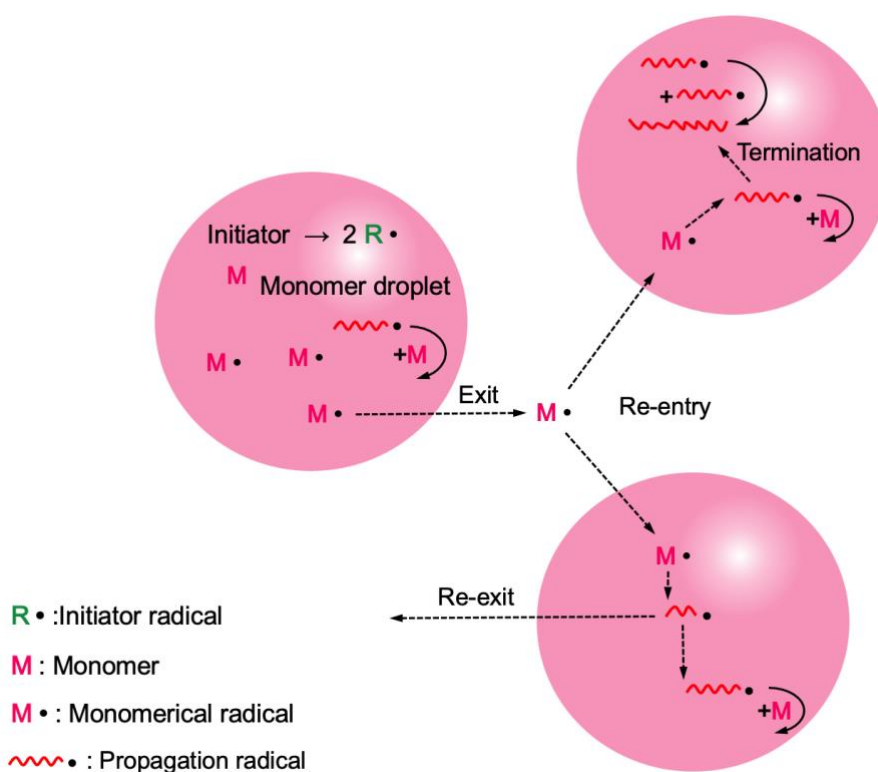
Scheme 1. The model of the fate of free radicals in microsuspension polymerization.

According to the model used in the simulation, the exiting rate of a primary radical is faster than the propagating rate, and the probability of the aqueous-phase propagation or termination can be neglected.[2] At that time, the exiting rate coefficient (k_e) of oligomer radicals is proportional to the transfer rate coefficient (k_{tr}), as shown in eq (1), where C_m refers to the monomer concentration in the particle.

$$k_e = k_{tr}C_m$$ eq (1)

Although there are a few other factors might be important in determining the exiting rate,[13] in this simulation model, the transfer rate is treated as the governing factor without considering the influence from monomer and chain transfer agent concentration.

Once the chain transfer agent was added, in this case of iodoform (CHI_3), the chain transfer rate coefficient of CHI_3 (k_{tr,CHI_3}) is much faster than the chain transfer rate coefficient of monomer ($k_{tr,m}$), which indicates the nascent radicals captured by chain transfer agent are difficult to escape from the monomer droplet basing on the increased hydrophobicity. Therefore, the escapable radicals are only derived from the free monomeric radicals.

And the rate of radical loss is proportional to the radical concentration. To understand it, the rate of radical loss is given as eq (2), in which ρ refers to the entry rate coefficient. In the two equations, $\bar{n}$ presents the relative average number of exiting radicals in the per particle. The sign of eq (2) refers to the tendency of radicals that are entering or exiting. For the first exiting, the rate of radical loss can be simplified to eq (3), where is no entering radicals. Therefore, to decrease the exiting oligomer radicals from monomer droplets which will arouse the homogenous nucleation in the aqueous phase, it is important to decrease the number of the generation of oligomer radicals in the early stage.

$$\frac{d\bar{n}}{dt} = (1 - 2\bar{n})\rho - 2k_e\bar{n}$$

eq (2)

$$\frac{d\bar{n}}{dt} = -2k_e\bar{n}$$

eq (3)

1.3.2 Calculation of chain transfer constant (C$_{tr}$) at different temperatures[14]

To give the reliable result of $k_{tr,CHI3}$, the chain transfer constant of CHI$_3$ would be calculated

practically under various assumptive conditions, as the following calculative process.

The main chain transfer appeared in the early stage of the polymerization showed as

below:

$$P_n\bullet + CHI_3 \xrightarrow{k_{tr}} P_n\text{-}I + CHI_2\bullet \qquad \text{Reaction (1)}$$
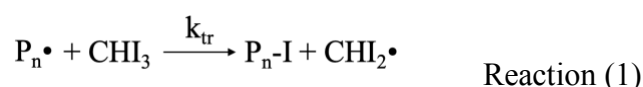
This reaction is a second-order reaction, therefore, the consumption of iodoform (CHI$_3$)

within the period of time (t) based on reaction (1) can be calculated by equation (4) through the

following mathematical procedures.

Consumption of [CHI$_3$]
$$-\frac{d[CHI_3]}{dt} = k_{tr}[P_n\bullet][CHI_3] \implies -\frac{d[CHI_3]}{[CHI_3]} = k_{tr}[P_n\bullet]\,dt$$

Integration
$$-\int_{[CHI_3]_0}^{[CHI_3]_t} \frac{d[CHI_3]}{[CHI_3]} = \int_0^t k_{tr}[P_n\bullet]\,dt \implies \ln\left(\frac{[CHI_3]_0}{[CHI_3]_t}\right) = k_{tr}[P_n\bullet]\,t$$

$$\text{eq (4)}$$

In the calculation, the k_{tr}, [CHI$_3$]$_0$, [CHI$_3$]$_t$ and [P$_n$•] refer to the chain transfer rate,

concentration of CHI$_3$ at time t = 0 and t = t, and concentration of polymer radicals, respectively.

For the generally propagation:

$$P_n\bullet + M \xrightarrow{k_p} P_{n+1}\bullet \qquad \text{Reaction (2)}$$
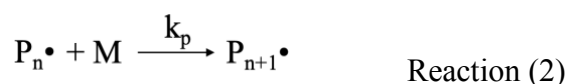
The generation of polymer within the period of time (t) based on reaction (2) can be

calculated by equation (2) through the following mathematical procedures.

Consumption of [M]

$$-\frac{d[M]}{dt} = k_p [P_n \bullet][M] \implies -\frac{d[M]}{[M]} = k_p [P_n \bullet] \, dt$$

Integration

$$-\int_{[M]_0}^{[M]_t} \frac{d[M]}{[M]} = \int_0^t k_p [P_n \bullet][M] dt \implies \ln\left(\frac{[M]_0}{[M]_t}\right) = k_p [P_n \bullet] \, t$$

eq (5)

The k_p, [M], $[CHI_3]_t$ and $[P_n\bullet]$ refer to the propagation rate, the concentration of monomer, the concentration of CHI_3 at time t, and the concentration of polymer radicals, respectively.

After dividing eq (1) by eq (2), it gives the below equation (6):

$$\ln\left(\frac{[CHI_3]_0}{[CHI_3]_t}\right) = \frac{k_{tr}}{k_p}\ln\left(\frac{[M]_0}{[M]_t}\right)$$

eq (6)

Because $C_{tr} = k_{tr}/k_p$, eq (6) can be converted into the following equation (7), which can be used to calculate C_{tr} experimentally in the form of conversion.

$$C_{tr} = \ln(1-p)/\ln(1-q)$$

eq (7)

In equation (7), the p and q represent the conversion of CHI_3 and monomer, respectively, which can be determined by GC. The measurement was proceeded in the bulk system with the

same concentration of materials as the recipe in the suspension system, which would be shown in the following chapter. As a small amount of I_2 generated in the early stage, which can work as the good scavenger for radicals and result in the inhibition of polymerization, the value of C_{tr} was focused within the early 15 minutes.

Table 1. Values of C_{tr} of CHI_3 at different temperatures with different monomers and initiators.

Monomer	T (˚C)	Initiator	C_{tr}
MMA [a)	60	BPO	3.18
MA [b)	70	BPO	50.62
	60	AIBN	5.43
	50	V-70	2.28
VAc [b)	40	V-70	21.54
	30	V-70	40.16

a) Barson, C.A.; Bevington, J.C.; Hunt, B.J., *Polymer* **1996**, *37*(25), 5699-5702
b) Calculated value

The values of C_{tr} at different temperatures in the existence of different monomers and initiators were given in Table 1, which would be plug into the kinetic simulation.

1.3.3 Simulation section[12]

As mentioned above, it is important to restrict the number of free monomeric radicals, which will arouse the homogenous nucleation in the aqueous phase. For simplifying the simulation, the original concentration of water-soluble radicals only takes the saturation solubilities of monomers, initiators, and iodoform in water into account. Afterwards, the polymerization rate in the aqueous phase (R_p^w) could be sumilated.

The kinetic scheme for simulation is given in Table 2. And the kinetic parameters input to the simulation model are given in Table 3.

Table 2. Kinetic scheme for simulation of ITP.

Primary radical formation		Chain transfer	
$I \rightarrow f \times (R\bullet + R\bullet)$	k_d	$P1(s)\bullet + P2\text{-}I(r) \rightarrow P1\text{-}I(s) + P2(r)\bullet$	k_{ex}
Initiation		$P1(s)\bullet + P3\text{-}I(r) \rightarrow P1\text{-}I(s) + P3(r)\bullet$	k_{ex}
$R\bullet + M \rightarrow P1(1)\bullet$	$k_{i,R\bullet}$	$P2(s)\bullet + P1\text{-}I(r) \rightarrow P2\text{-}I(s) + P1(r)\bullet$	k_{ex}
$CHI_2\bullet + M \rightarrow P2(1)\bullet$	$k_{i,CHI_2\bullet}$	$P2(s)\bullet + P2\text{-}I(r) \rightarrow P2\text{-}I(s) + P2(r)\bullet$	k_{ex}
$R\bullet + M \rightarrow P3(1)\bullet + RH$	$k_{itr,m}$	$P2(s)\bullet + P3\text{-}I(r) \rightarrow P2\text{-}I(s) + P3(r)\bullet$	k_{ex}
Propagation		$P3(s)\bullet + P1\text{-}I(r) \rightarrow P3\text{-}I(s) + P1(r)\bullet$	k_{ex}
$P1(s)\bullet + M \rightarrow P1(s+1)\bullet$	k_p	$P3(s)\bullet + P2\text{-}I(r) \rightarrow P3\text{-}I(s) + P2(r)\bullet$	k_{ex}
$P2(s)\bullet + M \rightarrow P2(s+1)\bullet$	k_p	$P3(s)\bullet + P3\text{-}I(r) \rightarrow P3\text{-}I(s) + P3(r)\bullet$	k_{ex}
$P3(s)\bullet + M \rightarrow P3(s+1)\bullet$	k_p	**Termination**	
Chain transfer		$P1(s)\bullet + P1(r)\bullet \rightarrow D11(s+r)$	k_{tc}
$R\bullet + CHI_3 \rightarrow RI + CHI_2\bullet$	k_{itr,CHI_3}	$P2(s)\bullet + P2(r)\bullet \rightarrow D22(s+r)$	k_{tc}
$P1(s)\bullet + RI \rightarrow P1\text{-}I(s) + R\bullet$	$k_{tr,RI}$	$P3(s)\bullet + P3(r)\bullet \rightarrow D33(s+r)$	k_{tc}
$P2(s)\bullet + RI \rightarrow P2\text{-}I(s) + R\bullet$	$k_{tr,RI}$	$P1(s)\bullet + P2(r)\bullet \rightarrow D12(s+r)$	k_{tc}
$P3(s)\bullet + RI \rightarrow P3\text{-}I(s) + R\bullet$	$k_{tr,RI}$	$P1(s)\bullet + P3(r)\bullet \rightarrow D13(s+r)$	k_{tc}
$P1(s)\bullet + M \rightarrow D1(s) + P3(1)\bullet$	$k_{tr,m}$	$P2(s)\bullet + P3(r)\bullet \rightarrow D23(s+r)$	k_{tc}
$P2(s)\bullet + M \rightarrow D2(s) + P3(1)\bullet$	$k_{tr,m}$	$P1(s)\bullet + P1(r)\bullet \rightarrow D1(s) + D1(r)$	k_{td}
$P3(s)\bullet + M \rightarrow D3(s) + P3(1)\bullet$	$k_{tr,m}$	$P2(s)\bullet + P2(r)\bullet \rightarrow D2(s) + D3(r)$	k_{td}
$P1(s)\bullet + CHI_3 \rightarrow P1\text{-}I(s) + CHI_2\bullet$	k_{tr,CHI_3}	$P3(s)\bullet + P3(r)\bullet \rightarrow D3(s) + D3(r)$	k_{td}
$P2(s)\bullet + CHI_3 \rightarrow P2\text{-}I(s) + CHI_2\bullet$	k_{tr,CHI_3}	$P1(s)\bullet + P2(r)\bullet \rightarrow D1(s) + D2(r)$	k_{td}
$P3(s)\bullet + CHI_3 \rightarrow P3\text{-}I(s) + CHI_2\bullet$	k_{tr,CHI_3}	$P1(s)\bullet + P3(r)\bullet \rightarrow D1(s) + D3(r)$	k_{td}
$P1(s)\bullet + P1\text{-}I(r) \rightarrow P1\text{-}I(s) + P1(r)\bullet$	k_{ex}	$P2(s)\bullet + P3(r)\bullet \rightarrow D2(s) + D3(r)$	k_{td}

Table 3. Kinetic input parameters for simulation and recipes of ITP of VAc or MA.

Coefficient	eq for MMA	eq for MA	eq for VAc
k **d** (s^{-1})	$=3.0\times10^{13}\exp(-123800/RT)$ [a] $R=8.314J\ K^{-1}mol^{-1}$	$=3\times10^{13}\exp(-123800/RT)$ [a] for BPO $R=8.314J\ K^{-1}mol^{-1}$	$=5.37\times10^{11}\exp(-94300/RT)$ [a] for V-70 $=5.82\times10^{15}\exp(-132400/RT)$ [a] for AIBN $R=8.314J\ K^{-1}mol^{-1}$
k **i,R•** $(M^{-1}s^{-1})$	$=k$p	$=k$p	$=k$p
k **i,CHI$_2$•** $(M^{-1}s^{-1})$	$=k$p	$=k$p	$=k$p
k **itrm** $(M^{-1}s^{-1})$	$=k$p/100	$=k$p/100	$=k$p/100
k **p** $(M^{-1}s^{-1})$	$=5.13\times10^{6}\exp(-26400/RT)$ [b] at 80 °C $R=8.314J\ K^{-1}mol^{-1}$	$=1.66\times10^{7}\exp(-17700/RT)$ [c] $R=8.314J\ K^{-1}mol^{-1}$	$=2.43\times10^{8}\exp(-30600/RT)$ [b] $R=8.314J\ K^{-1}mol^{-1}$
k **itr,CHI$_3$** $(M^{-1}s^{-1})$	$=k$tr,CHI$_3$	$=k$tr,CHI$_3$	$=k$tr,CHI$_3$
k **tr,RI** $(M^{-1}s^{-1})$	$=k$tr,CHI$_3$	$=k$tr,CHI$_3$	$=k$tr,CHI$_3$
k **trm** $(M^{-1}s^{-1})$	$=0.25\times10^{-4}\times k$p [d]	$=0.224\times10^{-4}\times k$p [d]	$=1.9\times10^{-4}\times k$p [d]
k **tr,CHI$_3$** $(M^{-1}s^{-1})$	$=3\times k$p [e]	$=C_{tr}\times k$p [e]	$=C_{tr}\times k$p [e]
k **ex** $(M^{-1}s^{-1})$	$=k$tr,CHI$_3$	$=k$ tr,CHI$_3$	$=k$ tr,CHI$_3$
k **t** $(M^{-1}s^{-1})$	$=6.8\times10^{8}\exp(-2840/RT)$ [g] $R=1.987cal\ K^{-1}mol^{-1}$	$=1.40\times10^{10}\exp(-5300/RT)$ [g] $R=1.987cal\ K^{-1}mol^{-1}$	$=2.08\times10^{11}\exp(-5204/RT)$ [f] $R=1.987cal\ K^{-1}mol^{-1}$
$[M]_{aq}$ (mol/L) [h]	1.50×10^{-1}	6.72×10^{-1}	3.19×10^{-1}
$[I]_{aq}$ (mol/L) [i]	4.6×10^{-4} for BPO	4.6×10^{-4} for BPO	6.5×10^{-3} for AIBN 3.70×10^{-4} for V-70
$[CHI_3]_{aq}$ (mol/L) [j]	2.54×10^{-4}	2.54×10^{-4}	2.54×10^{-4}

a) https://specchem-wako-jp.fujifilm.com/en/oilazo

b) M. S. Matheson, E. E. Auer, Ellen B. Bevilacqua, *et al.*, *J. Am. Chem. Soc.*, **1949**, *71*, 2610

c) X. Yu, J. Pfaendtner, and L. J. Broadbelt, *J. Phys. Chem. A.*, **2008**, *112*, 6772

d) Brandrup, J.; Immergut, E. H.; Grulke, E.A., *Polymer Handbook, Fourth Edition*. **1998**, II-99,101

e) C$_{tr}$ shown in Table 1

f) Matheson, S.; Auer, E. E.; Bevilacqua, Ellen B.; Hart, E. J., J. Am. Chem. Soc. **1949**, *71*, 2610

g) Matheson, S.; Auer, E. E.; Bevilacqua, Ellen B.; Hart, E. J., J. Am. Chem. Soc. **1949**, *71*, 497

h) D. Richon, and A. Viallard, *Fluid Ph. Equilibria.*, **1985**, *21*, 279

i) Calculated using Advanced Chemistry Development (ACD/Labs) Software V11.02

j) Kamal I. Al-Malah, *J. Mol. Modela.*, **2011**, *17*, 1029

1.3.4 Calculation of maximum monomer units of an oligomer radical (P_{max})

More specifically, from the view of the solubility of oligomers, the maximum monomer units of an oligomer radical (P_{max}), which can still exit from monomer droplets, are able to be calculated by the following calculation process.

The hydrophobic free energy (ΔG^{hyd}) can be seen as the important factor to influence the ratios of the adsorption to desorption rate coefficients.[2] If the oligomers in water phase possess the larger ΔG^{hyd}, the oligomers have higher possibility of "instantaneous" entry to the monomer droplets, that is, they are less likely to desorb after entering and proceed to propagation in the monomer droplet.

The ΔG^{hyd} of small solute molecules in water was calculated by the eq (8), which proposed by Israelachvili and Pashley.[15] Here σ is the diameter of the solute molecule. In the case of polymerization with water-insoluble initiator BPO, the σ of a styryl unit, a methene group and a carbon monoxide are 0.6 nm,[16] 0.15 nm[1] and 0.13 nm,[17] respectively. While, in the case of AIBN and V-70, only the lengths of C-H (0.109 nm) and C-C bond (0.15 nm) are taken into consideration.

$$\Delta G_1^{hyd} \text{ (kJ/mol)} \cong -20\,\sigma \qquad \text{eq (8)}$$

The ΔG^{hyd} of monomer in water was calculated by the eq (9),[2] where the [$M_{aq,sat}$] refers to the saturation solubility of the monomer in the aqueous phase (mol L^{-1}), gas constant (R) is 1.987 cal K^{-1}mol^{-1} and T is thermodynamic temperature.

$$\Delta G_2^{hyd}(kJ/mol) \cong 0.004RTln[M_{aq, sat}] \qquad \text{eq (9)}$$

In the calculation, a criterion was set up that the ΔG^{hyd} for oligomers is approximate to the sum of the ΔG^{hyd} of monomer units. Before the oligomers become incipiently insoluble in water, there is a maximum monomer units of oligomer radicals (P_{max}) which can still exit from monomer droplets. This maximum value can be estimated roughly by considering the n-alkyl chain length, that the ΔG^{hyd} of both oligomer and n-alkyl specie is equal. In the case of emulsifier-free emulsion polymerization using BPO as initiator, the ΔG^{hyd} of n-alkyl benzoate is required. For n-alkyl benzoate in the aqueous phase, which is found "absolutely" insoluble in water when the number of methene groups is 4. It is determined by comparing with the water solubility of heptadecyl sulfate, which is found experimentlly that oligomeric species becomes insoluble in water.[1, 18, 19] For using AIBN and V-70 as intiator, the "absolutely" insoluble species appeare when the number of methene groups are 16 and 14, respectively, after comparing the predicted water solubility to the heptadecyl sulfate.

When $|\Delta G_2^{hyd}|$ of initial radicals is higher than the $|\Delta G_1^{hyd}|$ calculated by eq (8), the insoluble oligomer radicals will start to appear.

Therefore, the value of the P_{max} can be obtained by eq (10). Here the integer function (int) rounds off the quantity to the lower integer value.

$$P_{max} = int(\Delta G_1^{hyd}/\{0.004RTln[M_{aq, sat}]\}) \qquad \text{eq (10)}$$

The exact maximum units of oligomer which can still exit to water phase at different temperatures were shown in Table 4.

Table 4. Calculated Values of P_{max} for MA and VAc at various temperature using different initiators.

Monomer	T (°C)	Initiator	$[M_{aq,\ sat}]$ (mol/L)	ΔG_1^{hyd} (KJ/mol)	P_{max}
MMA	80	BPO	0.150	-26.6	4
MA	70	BPO	0.697	-26.6	26
VAc	60	AIBN	0.290	-55.4	16
	50	V-70			17
	40	V-70			17
	30	V-70			18

According to this result, the R_p^w of polymerization processes could be evaluated at a monomer conversion of at most 10%. Hence, in this work, the comparison of the R_p^w was focused within a conversion of 20%.

1.4 Conclusion

The kinetic model was explained in this chapter, to verify and predict the suitable condition of hydrophilic monomers for synthesizing micrometer-sized particles without submicrometer-sized byproduct particles in the following chapters. The comparison of the R_p^w of polymerization processes would be emphasized at a conversion of 20%, according to the calculation results of P_{max}s.

1.5 References

1. B. S. Casey, B. R. Morrison, R. G. Gilbert, *Prog. Polym. Sci.*, **18**, 1041-1096 (1993)

2. I. A. Maxwell, B. R. Morrison, D. H. Napper, R. G. Gilbert, *Macromolecules*, **24** (7), 1629-1640 (1991)

3. J. M. M. Simons, J. T. F. Keurentjes, J. Meuldijk, *Macromol. Symp*, **333**, 102-112 (2013)

4. M. Okubo, H. Yonehara, T. Kurino, *Colloid Polym. Sci.*, **281** (10), 1002-1005 (2003)

5. G. H. Ma, H. Sone, S. Omi, *Macromolecules*, **37**, 2954-2964 (2004)

6. Z. Wang, R. Hong, *J. Polym. Res.*, **23**, 1-10 (2015)

7. P. Chaiyasat, S. Namwong, M. Okubo, A. Chaiyasat, *RSC Adv.*, **6** (97), 95062-95066 (2016)

8. J. K. Guillory, *J. Med. Chem.*, **46** (19), 4213-4213 (2003)

9. P. Chaiyasat, S. Noppalit, M. Okubo, A. Chaiyasat, *Sol. Energy Mater. Sol. Cells*, **157**, 996-1003 (2016)

10. A. P. Altshuller, H. E. Everson, *J. Am. Chem. Soc.*, **75** (7), 1727-1727 (1953)

11. D. Richon, A. Viallard, *Fluid Phase Equilib.*, **21** (3), 279-293 (1985)

12. M. Okubo, Y. Kitayama, N. Yamashita, X. Liu, C. Huang, *Macromol. Theory Simul.*, **27** (5), 1800029 (2018)

13. G. Lichti, D. F. Sangster, B. C. Y. Whang, D. H. Napper, R. G. Gilbert, *J. Chem. Soc., Faraday Trans.*, **78** (7), (1982)

14. P. Lacroix-Desmazes, J. Tonnar, Degenerative Transfer with Alkyl Iodide. In *Polymer Science: A Comprehensive Reference*, 2012; pp 159-180.

15. R. P. Jacob Israelachvili, *Nature*, **300**, 341-342 (1982)

16. M. J. Rosen, J. T. Kunjappu, *Surfactants and Interfacial Phenomena, Fourth Edition*. 2012; p 616 pp.

17. J. Lin, E. Pozharski, M. A. Wilson, *Biochemistry*, **56** (2), 391-402 (2017)

18. L. C. Becker, W. F. Bergfeld, D. V. Belsito, R. A. Hill, C. D. Klaassen, D. Liebler, J. G. Marks, Jr, R. C. Shank, T. J. Slaga, P. W. Snyder, F. A. Andersen, *Int. J. Toxicol.*, **31** (6 Suppl), 342S-372S (2012)

19. H. V. Tartar, K. A. Wright, *J. Am. Chem. Soc.*, **61** (3), 539-544 (1939)

Chapter 2

Synthesis of micrometer-sized poly(methyl acrylate) by temperature-step microsuspension polymerization with iodoform based on "radical exiting depression" (RED) effect

2.1 Introduction

Methyl acrylate (MA) as a monomer owning the high water solubility (solubility in water: 6 g/100 mL, 20°C),[1] which is 4 times higher than methyl methacrylate (MMA, water solubility in water: 1.5 g/100mL, 20°C),[2] is difficult to synthesize micrometer-sized particles without submicrometer-sized particle. After trying the condition of 8 wt% benzyl peroxide (BPO) (relative to MA) at 80°C, at which the *ms* ITP of MMA succeeded to prepare micrometer-sized particles without submicrometer-sized ones,[3] it failed. In contrast, the product was 100% submicrometer-sized poly(methyl acrylate) (PMA) particles. As mentioned in Chapter 1, the generation of free monomeric radicals in the aqueous play a role in the submicrometer-sized particles. To restrain the amount of these free radicals in the preliminary stage of polymerization, a work was done by decreasing the amount of BPO. It succeeded in synthesis of micrometer-sized particles without the submicrometer-sized byproduct particles only at a very low BPO concentration (0.8 wt % relative to monomer). However, in this work, the conversion

was low and it needed a longer time to complete the polymerization.[4]

To realize the 100% micrometer-sized particles efficiently from the viewpoint of industrial applications, in this chapter, the microsuspension polymerization with iodoform (*ms* I) of MA will be carried out using a high concentration of BPO with a two-step temperature process, which is based on the idea of *Radical Exiting Depression* (RED) effect, under the instruction of simulation. For the control/livingness in the case of MA at high temperature is relatively poor, we refer to microsuspension polymerization with iodoform as "*ms* I" instead of "*ms* ITP" in this chapter.

2.2 Experimental

2.2.1 Materials

MA (Nacalai Tesque, Inc. Kyoto, Japan; purity, 98%) was purified by passing through the column packed with basic aluminum oxide (Alumina Activated 200, Nacalai Tesque, Inc. Kyoto, Japan). Iodoform (CHI_3) of analytical grade (Nacalai Tesque, Inc. Kyoto, Japan; purity, 99%) and poly(vinyl alcohol) (PVA; Nippon Synthetic Chemical Industry Co., Ltd, Osaka, Japan; degree of saponification 86.5-89%, molecular weight 7×10^4) and BPO (Nacalai Tesque, Inc. Kyoto, Japan; purity $\geqq$ 98.0%) were used as received. Deionized water used in all experiments was obtained from a water purification machine (Elix UV, Millipore Co., Ltd., Japan) and had a resistivity of 15 MΩ cm.

2.2.2 Synthesis of PMA Particles in an aqueous phase

PMA particles were synthesized by *ms* I and *ms* CRP. BPO (3.0 g) and CHI_3 (0.036 g) (only for *ms* I) were dissolved in MA (3 g), which was added to a 100-mL glass vial. Next, 1 wt% PVA aqueous solution (27 g) was poured into the monomer phase, followed by vibration for 1 min with a vortex mixer (MIXER MF-71) at 200 rpm/min to obtain a monomer dispersion. Subsequently, the monomer dispersion was evenly divided into six glass tubes, which were sealed off after degassing with five times vacuum/N_2 gas cycles. Finally, *ms* CRP was carried out at 70°C for 1 h, while *ms* I was carried out at two-step temperatures: first step: 60 or 70°C for 2 h; second step: 80°C for 4 h. In all polymerizations, the sealed tubes were placed in a water bath with a horizontal shaking rate of 120 rpm/min.

2.2.3 Chain extension in bulk system

Chain extension was conducted in a bulk system with styrene using PMA prepared by *ms* I as a macroinitiator agent. PMA (0.15g) was dissolved in styrene (3 g), and the solution was added to a glass tube. After degassing with five times vacuum/N_2 gas cycles, the glass tube was sealed off under vacuum. The polymerization was proceeded at 70°C for 48 h with the horizontal shaking rate of 120 rpm/min.

2.2.4 Simulation

Simulation for ITP and CRP of MA was conducted with PREDICI software from CiT GmbH (Rasfede, Germany), using the kinetic parameters shown in the Table 3, Chapter 1.

2.2.5 Characterization

The monomer conversions were measured by both gravimetry and gas chromatography (GC-18A, SHIMADZU, Japan). Appearances of dispersion at each conversion and its upper layer after centrifugation at a speed of 5,000 rpm for 10 min, where the micrometer-sized particles sedimented out and the submicrometer-sized particles still dispersed in the aqueous medium, were observed with naked eyes. The particles were observed utilizing an optical microscope (OM, ECLIPSE 80i, Nikon). The weight-average diameters ($\overline{D}_w$) and the number-average diameters ($\overline{D}_n$) of the particles were measured using dynamic light scattering (DLS, FPAR-1000RK, OTSUKA ELECTRONICS Co., LTD). Weight-average and number-average molecular weights (M_w and M_n, respectively) and molecular weight distribution (M_w/M_n) were measured by gel permeation chromatography (GPC) with two styrene/divinylbenzene gel columns (TOSOH Corporation, TSK gel GMH$_{HR}$-H, 7.8 mm i.d × 30 cm, separation range per column: approx. $50 - 4 \times 10^8$ g/mol (exclusion limit)) using DMF as eluent at 40°C at a flow rate of 1.0 mL/min employing refractive index (TOSOH RI-8020/21). The columns were calibrated with seven standard PS samples ($1.11 \times 10^3 - 5.48 \times 10^6$, $M_w/M_n = 1.01 - 1.07$).

2.3 Results and discussion

2.3.1 Simulation of R_p^w in the case of *ms* I of MA under different temperatures

In the principle of *ms* I, the primary radicals derived from the decomposition of the initiator react with a few monomers to generate oligomer radicals, and then the oligomer radicals react with the chain transfer agent in the monomer droplets. However, in the case of hydrophilic monomers, a number of oligomer radicals would exit from monomer droplets to the aqueous phase before captured by the chain transfer agent. In this study, we assume that a lower polymerization temperature (decreasing the decomposition rate of the initiator and lowering the polymerization rate) should decrease the number of the generation of oligomer radicals in the

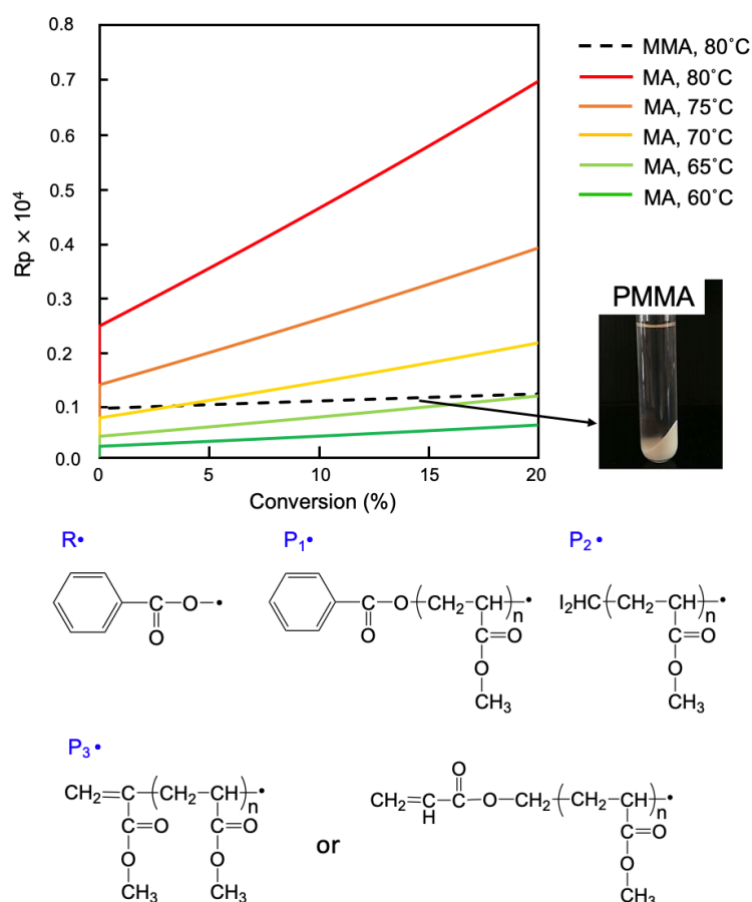early stage, resulting in the decrease of exiting oligomer radical from monomer droplet.

Figure 1. Relationships between the conversion and the polymerization rate in the aqueous phase (R_p^w) simulated in the system of microsuspension polymerization with iodoform (*ms* I) of methyl acrylate (MA) at various temperatures under the assumption that the same total number of $P_1\bullet$, $P_3\bullet$ and $R\bullet$ radicals within monomer droplets exist in the aqueous media. The broken line indicates the simulation result for methyl methacrylate (MMA) at 80°C and 8 wt% benzoyl peroxide (BPO) (relative to MMA). Inset: appearance of micrometer-sized poly(MMA) (PMMA) dispersion after centrifugation and structures of $P_1\bullet$, $P_2\bullet$, $P_3\bullet$, and $R\bullet$ radicals.

To better understand the kinetics of *ms* I, simulation results of R_p^w of polymerization with iodoform as chain transfer agent at a various polymerization temperature of 60 – 80°C are shown in Fig. 1. This simulation is manipulated under the assumption that the amount of

preliminary monomeric radicals (i.e., $P_1\bullet$, $P_3\bullet$, and $R\bullet$ radicals) are equal to the saturate water solubility of initiator and monomer. The chemical structures of $P_1\bullet$, $P_3\bullet$, and $R\bullet$ radicals are shown at the bottom half of Fig. 1, refer to PMA oligomer radicals with BPO initiator fragment, a vinyl group as end group, and benzoyloxy radicals, respectively. These are the main radicals that were considered to exit from MA droplets and form the nucleus of byproduct particles in the aqueous medium. While $P_2\bullet$ radicals, which are attached to diiodomethyl group, display a good RED effect, which depresses the exiting of monomer and oligomer radicals from monomer droplets to the aqueous phase based on capturing by high hydrophobicity of iodine group within the monomer droplets.[3, 4] A broken line indicates simulated R_p^w of MMA under which polymerization within monomer droplets succeeds at the condition of 8 wt% BPO (relative to monomer) at 80°C. On the other hand, the simulated rate of polymerization for MA (red solid line) was higher than that of MMA over an entire conversion. Indeed, the microsuspension polymerization was failed.[5] Specifically, from the view of water soluble nascent radicals, the maximum monomer units of an oligomer radical (P_{max}) at 80°C, which can still exit from monomer droplets is 4 of PMMA oligomer, while that of PMA oligomer is 26, which were calculated in Chapter 1. This higher water solubility of PMA oligomer caused the difficulty of microsuspension of MA. Therefore, an appropriate temperature for polymerization of MA would be an equal or lower R_p^w than that of MMA at the beginning of polymerization, that is, the temperature should be equal to or lower than 70°C. Based on this simulation, the recipe of *ms* ITP of MMA with the high BPO concentration (8 wt% relative to monomer) was applied to MA as *ms* I under different temperature steps.
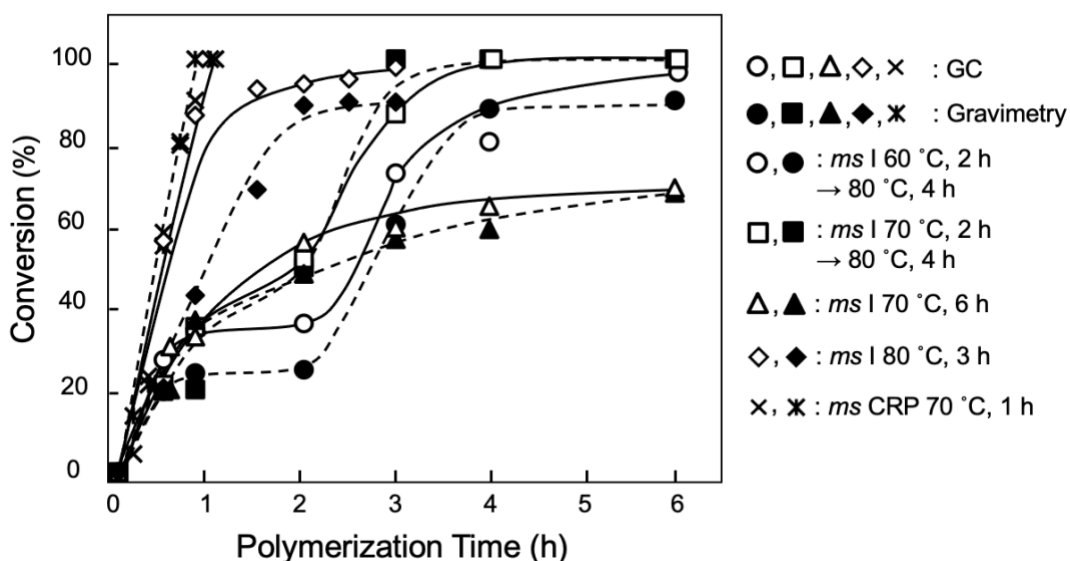
2.3.2 *ms* CRP and *ms* I with different temperature steps

As the simulation result shown, the recipe of *ms* ITP of MMA with the high BPO concentration

(8 wt% relative to monomer) was applied to MA as *ms* I under different temperature steps.

Figure 2. Conversion-time plots of *ms* I and microsuspension conventional radical polymerization (*ms* CRP) of MA at different temperature steps. The conversions were measured by GC (open symbols) and gravimetry (closed symbols).

Figure 2 shows conversion time plots of *ms* I and *ms* CRP of MA with different

temperature steps, where the conversion was measured by both GC ($\bigcirc$, $\square$, $\triangle$, $\diamondsuit$, $\times$) and

gravimetry ($\bullet$, $\blacksquare$, $\blacktriangle$, $\blacklozenge$, $\ast$) to enhance the credibility. *ms* CRP of MA at 70°C shown as

cross symbols ($\times$, $\ast$) was completed within 1 h and the appearance of dispersion showed

bluish white color as shown in Figure 3c and $\bar{D}_w$ of prepared particles was 137 nm as shown in

Figure 4e'. These indicate that emulsion polymerization proceeds based on homogenous

nucleation in the aqueous medium. In contrast, in the case of *ms* I at 70°C for 6 h ($\triangle$, $\blacktriangle$),

micrometer-sized particles were obtained as shown in Figure 4c, where the $\overline{D}_w$ was 31.7 μm.

This result supported the aforementioned idea and emphasized the RED effect would be

important at the beginning of the polymerization: The $R_p{}^w$ (less than 10% conversion) of MA

for polymerization with iodoform system was lower than that of MMA (Figure 1). When the

polymerization rate is relatively low, almost generated radicals (or propagating radicals) in the

monomer droplet would be able to be captured by diiodomethyl radicals or reacted with iodine

radicals resulting in the formation of iodinated chains (high insolubility in water). However, the

polymerization proceeded gently and attained around 60 % at 6 h, that is, the polymerization

rate of *ms* I slowed down in comparison with that of *ms* CRP at 70°C described above, which

should be unappealing in the industrial application. On the other hand, in the case of *ms* I under

80°C, although the polymerization completed within 3 h due to the higher propagation rate as

shown in Figure 2 (◇, ◆), synthesis of micrometer-sized particles was failed, where the $\overline{D}_w$

was 270 nm (Figure 4d').

Thus, *ms* I was undergoing a continuous two-step temperature process to realize both

suppression of byproduct and practical polymerization time.

The circle plots (○, ●) refer to *ms* I carried out under 60°C for 2 h followed by 80°C

for 4 h, while the square plots (□, ■) refer to *ms* I carried out under 70°C for 2 h with following

80°C for 4 h. The staged conversion among the two-step temperature process can be observed

based on the different polymerization rates under different temperatures.

Moreover, the retardation period, which can be recognized as the platform of circle (○,

●) and square (□, ■) plots, is attributed to the generation of iodine molecules and ions. According to the mechanism of polymerization with iodoform in the aqueous phase (Scheme 1), CHI$_3$ is easily disassociated to CHI$_2$• radical and iodine (I•) radical, which would react with propagating radical to generate an iodinated chain transfer agent (Polymer-I). However, there exists a competitive reaction in the early stage, which is similar to the reverse ITP (RITP)[6-9] process that the excess initiator radicals react with CHI$_3$ to form the R-I adducts. Afterwards, a small portion of iodine radicals released from the unstable R-I adducts tends to combine with others to form iodine molecules.[10] Due to the presence of water, iodine molecules can react with water to generate the anions (I$^-$, IO$^-$ and I$_3^-$).[11] There might be a possibility to form the complex of generated I$_3^-$ with PVA, which affects the kinetics of the polymerization.
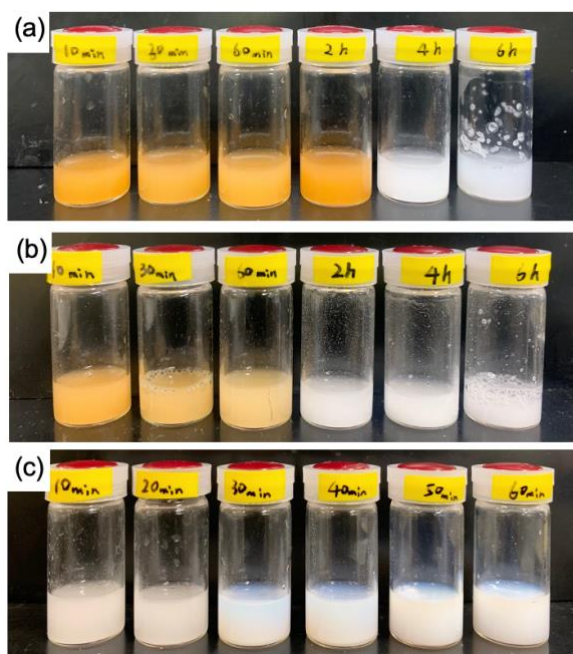

Figure 3. Time-dependent appearance of PMA dispersions prepared by *ms* I with different temperature steps [(a) 60°C, 2 h → 80°C, 4 h; (b) 70°C, 2 h → 80°C, 4 h], and by *ms* CRP (c) 70°C, 1 h.

However, the formation of the complex would be neglected because of the very low concentration of these anions.[12] Indeed, iodine molecules and triiodide (I_3^-) can be recognized as a characteristic orange color as shown in Figure 3(a, b). Subsequently, the generated iodine molecules would react with the propagating radicals to form Polymer-I, where the polymerization proceeds further as the degeneration transfer process (Scheme 1), resulting disappear of the color of iodine and triiodide (Figure 3).
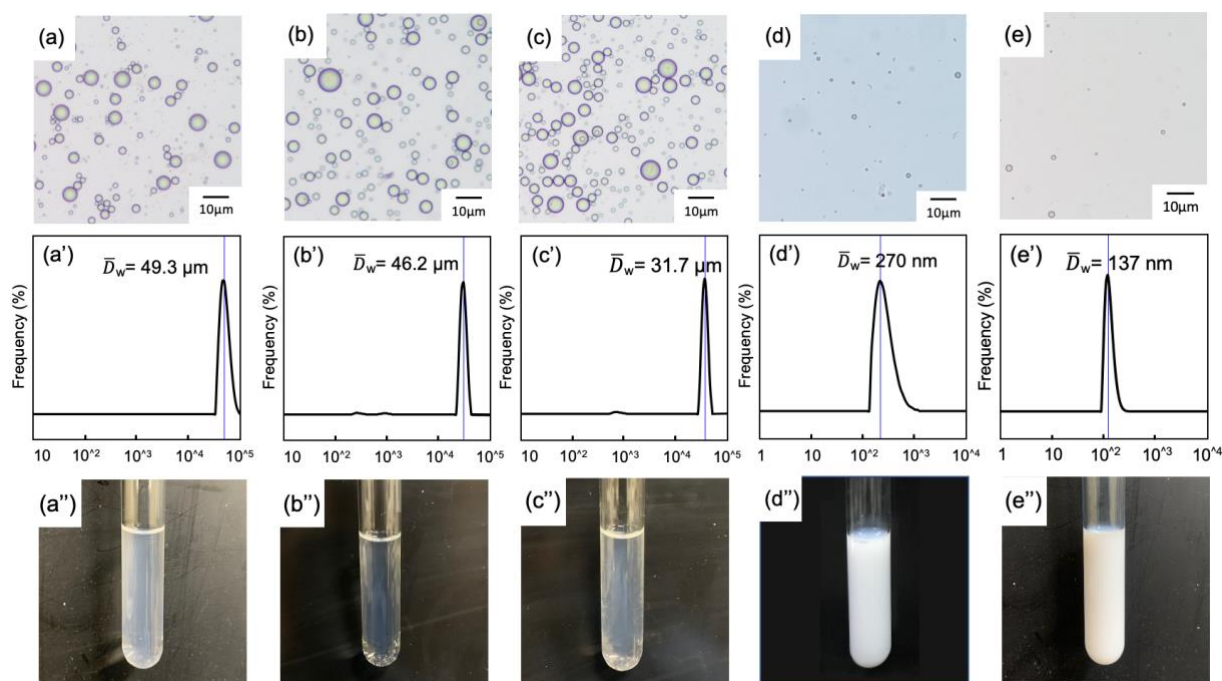
Figure 4. optical images (a-e), weight-average diameter (a'-e'), and digital photo images (a"-e") of supernatant after centrifugation at 5000 rpm for 15 min of PMA prepared by *ms* I with different temperature steps [(a-a") 60°C, 2 h → 80°C, 4 h; (b-b") 70°C, 2 h → 80°C, 4 h; (c-c") 70°C, 6 h; (d-d") 80°C, 3 h] and by *ms* CRP (e-e") 70°C, 1 h.

To confirm whether the two-step temperature polymerization successfully prepared the micrometer-sized particles without submicrometer-sized byproduct particles, optical images and DLS data were held up in Figure 4(a-e, a'-e') as evidence for particle size. While, Figure

4(a''-e'') shows the direct observation of the supernatant of PMA dispersion prepared at different temperatures, which was obtained after centrifugation. It is obvious that *ms* I underwent the lower temperature in the first stage obtained almost micrometer-sized particles (Figure 4(a-b, a'-b')) and showed the clearer supernatant after centrifugation (Figure 4(a'', b'')), indicating that the nucleation was almost restricted within the droplet. However, in the case of the [60°C, 2 h → 80°C, 4 h] process (Figure 4(a-a'')), the supernatant was slightly turbid indicating the formation of a few submicrometer-sized byproduct particles, which were also obvious from the number-average diameter ($\bar{D}_n$) as shown in Figure 5.
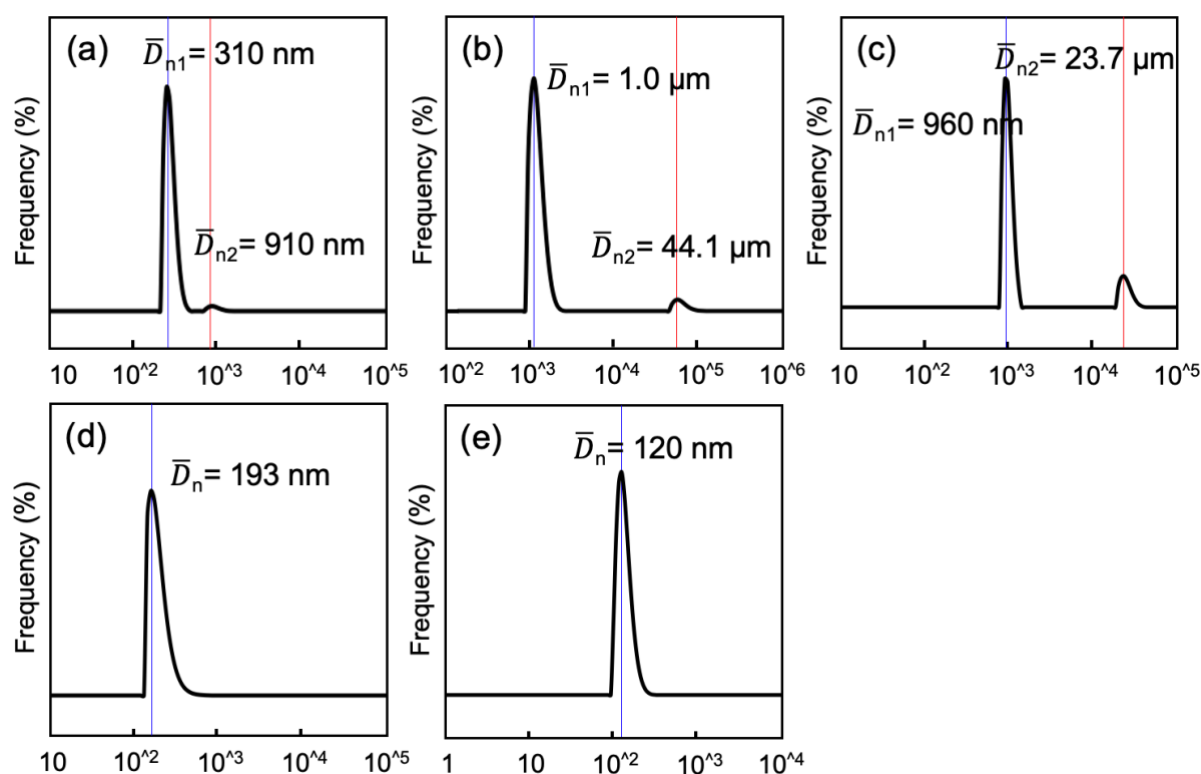

Figure 5. Number-average particle size (d_n) (a-e) of PMA particles prepared by *ms* I with different temperature steps [(a) 60°C, 2 h → 80°C, 4 h; (b) 70°C, 2 h → 80°C, 4 h; (c) 70°C, 6 h; (d) 80°C, 3 h], and by *ms* CRP (e) 70°C, 1 h.

It was because iodine radicals weren't consumed entirely during the 60°C first step, which can be proved by the appearances of *ms* I (orange color still remained even after 2 h at 60°C first step) (Figure 3b). In other words, the untrapped $P_1\bullet$, $P_3\bullet$, and $R\bullet$ radicals by iodine radical would have a chance to exit from MA monomer droplets. With the continual 80°C treatment, it results in a higher polymerization rate in the aqueous phase, which further causes submicrometer-sized byproduct particles. Meanwhile, in the [70°C, 2 h → 80°C, 4 h] process (Figure 4(b-b'')), the $\overline{D}_w$ was about 46.2 μm without submicrometer-sized byproduct and the appearance of supernatant was the clearest.

The M_n and M_w/M_n are shown in Figure 6. In *ms* CRP, the larger M_n (274,100) and broader M_w/M_n (6.07) (Figure 6, plot (d)) were displayed. In the case of *ms* I under 80°C for 6 h in our previous work,[4] the M_n and M_w/M_n of PMA decreased effectively, showing as 55,900 and 2.03 respectively (Figure 6, plot (c)). It is ascribed to the chain transfer behavior in the polymerization. However, it still accompanied by emulsion polymerization, leading to a large number of submicrometer-sized byproduct particles (Figure 4(d-d'')), which implied a large number of radicals existed in the aqueous phase during the initial stage even in *ms* I system at such high initial temperature. After applying the two-step temperature procedure to *ms* I, in the case of [60°C, 2 h → 80°C, 4 h] process, the board M_w/M_n (2.29) with a side peak (7×10^6) was observed (Figure 6, plot (a)), which refers to the generation of submicrometer-sized byproduct particles. While, in the case of *ms* I under [70°C, 2 h → 80°C, 4 h] process, the lower M_w/M_n (1.89) represents the depression of the submicrometer-sized byproduct particles (Figure 6, plot(b)).
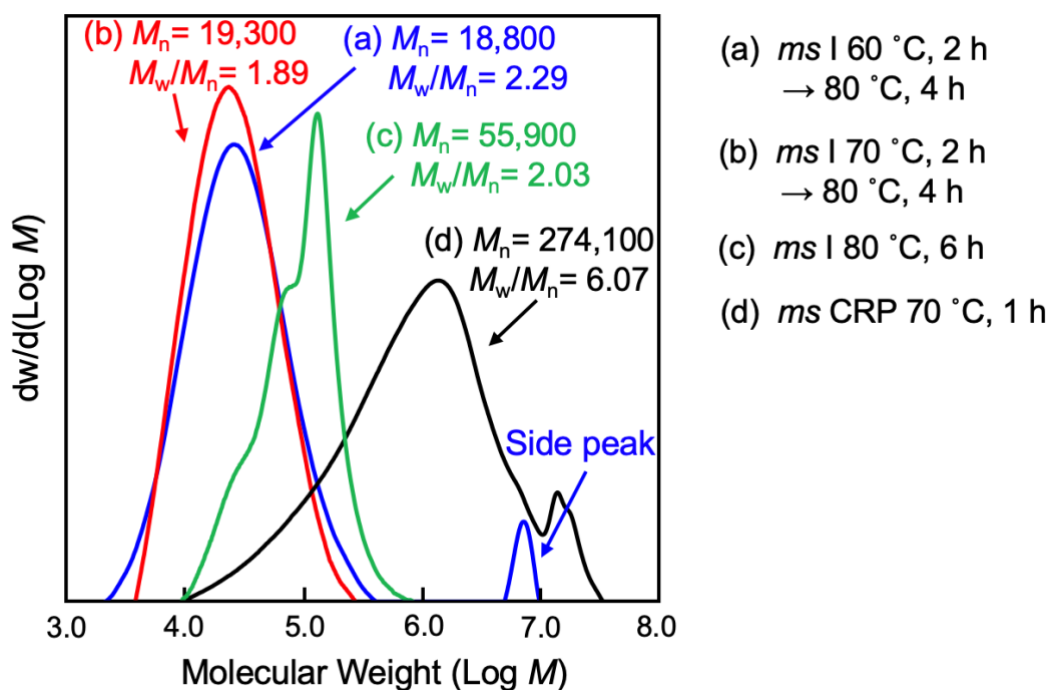
Figure 6. Number-average molecular weight (M_n) and molecular weight distribution (M_w/M_n) of PMA prepared by ms I with different temperature steps [(a) 60°C, 2 h → 80°C, 4 h; (b) 60°C, 2 h → 80°C, 4 h; (c) 80°C, 3 h], and by ms CRP (d) 70°C, 1 h.

As a conclusion, [70°C, 2 h → 80°C, 4 h] seems the best condition to prepare the micrometer-sized particles and maintain the high conversion.

2.3.3 *ms* I under the process of [70°C, 2 h → 80°C, 4 h]

Figure 7(a, b) shows M_n and M_w/M_n of PMA prepared by *ms* I [70°C, 2 h → 80°C, 4 h] at various conversions. The molecular weight distribution was slightly shifted to higher molecular weight with increasing conversion, however, the M_n doesn't match with $M_{n,th}$, that is, it doesn't behave in a good controlled/livingness manner. In the first step at 70°C, the molecular weights of PMA grew with conversion (15,500, 20 % → 18,100, 50 %), but much higher than the theoretical one. It can be ascribed to a lower chain transfer rate than the propagation rate at

70°C.[13-15] Moreover, the relatively high M_w/M_n in the range from 1.8 to 2 could be explained by this low chain transfer reaction. However, in the second temperature step at 80°C, M_n (19,300) nearly unchanged (Figure 7b), which was significantly lower than $M_{n,th}$. We assumed this behavior resulted from the fast termination reaction, that is, the degeneration chain transfer rate of Polymer-I was considerably lower than irreversible termination (coupling with excess R• or propagating chains). It was also considered as the reason for the low conversion of *ms* I of MA at 70°C for 6 h.

To verify the livingness of polymer chains, the chain extension of PMA-I with styrene was carried out in the bulk system. The molecular weight distribution and number distributions (plots of $w(\text{Log } M)/M^2$) of living chains were determined from GPC data, using RI and UV detector, as shown in Figure 7(c,d). Although the M_n after chain extension shifted to the higher molecular weight, the M_w/M_n also turned broader due to the relative polydispersity of PMA-I. However, the fraction of block copolymer chains containing polystyrene (PS) blocks was only 14.2%, which was calculated from the proportion of PMA-*b*-PS obtained by UV relative to all of the polymer chains obtained by RI, according to previous paper.[16] This low livingness should be based on that the polymer chains were ended with R• or MA by coupling reaction rather than I•.

Although *ms* I with temperature-step process showed the unideal controlled/livingness behavior, it is still acceptable when compared with the result of *ms* CRP. Significantly, the idea of this work is underlined that hydrophilic monomer, polymerization of MA can be efficiently

restricted within micrometer-sized droplets by using *ms* I, resulting in micrometer-sized particles without submicrometer-sized byproduct particles.
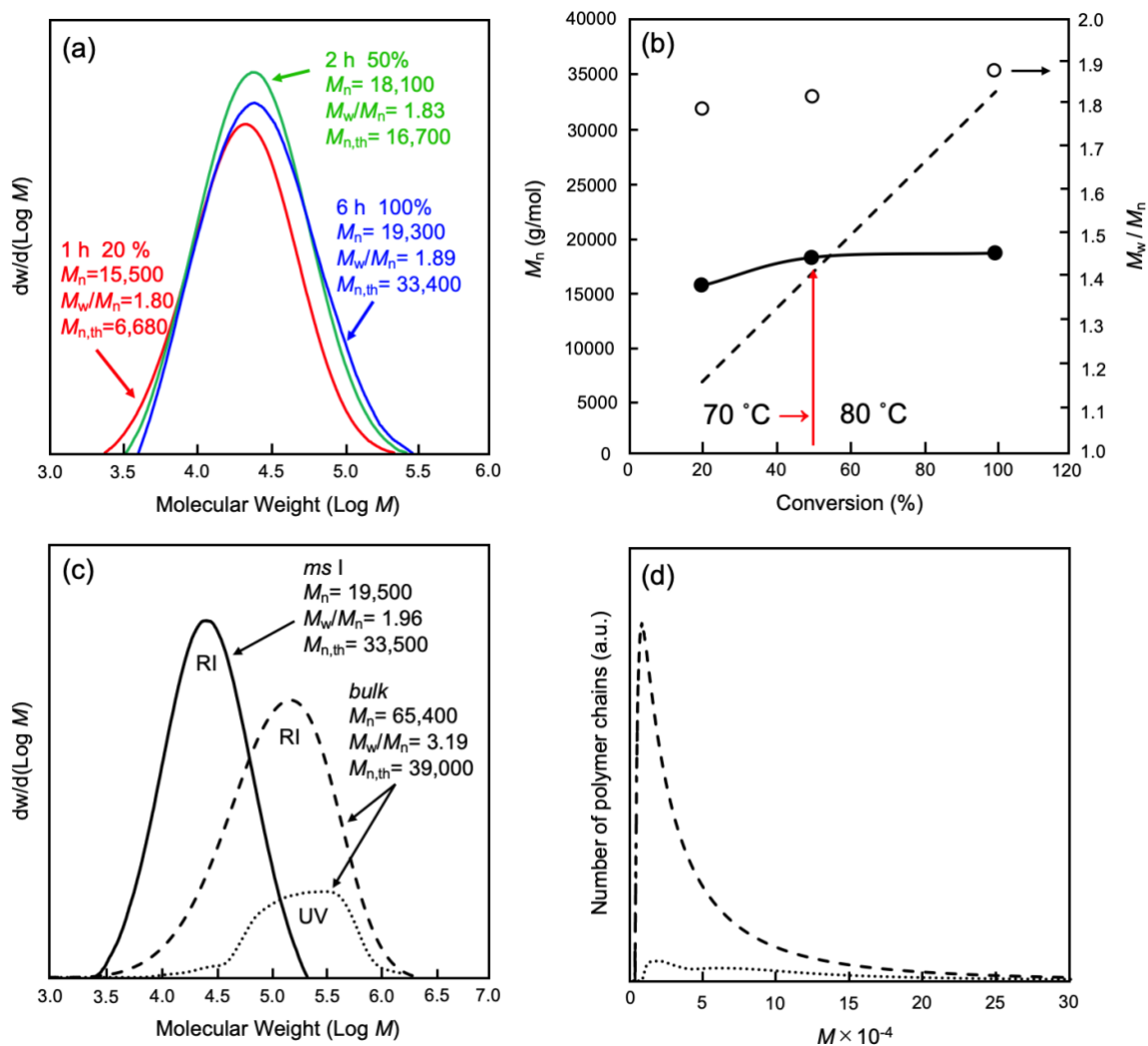

Figure 7. Evolution molecular weight distributions (a) and M_n (closed circle) and M_w/M_n (open circle) (b) of PMA prepared via *ms* I under 70°C for 2 h followed by 80°C for 4 h (inset redline refers to the temperature changing point). The dash line represents the theoretical molecular weight ($M_{n,th}$).

Molecular weight distributions (c) and number distributions (d) (based on GPC data with RI and UV detectors, Polystyrene-equivalent) of PMA prepared by *ms* I with [70°C, 2 h → 80°C, 4 h] process (solid line) and the obtained polymer after chain extension by bulk polymerization (70°C, 48 h) of styrene (RI, broken line; UV, dotted line).

2.4 Conclusions

The micrometer-sized PMA particles were successfully synthesized without submicrometer-sized byproduct particles by conveniently applying *ms* I with a two-step temperature process at a threshold content of BPO for the maximum industrial efficiency. By varying the pretreatment temperature, the number of oligomer radicals in the preliminary stage was controlled and captured in the oil droplets effectively. These experimental results were strongly supported the idea that only lowering the temperature in an early stage can decrease the number of exiting oligomer radicals (including initiator radicals), resulting in depression of homogenous nucleation in the aqueous medium. With the decrease in decomposition rate of BPO, there is sufficient chance for CHI_3 to react with oligomer radicals within oil droplets although *ms* I proceeded with limited control manner. Moreover, the two-step temperature process was able to complete the polymerization within practical polymerization time from the viewpoint of industrial applications.

2.5 References

1. D. Richon, A. Viallard, *Fluid Phase Equilib.*, **21** (3), 279-293 (1985)

2. J. K. Guillory, *J. Med. Chem.*, **46** (19), 4213-4213 (2003)

3. P. Chaiyasat, S. Namwong, M. Okubo, A. Chaiyasat, *RSC Adv.*, **6** (97), 95062-95066 (2016)

4. C. Huang, N. Yamashita, A. Chaiyasat, X. Liu, M. Okubo, *Polymer*, **154**, 128-134 (2018)

5. M. Okubo, Y. Kitayama, N. Yamashita, X. Liu, C. Huang, *Macromol. Theory Simul.*, **27** (5), 1800029 (2018)

6. C. Boyer, P. Lacroix-Desmazes, J. J. Robin, B. Boutevin, *Macromolecules*, **39** (12), 4044-4053 (2006)

7. J. Hui, Y. Shi, T. Li, J. Wu, Z. Fu, *RSC Adv.*, **5** (55), 44326-44335 (2015)

8. P. Lacroix-Desmazes, R. Severac, B. Boutevin, *Macromolecules*, **38** (15), 6299-6309 (2005)

9. J. Gu, X. Yan, Z. Fu, W. Yang, Y. Shi, *J. Appl. Polym. Sci.*, **128** (4), 2291-2296 (2013)

10. X. Liu, L. Zhang, Z. Cheng, X. Zhu, *Polym. Chem.*, **7** (21), 3576-3588 (2016)

11. J. Tonnar, P. Lacroix-Desmazes, B. Boutevin, *Macromolecules*, **40** (2), 186-190 (2007)

12. K. Tashiro, H. Kitai, S. M. Saharin, A. Shimazu, T. Itou, *Macromolecules*, **48** (7), 2138-2148 (2015)

13. I. P. Kim, E. I. Kats, V. A. Benderskii, *High Energy Chem.*, **53** (4), 265-275 (2019)

14. J. P. Xinrui Yu, and Linda J. Broadbelt, *J. Phys. Chem. A*, **112**, 6772–6782 (2008)

15. C. Barner-Kowollik, S. Beuermann, M. Buback, P. Castignolles, B. Charleux, M. L. Coote, R. A. Hutchinson, T. Junkers, I. Lacík, G. T. Russell, M. Stach, A. M. van Herk, *Polym. Chem.*, **5** (1), 204-212 (2014)

16. R. McHale, F. Aldabbagh, P. B. Zetterlund, H. Minami, M. Okubo, *Macromolecules*, **39** (20), 6853-6860 (2006)

Chapter 3

Synthesis of micrometer-sized poly(vinyl acetate) particles through microsuspension iodine transfer polymerization: : effect of iodine species in a water medium

3.1 Introduction

Vinyl acetate (VAc), besides as a monomer possessing high water solubility (solubility in water: 2.5 g/100 mL at 25°C),[1] is also an important monomer, whose corresponding polymer, poly(vinyl acetate) (PVAc), has a wide range of industrial uses. As one of its main applications, the hydrolysis of PVAc produces poly(vinyl alcohol) (PVA), which is attractive in the chemistry and biology fields because of fascinating properties such as low toxicity, high hydrophilicity, adhesivity, biodegradation, and biocompatibility.[2, 3] The performance of PVA or PVA-based materials is strongly influenced by their molecular weight and molecular weight distribution. Therefore, the synthesis of PVAc with desirable molecular weight and molecular weight distribution is of great significance for further development of its potential applications.

Although the synthesis of PVAc through RDRP has been achieved to meet the emerging demands,[4] the high reactivity of VAc (unconjugated monomer) radicals makes the polymerization more difficult to control than that of (meth)acrylates and styrene, which are conjugated monomers.[5] Specifically, the highly active propagating radicals of VAc easily

undergo combination termination, degradation,[6, 7] and chain transfer to the methine or the methyl groups on the polymer.[8-10] Owing to this drawback, the most widely used RDRP method to polymerize VAc is reversible addition-fragmentation chain-transfer (RAFT) polymerization,[11, 12] which is tolerant toward unprotected functional groups. Meanwhile, only a few reports have described the use of ITP to prepare PVAc,[5, 13, 14] mainly focusing on homogenous systems, with only one example reported by Lacroix-Desmazes et al. using a miniemulsion system.[5] When employing a hydrophilic monomer in a suspension or microsuspension system, the initiator or oligomeric radicals generated in the monomer droplets can easily exit from the droplets to the aqueous medium, resulting in the formation of submicrometer-sized byproduct particles through emulsion polymerization,[15-18] which hinders the control of the molecular weight and molecular weight distribution in RDRP. Therefore, the synthesis of micrometer-sized particles through microsuspension polymerization of VAc without obtaining submicrometer-sized particles as a byproduct is challenging.

In the Chapter 2,[19] it mentioned that improved result was obtained in aqueous microsuspension iodine transfer polymerization (*ms* ITP) of methyl acrylate (MA) using iodoform (CHI_3) as a chain transfer agent. The success of this reaction lies on the radical exit depression (RED) effect, according to which the capture of the monomer and oligomer radicals by the highly hydrophobic diiodomethyl group from CHI_3 inhibits their transfer from the monomer droplets to the aqueous phase.

Following this line of work, *ms* ITP is employed in this chapter to obtain micrometer-sized PVAc particles. To the best of our knowledge, this is also the first trial on the

polymerization of VAc through ITP in a microsuspension system. In this chapter, the polymerization condition and the mechanism, including the kinetics of *ms* ITP of VAc, are analyzed by taking the effect of temperature and iodine species into account. Moreover, the preparation of well-defined PVA with narrow molecular weight distribution by subjecting *ms* ITP-obtained PVAc to alcoholysis is demonstrated.

3.2 Experimental

3.2.1 Materials

VAc (Nacalai Tesque, Inc. Kyoto, Japan; stabilizer: hydroquinone 5 ppm) and MMA (Nacalai Tesque, Inc., Kyoto, Japan) were purified by passing it through a column packed with basic aluminum oxide (Alumina Activated 200, Nacalai Tesque, Inc. Kyoto, Japan). CHI_3 of analytical grade (Nacalai Tesque, Inc., Kyoto, Japan; purity, 99%), PVA (GH-17, Nippon Synthetic Chemical Industry Co., Ltd, Osaka, Japan; degree of saponification, 86.5% − 89%; molecular weight, 7×10^4), 2,2′-azobis(2-methylpropionitrile) (AIBN; Nacalai Tesque, Inc., Kyoto, Japan; purity ≥ 98.0%), 2,2'-azobis(4-methoxy-2,4-dimethylvaleronitrile) (V-70; Fujifilm Wako Pure Chemical Co., Osaka, Japan; purity ≥ 95.0%), sodium hydroxide (NaOH; Nacalai Tesque, Inc., Kyoto, Japan; purity ≥ 97.0%), *N,N*-dimethylformamide (DMF; Nacalai Tesque, Inc., Kyoto, Japan; purity ≥ 99.0%), *N,N*-dimethylacetamide (DMAC; Nacalai Tesque, Inc., Kyoto, Japan; purity ≥ 98.0%), and methanol (MeOH; Nacalai Tesque, Inc., Kyoto, Japan; purity ≥ 99.8%) were used as received. Deionized water used was obtained using a water purification machine (Elix UV, Millipore Co., Ltd., Japan) and had a resistivity of 15 MΩ cm.

3.2.2. Synthesis of PVAc particles in a microsuspension system

PVAc particles were synthesized using *ms* ITP and microsuspension conventional radical polymerization (*ms* CRP). V-70 (0.03 g) and CHI$_3$ (0.036 g, only for ITP) were dissolved in VAc (3 g) in a molar ratio of [VAc]:[V-70]:[CHI$_3$] = 381:1.06:1, and the mixture was poured into an aqueous phase consisting of a 1 wt% PVA aqueous solution (27 g). After homogenizing for 5 min using a homogenizer at 3,700 rpm, a monomer dispersion was obtained. Subsequently, the monomer dispersion was evenly divided into eight glass tubes, which were sealed off after being degassed five times with vacuum/N$_2$ gas cycles. Finally, both *ms* ITP and *ms* CRP were conducted at 30°C for 24 h. In all the polymerizations, the sealed tubes were placed in a water bath with a horizontal shaking rate of 120 rpm. The polymers were collected after being centrifuged three times with water and freeze-dried overnight.

3.2.3 Dispersion ITP for chain extension

Chain extension was conducted through dispersion ITP with MMA using the PVAc, which was synthesized by *ms* ITP, as a macro chain transfer agent. Briefly, the washed PVAc dispersion (0.05 g in 0.15 g water), MMA (0.099 g), and V-70 (0.0009 g) (molar ratio [MMA]:[V-70]:[PVAc] = 350:1.02:1) were dissolved in Methanol (1.2 g), and the solution was added to a glass tube. After degassing five times with vacuum/N$_2$ gas cycles, the glass tube was sealed off under vacuum. The polymerization was performed at 30°C for 24 h with a horizontal shaking rate of 80 rpm.

3.2.4 Alcoholysis of PVAc

The PVAc for alcoholysis was collected after being centrifuged five times with deionized water to remove the excess amount of PVA and freeze-dried overnight. The washed PVAc (0.15 g) was dissolved in MeOH (5 g) in a 20 mL vial. Then, 2 g of an MeOH solution containing NaOH (2.5 mol% relative to ester groups) was poured into the PVAc solution. After sealing the vial with a polytetrafluoroethylene tape, the alcoholysis reaction was conducted at 50°C for 30 min with magnetic stirring (400 rpm). The precipitated product was collected, washed three times with methanol, and then dried under vacuum overnight at room temperature.

3.2.5. Characterization

The monomer conversions were measured using gravimetry. The remaining percentage of CHI_3 and the conversion in the bulk system were determined by gas chromatography. The appearance of latex prepared at high temperature before and after dissolving in DMF, the appearance of the dispersion at each conversion, the appearance of the *ms* ITP mixture after 18 h polymerization and the *ms* CRP mixture after 8 h polymerization, and the upper layer of the final dispersion after centrifugation at a speed of 5,000 rpm for 10 min, where the micrometer-sized particles sedimented out and the submicrometer-sized particles were still dispersed in the aqueous medium, were observed with naked eyes. The percentage of submicrometer-sized byproduct particles was calculated using the equation $\left(\frac{\text{Weighted amount} \times \text{Solid content of supernatant after centrifugation}}{\text{monomer content in the weighted amount} \times \text{Conversion}} \right)$ after measurement of the solid content of the supernatant using gravimetry. The particles were observed utilizing an optical

microscope (OM, ECLIPSE 80i, Nikon). The weight-average diameters ($\bar{D}_w$) of the particles

were measured using dynamic light scattering (DLS; FPAR-1000RK, OTSUKA

ELECTRONICS Co., LTD). Weight-average and number-average molecular weights (M_w and

M_n, respectively), molecular weight distribution (M_w/M_n), and number distributions (plots of

w(Log M)/M^2) were determined using gel permeation chromatography (GPC) using two

methacrylate gel columns (TOSOH Corporation, TSK gel α 5000, 7.8 mm i.d $\times$ 30 cm,

separation range per column: approximately $50 - 7 \times 10^6$ g/mol (exclusion limit) using DMF

as an eluent for PVAc at 40°C, and a flow rate of 1.0 mL/min. TSK gel GMPWXL using water

as an eluent for PVA at 35°C and a flow rate of 0.8 mL/min) employing a refractive index (RI)

detector (TOSOH RI-8020/21). The columns were calibrated with seven standard polystyrene

samples for DMF ($1.11 \times 10^3 - 5.48 \times 10^6$, $M_w/M_n = 1.01 - 1.07$) and seven standard

polyethylene oxide/glycol samples for water ($585 - 1.24 \times 10^6$, $M_w/M_n = 1.02 - 1.21$). The

fraction of living chains was calculated according to the proportion of blocked polymers

obtained by ultraviolet (UV) detection relative to all of the polymer chains obtained by RI

($\frac{Blocked\ polymer\ chains\ (UV)}{All\ polymer\ chains\ (RI)}$), according to the previous paper.[20] The characteristic substituents

of PVAc and PVA were determined by fourier transform infrared spectrometer (FTIR; FT/IR-

6200, Jasco, Inc.).

3.3 Results and discussion

3.3.1 *ms* ITP of VAc initiated with AIBN at 60°C

In the early stage of the microsuspension polymerization, the water-soluble primary species

(oligomeric radicals) trigger the formation of submicrometer-sized byproduct particles. Specifically, for hydrophilic monomers, some amount of the oil-soluble initiator and oligomeric radicals generated inside the oil droplets can easily exit to the aqueous medium, which work as the loci of emulsion polymerization. These soluble oligomers have a certain number of maximum monomer units, which can be calculated utilizing the hydrophobic free energy (Table4, Chapter 1). The polymerization rate in the aqueous phase (R_p^w) is one of the key points that should to be maintained as low as possible to hamper the formation of submicrometer-sized byproduct particles, as discussed in Chapter 1. The R_p^w can be reduced by increasing the hydrophobicity and decreasing the number of primary species (initiator and oligomeric radicals) in the early stages of the polymerization.[19, 21] Therefore, in this work, AIBN (water solubility: 0.40 g/L, 20°C),[22] whose water solubility is approximately one-third that of benzoyl peroxide (BPO; water solubility: 1.27 g/L, 20°C),[23] was used, and the amount of initiator was decreased to 1 wt% relative to the monomer.

The result of the simulation of the R_p^w of VAc at 60°C is illustrated in Figure 1. The chemical structures of the $P_1\bullet$, $P_3\bullet$, and $R\bullet$ radicals, which refer to PVAc oligomer radicals containing an initiator fragment or a vinyl group as the end group and initiator radicals, respectively, are shown on the right-hand side of Figure 1.

It should be noted that the initiator fragment of $P_1\bullet$ and $R\bullet$ are altered with the change of initiator used. These are the main radicals that were considered to exit from the monomer droplets and form the nucleus of the byproduct particles in the aqueous medium. In contrast, the $P_2\bullet$ radical, which is attached to a diiodomethyl group, has high hydrophobicity due to the

iodine group, resulting in a good RED effect. This simulation was performed under the assumption in Chapter 1, that all amount of the water-soluble monomeric radicals: $P_1\bullet$, $P_3\bullet$, and $R\bullet$ radicals equal to their saturated water solubility. Therotically, a high R_p^w value indicates that the micrometer-sized particles are difficult to obtain without submicrometer-sized byproduct particles. The black line represents the successful synthesis of micrometer-sized poly(methyl acrylate) (PMA) particles without submicrometer-sized byproduct particles under the threshold condition of 8 wt% BPO (relative to MA) as an initiator for 2 h of pretreatment at 70°C.[19] At the early stage of the polymerization, a lower R_p^w was observed for VAc than those for MA.
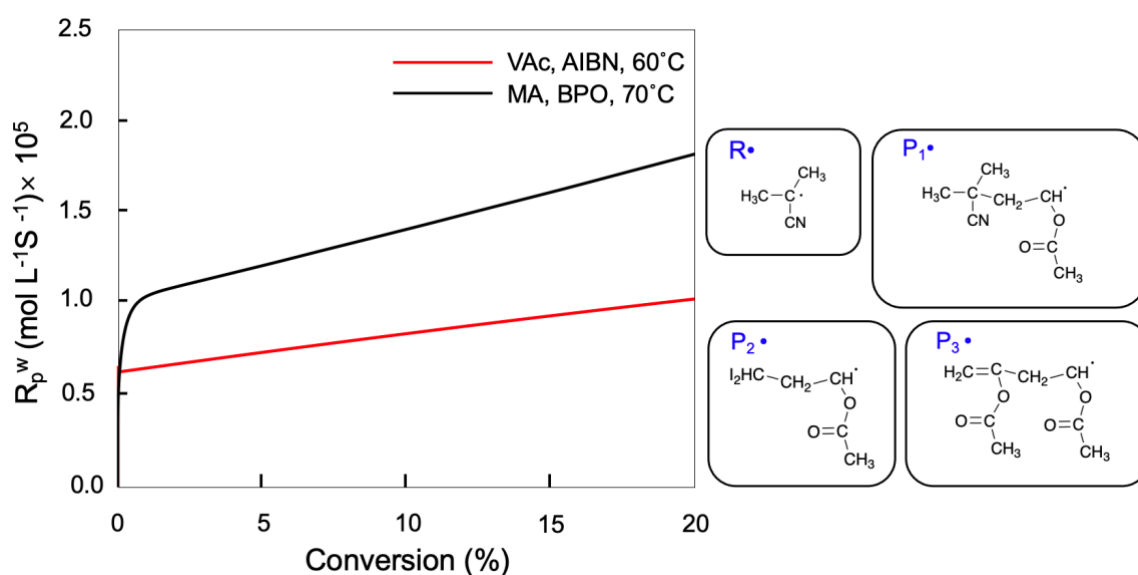
Figure 1. Relationships between the conversion and the polymerization rate in the aqueous phase (R_p^w) simulated in the *ms* ITP of VAc (red line) using 1 wt% AIBN (relative to VAc) as an initiator at 60°C and MA (black line) using 8 wt% benzoyl peroxide (BPO; relative to MA) as an initiator at 70°C, assuming that the same number of $P_1\bullet$, $P_3\bullet$, and $R\bullet$ radicals within monomer droplets exist in the aqueous media.

According to the simulation, the *ms* ITP of VAc under the condition of 1 wt% AIBN as the initiator at 60°C would proceed easier than that of MA to obtain exclusively micrometer-

sized particles. However, the application of this theoretical condition was not satisfactory experimentally. After 2 h of polymerization, the suspension became unstable, and coagulation was observed, as illustrated in Figure 2(a). Moreover, the obtained PVAc had a crosslinking structure. The dried coagulation (0.06 g) was dipped in 5 g DMF (good solvent for PVAc) and allowed to stand for 24 h, however, the coagulation was hardly dissolved and only swelled in DMF (Figure 2(b,c)). A gravimetric analysis revealed that almost no coagulation was dissolved (0.05 g/0.06 g); this could be ascribed to the side reactions depicted in Scheme 1.
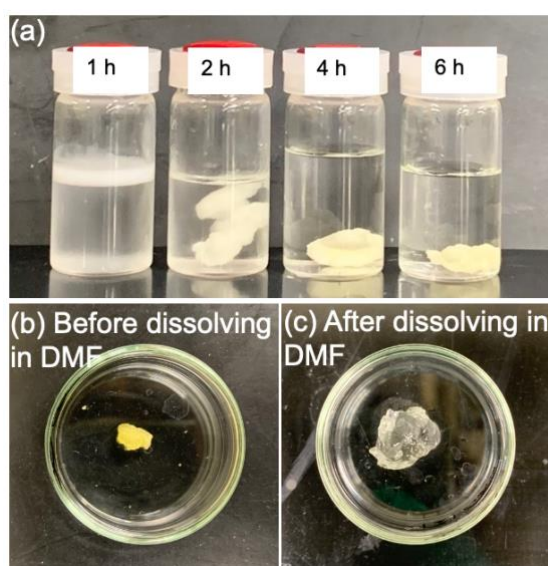

Figure 2. Time-dependent appearance of PVAc dispersions prepared by *ms* ITP using AIBN as initiator at 60°C (a), and the appearance of PVAc coagulation before (b) and after (c) dissolving in DMF for 24 h.

Abdollahi et al. reported that in a bulk system, poly(vinyl acetate) with an iodine end group (PVAc-I) was very sensitive to humidity.[7] As described in Scheme 1, a portion of the living chains having an iodide end group is inevitably degraded into aldehyde, hydroiodic acid (HI), and acetic acid due to the reaction with water at high temperature (Scheme 1(a)). The

resulting side product, PVAc having an aldehyde end group, produces a double bond between

the carbonyl group at α and ß positions and acetic acid through an aldol reaction (Scheme 1(c)).

Moreover, an increase in the reaction temperature was found to not only accelerate the side

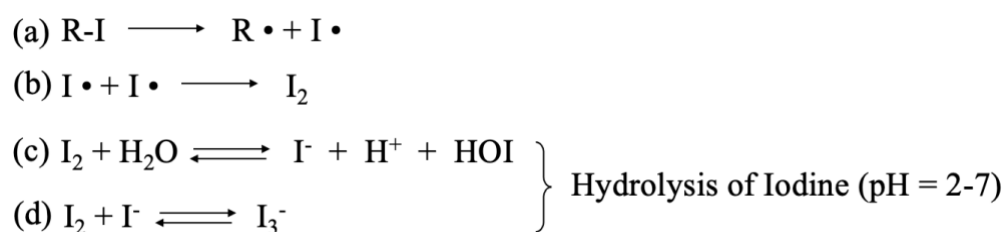reaction, but also increase the percentage of degradation and olefination.
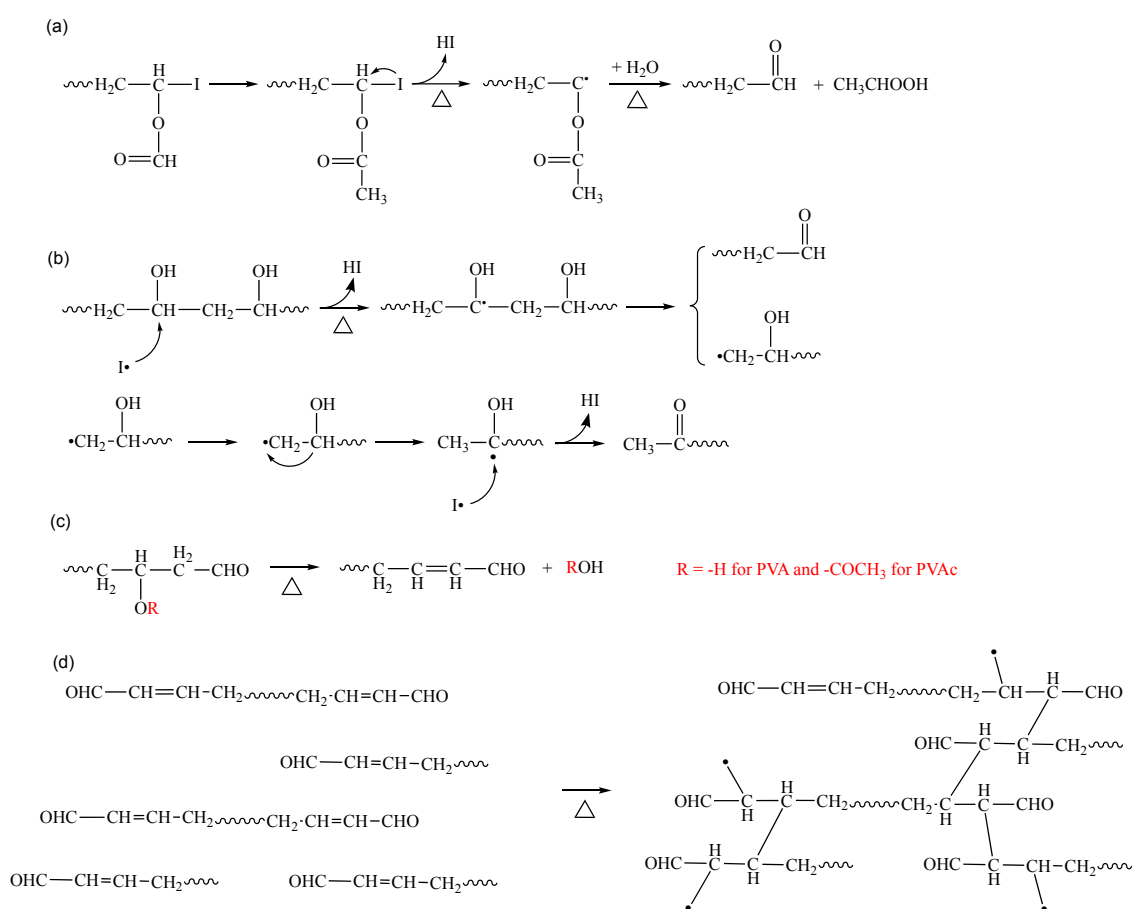
Scheme 1. (a) Degradation of iodide-terminated PVAc chains, (b) degradation of PVA dispersant in the presence of free iodine radicals, (c) aldol reaction of aldehyde-terminated polymers, and (d) crosslinking reaction between aldol-condensed polymers.

Meanwhile, PVA also tends to be oxidized by iodine radicals at high temperature.[24, 25]

Although the hydrolysis of PVAc carried out with a acid catalyst in a pure water system is

inhibited,[26] the PVA dispersant was regarded as one of the reasons for the side reactions, in

which the high amount of hydroxyl groups (–OH) of PVA dispersant relative to iodine groups

(–I) existed. A portion of PVA is degraded into ketone and aldehyde specimens by reacting with

free iodine radicals (Scheme 1(b)). This reaction is further promoted by HI, which is generated

from the degradation of PVAc-I and the hydrolysis of iodine molecules (Scheme 2). Afterwards,

the double bonds are formed through aldol reactions as describe above. These double bonds can

react with other double bonds in PVA or PVAc, resulting in the formation of a crosslinking

structure (Scheme 1(d)) and coagulation.

(a) $R\text{-}I \longrightarrow R\cdot + I\cdot$

(b) $I\cdot + I\cdot \longrightarrow I_2$

(c) $I_2 + H_2O \rightleftharpoons I^- + H^+ + HOI$

(d) $I_2 + I^- \rightleftharpoons I_3^-$

$\left.\right\}$ Hydrolysis of Iodine (pH = 2-7)

Scheme 2. General reaction of the generation of iodine species in the polymerization.

These results suggest that the polymerization of VAc is difficult to accomplish through

ITP in the presence of water at high temperature. Therefore, the polymerization must be

performed at low temperature to minimize the side reactions. The *ms* ITP of VAc was

subsequently studied at low temperature in detail, by replacing AIBN with V-70 as the initiator.

3.3.2 *ms* ITP of VAc initiated with V-70

As mentioned, the R_p^w is an important indicator of the occurrence of homogeneous nucleation

in a polymerization system. The simulation results of the R_p^w of the polymerization using CHI_3

as a chain transfer agent and V-70 as an initiator at various polymerization temperatures from

30 to 50°C are provided in Figure 3. A comparison between the R_p^w plots of VAc and that of

MA revealed the temperature should be equal to or lower than 40°C. Considering the side

reactions and the practical condition, 30°C was selected as the appropriate temperature to

prepare the micrometer-sized PVAc particles. The amount of initiator was maintained as 1 wt%

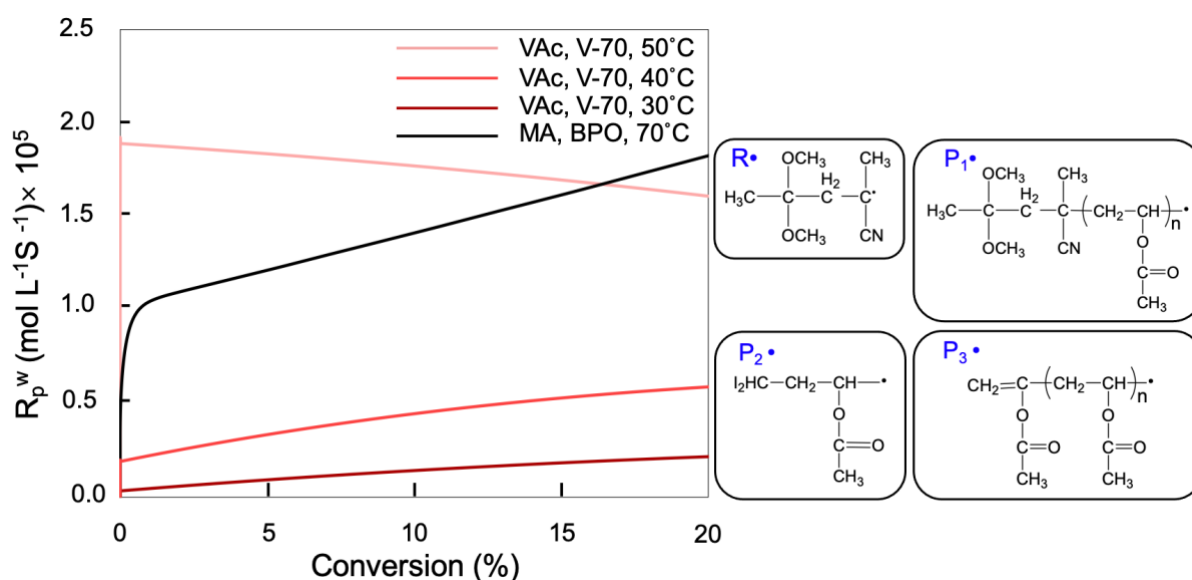relative to monomer for an appropriate polymerization time, which meets the demand of the

industry.

Figure 3. Relationships between the conversion and the polymerization rate in the aqueous phase (R_p^w) simulated in the *ms* ITP of VAc using 1 wt% V-70 (relative to VAc) as an initiator at various temperatures (colored lines) and MA (black line) using 8 wt% benzoyl peroxide (BPO; relative to MA) as an initiator at 70°C, assuming that the same number of $P_1\bullet$, $P_3\bullet$, and $R\bullet$ radicals within monomer droplets exist in the aqueous media.

Unlike the situation at 60°C, the polymerization system was stable at 30°C. Figure 4

presents optical images and weight-average particle size distributions of PVAc particles

prepared using *ms* ITP and *ms* CRP, respectively, at 30°C for 24 h. Only micrometer-sized

particles were observed in the *ms* ITP system at 30°C, whereas in the *ms* CRP of VAc, the

obtained micrometer-sized particles were accompanied by submicrometer-sized particles, indicating that homogeneous nucleation occurred.
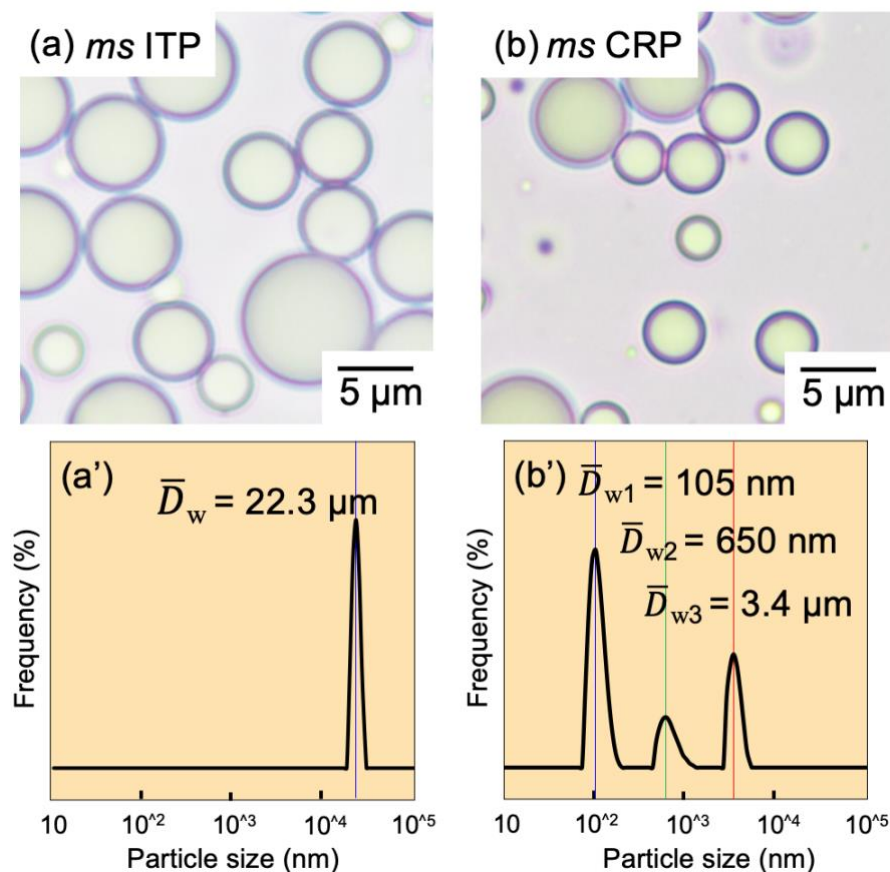

Figure 4. Optical images (a, b) and weight-average particle sizes (a', b') of poly(vinyl acetate) particles prepared by *ms* ITP (a, a') and *ms* CRP (b, b') using V-70 as the initiator.

The content of byproducts in the case of *ms* ITP was only 1%, and the supernatant was clear after centrifuging, whereas *ms* CRP afforded 43% of submicrometer-sized byproducts and a bluish supernatant (Figure 5). These results demonstrate that micrometer-sized PVAc particles without submicrometer-sized byproduct particles can be successfully synthesized through *ms* ITP using V-70 as an initiator at 30°C. This is because the low polymerization temperature results in a lower propagation rate, which leads to not only a decrease in the generation rate and

number of hydrosoluble oligomer radicals in the early stage but also a minimization of the side reactions. The capture of these radicals by hydrophobic diiodomethyl groups restricts the release of primary radicals from the oil droplets to the aqueous phase.
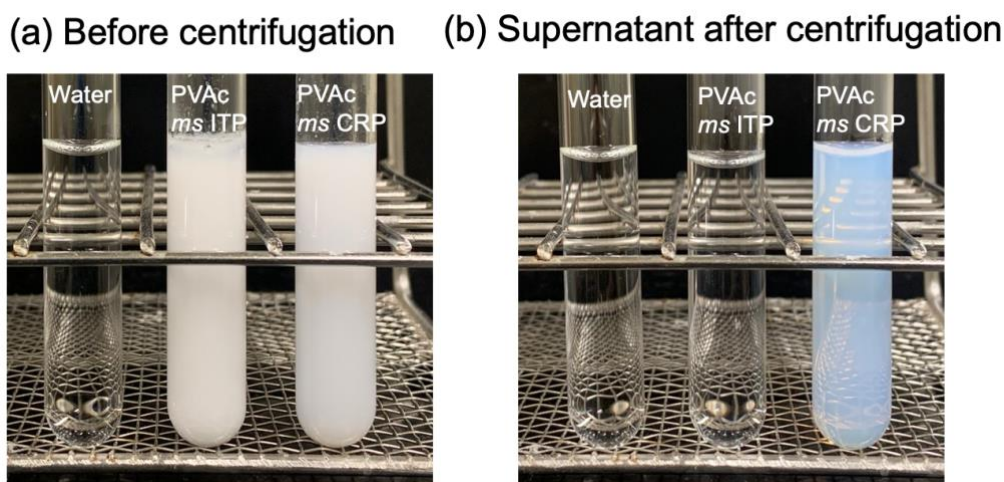

Figure 5. Appearance of PVAc prepared by *ms* ITP and *ms* CRP at 30°C (a) before centrifugation and (b) after centrifugation. Deionized water is shown for comparison.
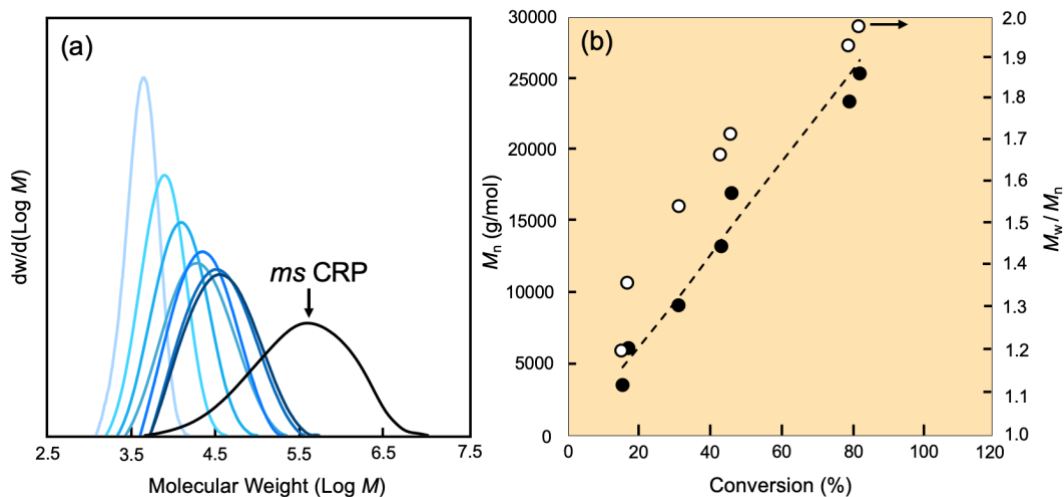

Figure 6. (a) Evolution of the molecular weight of PVAc obtained by *ms* ITP (colored lines) and *ms* CRP (black line) using V-70 as an initiator at 30°C for 24 h and 6 h, respectively. (b) Evolution of the molecular weight (closed circle ●), theoretical molecular weight (dash line), and molecular weight distribution (open circle ○) vs. monomer conversion of PVAc obtained by *ms* ITP at 30°C for 24 h.

To clarify the *ms* ITP of VAc proceeds with control/livingness, the M_n, theoretical molecular weight ($M_{n,th}$), and M_w/M_n of PVAc prepared using both *ms* ITP and *ms* CRP were estimated by GPC analysis as illustrated in Figure 6 and Table 1.

In *ms* CRP, the M_n and M_w/M_n values of PVAc particles were 1.2×10^5 and 5.08, respectively, which indicate that the polymerization proceeds in an uncontrolled manner. Meanwhile, in the case of *ms* ITP, M_n decreased considerably to 26,000, which is consistent with the $M_{n,th}$ (26,900), although the M_w/M_n value were relatively broad (2.00). Moreover, a linear relationship was observed between M_n and the monomer conversion, indicating the controlled behavior of the polymerization. However, the control of the *ms* ITP of VAc became poor with increasing M_n.

Table 1. Evolution molecular weight, theoretical molecular weight, and molecular weight distribution of PVAc.

	Time (h)	Conversion (%)	M_n (g/mol)	$M_{n,th}$ (g/mol)	M_w/M_n
ms ITP	4	14.9	3,700	4,900	1.19
	8	16.5	6,300	5,400	1.36
	12	42.9	13,600	14,000	1.68
	18	79.4	24,000	25,900	1.95
	24	82.2	26,000	26,900	2.00
ms CRP	6	48.4	122,600	—	5.08

In addition, after subjecting the obtained PVAc to chain extension through dispersion ITP with MMA, the main M_n peak of polymer after chain extension slightly shifted to the higher M_n. Meanwhile, the M_n detected by UV detector, which response from iodine end group, should

be M_n of living polymer. The M_n shifted to higher M_n and the value overlapped with the main

peak detected by RI (Figure 7(a, b)). Moreover, the side peak appeared at higher M_n (495,000)

after chain extension was the polymer subjected to the free radical polymerization. From the

number distribution data (Figure 7(c)), only 11.8% fraction of the block copolymer was

obtained after chain extension (Figure 7(c)). These phenomena indicates that the PVAc chains

with high M_n lost livingness. These results can be attributed not only to the transformation of

the iodine end group to an aldehyde end group (Scheme 1(a)) but also to the unequilibrium of

the different iodine species between the different phases (at the interface of the monomer droplet

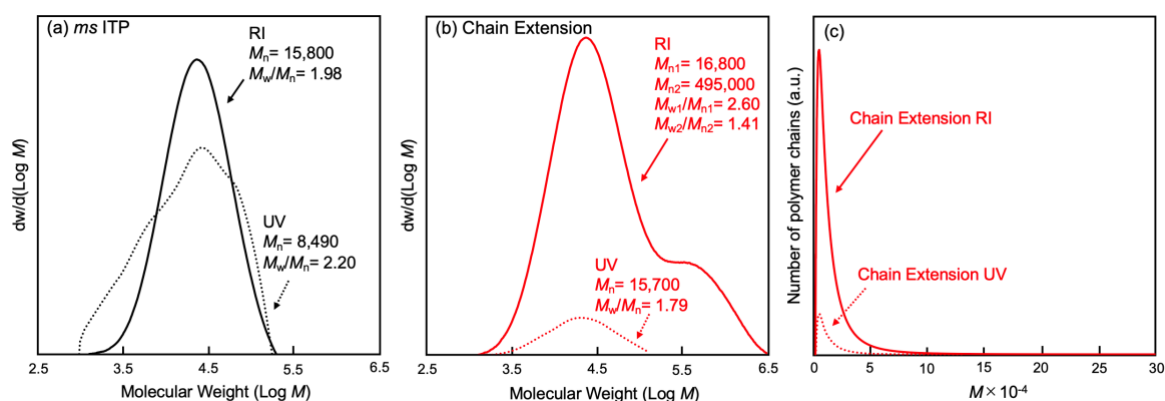and the aqueous phase) in the aqueous system, which is discussed below.

Figure 7. Molecular weight distributions of PVAc prepared by *ms* ITP (a) and the obtained
Polymer after chain extension ITP in dispersion (b), and number distributions of the obtained
polymer after chain extension ITP in dispersion (c). (RI, solid line; UV, dash line).

3.3.3 Effect of iodine species

Next, the kinetics of the polymerization was studied to understand the ITP behavior in an
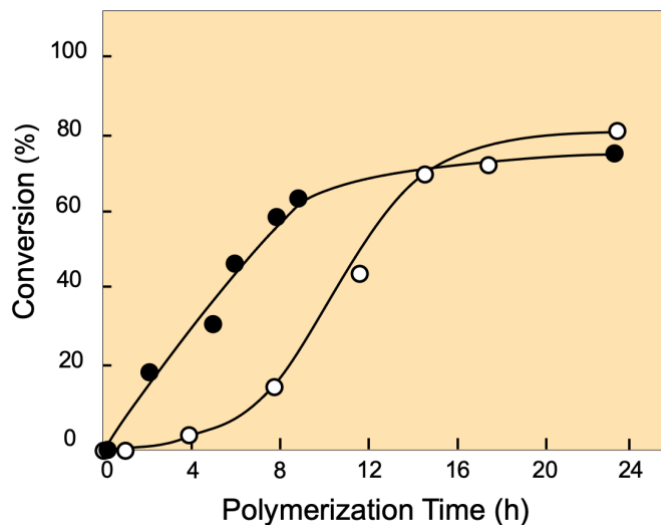
aqueous heterogeneous system.

Figure 8. Time conversion plots of PVAc prepared by *ms* ITP (open circle ○) and *ms* CRP (closed circle ●) measured by gravimetry.

Figure 8 shows the conversion time plots of both *ms* ITP and *ms* CRP of VAc with V-70 as an initiator at 30°C. When compared with the kinetic plot of *ms* CRP, the polymerization rate of *ms* ITP was found to be slower within the first 8 h, and an induction period appeared within the first 1 h, which cannot be explained simply by the general ITP reaction. At this stage, a side reaction involving iodine species occurs in the microsuspension system (Scheme 2). If all CHI_3 decomposes to iodine radicals and diiodomethyl groups (Scheme 2(a)), the concentration of the iodine radical ($[I\bullet]$) would be 2.85×10^{-2} mol/L in the oil phase. At this high $[I\bullet]$, the iodine chain-transfer reaction would compete with the iodine radical combination.[27, 28] This means that the iodine radical generated at the beginning of the polymerization can also be coupled with another iodine radical to form an iodine molecule (I_2) (Scheme 2(b)). This is the reason behind the induction observed in the early stage,[5] as I_2 is a good scavenger for radicals. This reaction could be witnessed as the orange color of the sample after 1 h of polymerization in Figure 9.

Figure 9. Evolution appearance of PVAc dispersions prepared by *ms* ITP using V-70 as initiator at 30°C.

At the interface of the monomer droplet and the water phase, the iodine molecule has the opportunity to react with water (Scheme 2(c)). The water solubility of the iodine molecule ($[I_2]_{aq}$) is 1.34×10^{-3} mol/L at 25°C,[29] which is close to that of the remaining iodine in the reaction mixture ($[I_2] = 1.69 \times 10^{-3}$ mol/L, if all I• are supposed to form I_2 in the aqueous phase). With the assistance of halogen bond interaction,[18] some I_2 are probably leave from the surface of monomer droplet to the aqueous phase. Concurrently, by reacting with the hydrosoluble oligomer radicals generated by the propagation step depicted in Scheme 2, the iodine molecules can also exit from the monomer droplet to the aqueous phase. It was confirmed by the UV-vis measurement that the absorption peaks of the polymerized suspension appeared around 295 and 372 nm can be attributed to the escaped I_2, whose characteristic peaks appeared around 204, 285, 353 nm (Figure 10). These escaped I_2 could also explain the relatively high M_w/M_n (Figure 6 and Table 1).

Various equilibria occur in the presence of iodine in the aqueous phase. In practice, the pH of the water phase was 6.5 before the polymerization and 2.1 after the polymerization. Within the pH range of $2 - 7$, the chemical equilibrium of iodine can be expressed as $[I_2 + H_2O$

$\rightleftharpoons I^- + H^+ + HOI]$ (Scheme 2(c)).[5, 30] After the consumption of I_2 (triiodide (I_3^-) is also eliminated, Scheme 2(d)), the polymerization reinitiates. Additionally, the final concentration of H^+ can be assumed to originate from HI (Scheme 1 and Scheme 2(c)), if the source of H^+ from acetic acid is neglected. According to the pH of the suspension after the polymerization ($[H^+] \approx [I^-]$), the number of I^- was almost equal to the original number of I• given by CHI3. This result indicates that the livingness of PVAc in *ms* ITP is probably low. And this problem is the inherent drawback of ITP.

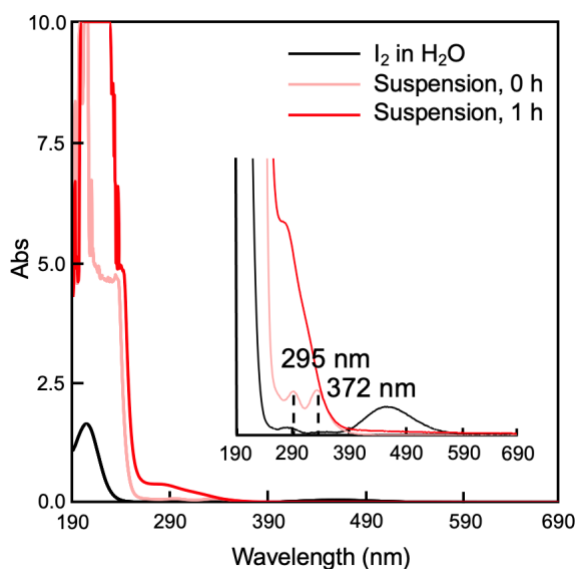**Figure 10.** UV-vis absorption spectra of I_2 (black line) and polymerization suspension at 30°C for 0h (pink line) and 1h (red line). (Conc. 0.65 mM; calculated by iodine group (–I) concentration).

Although the livingness is low, it is worth noting that the *ms* ITP system maintained the colloidal stability of the particles during the polymerization, with much less coagulation than that observed in the case of *ms* CRP (Figure 11). As the formation of submicrometer-sized byproduct particles was effectively minimized in the case of *ms* ITP, to some extent, the

depletion force would decrease to prevent the coagulation.[31] At the same time, besides the sterical repulsion exerted by the dispersant, the existence of I^- surrounding the micrometer-sized particles would enhance the stability through electrostatic repulsion among the particles. This was evidenced by the apparent decrease in the zeta potential to -14.02 mV in the case of *ms* ITP after removal of the dispersant, whereas that of *ms* CRP was -4.67 mV (Table 2).
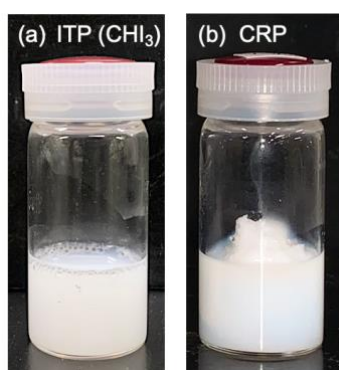

Figure 11. Appearance of PVAc prepared by *ms* ITP for 18 h (a) and *ms* CRP for 8h using V-70 as initiator at 30°C.

Table 2. Zeta potential (ζ) and pH of PVAc prepared by *ms* CRP and *ms* ITP.

Method	*ms* CRP			*ms* ITP	
Time	6 h	10 h	after wash	18 h	after wash
pH	6~7	5~6	7	2~3	6~7
ζ (mV)	-4.13	-2.64	-4.67	-1.34	-14.02
State	stable	coagulation	supernatant	suspension	suspension

3.3.4 Alcoholysis of PVAc

As mentioned in the introduction, well-defined PVA, which has fascinating properties, attracts attention in the fields of chemistry and biology. Hence, the PVAc products obtained from *ms* ITP and *ms* CRP were hydrolyzed using MeOH to prepare PVA. The generation of PVA was

confirmed by FTIR (Figure 12). In both cases, the characteristic peaks of the ester group (1,024 and 1,239 cm^{-1}) and the carboxyl group (1,749 cm^{-1}) of PVAc were weakened, and the peak of the hydroxyl group (3,000–3,700 cm^{-1}) was strengthened, confirming that the alcoholysis proceeded successfully.
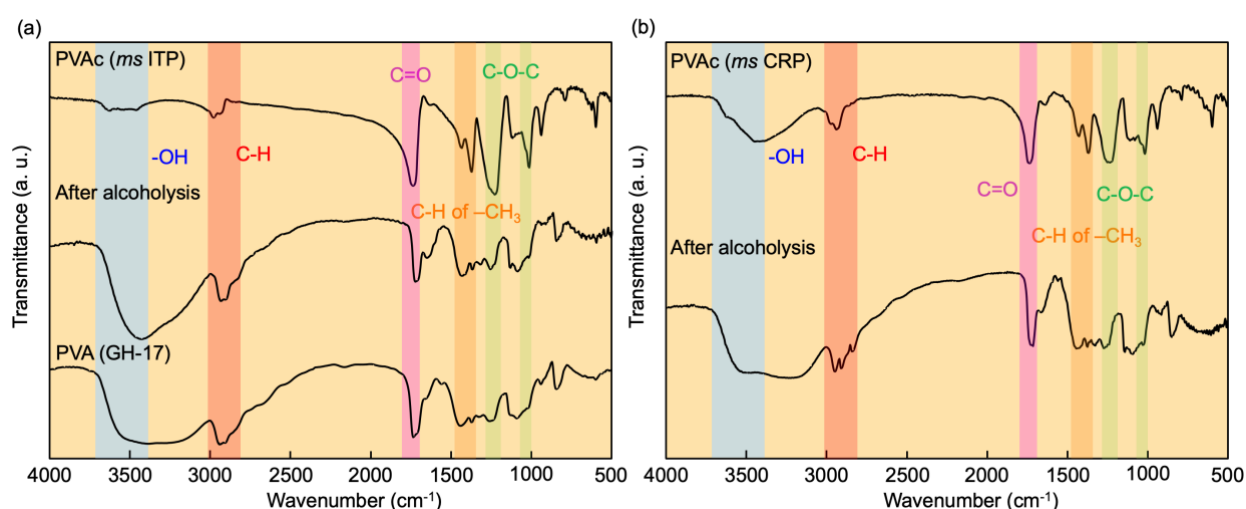

Figure 12. FTIR spectra of (a) PVAc prepared by *ms* ITP before and after alcoholysis, and compared with commercial PVA (GH-17), (b) PVAc prepared by *ms* CRP before and after alcoholysis.

The M_n and M_w/M_n of PVAc before and after the alcoholysis are displayed in Figure 13 and Table 3. In general, the chain transfer of VAc radical to the methine or the methyl group of the acetoxy substituents on PVAc is likely to occur in the radical polymerization of VAc (Scheme 3(a)).[8-10] Once the chain is transferred, the propagation reaction continues from the side chain. After alcoholysis, the PVAc segments grafted from the side chains leave the original polymer chains, resulting in a decrease in M_n of PVA (Scheme 3(b)). The PVAc prepared through *ms* CRP ($M_n = 3.77 \times 10^5$, $M_w/M_n = 4.81$) was hydrolyzed into a PVA with broad M_w/M_n ($M_n = 63800$, $M_w/M_n = 4.59$). By contrast, a well-defined PVA with M_n of 11,200, which was

consistent with $M_{n,th}$ of 11,200, and M_w/M_n of 1.96 was generated from PVAc (M_n = 22,200, M_w/M_n = 2.41) synthesized through *ms* ITP in a controlled manner (Scheme 3(c, d)). Though the M_n of PVA was limited by the livingness of PVAc, the chain transfer to the methine group and the methyl group of the acetoxy substituents on the polymer would be effectively prevented by the faster transfer of the monomer to the iodine end groups, which was evidenced by their C_{tr}s (Table 4). To calculate C_{tr} to the iodine end group of PVAc, ethyl iodoacetate (EI) was used as the chain-transfer agent, since its structure is same as that of the monomer unit. Therefore, C_{tr} to the iodine end group of PVAc is similar to that of EI.
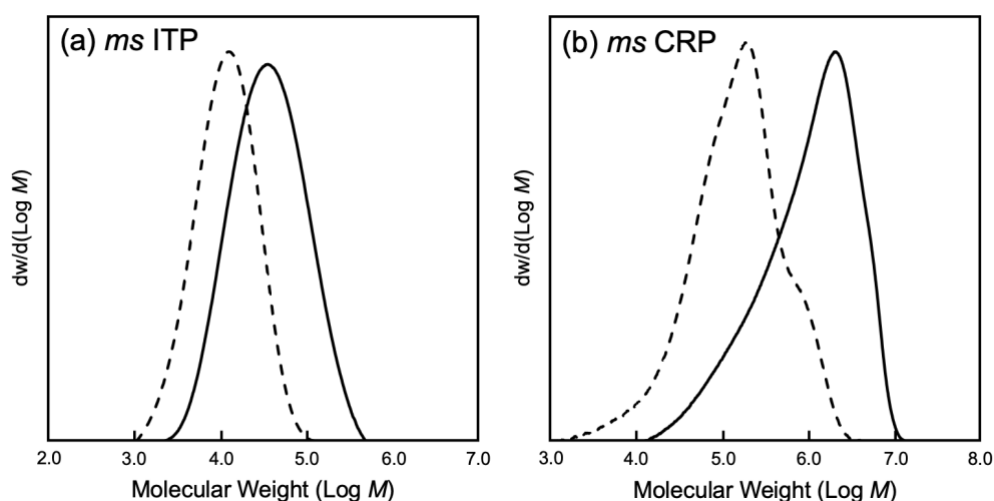

Figure 13. The molecular weight and molecular weight distribution of PVAc prepared by (a) *ms* ITP and (b) *ms* CRP before alcoholysis (solid line) using DMF as the eluent at 40°C and after alcoholysis (dash line) using water as the eluent at 35°C.
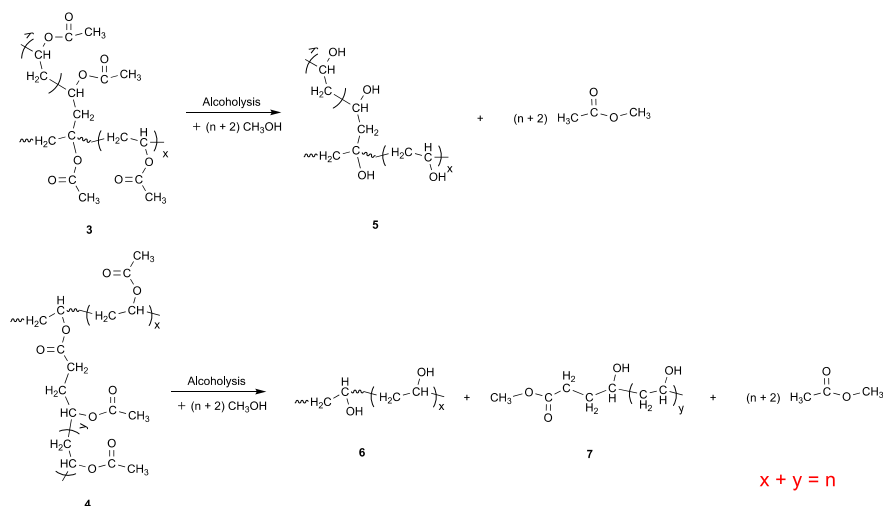
Table 3. The M_n and M_w/M_n of PVAc prepared by *ms* CRP (a) and *ms* ITP (b) before and after alcoholysis.

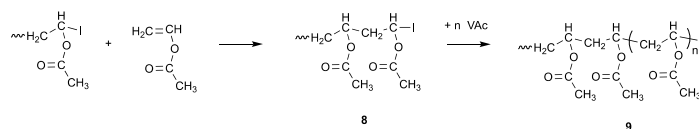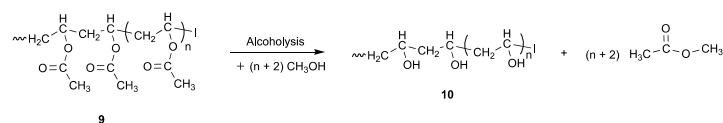|	Before		After	
	M_n	M_w/M_n	M_n	M_w/M_n
ms ITP	22,200	2.41	11,200	1.96
ms CRP	37.7×104	4.81	63,800	4.59

(a) Branching
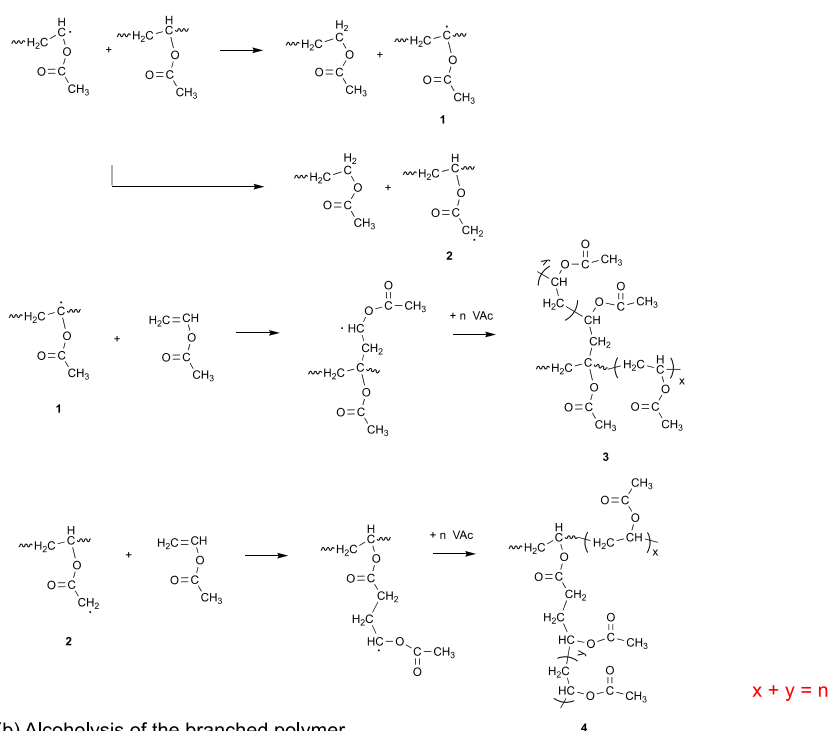
(b) Alcoholysis of the branched polymer

(c) Without branching

(d) Alcoholysis of the polymer without branching

Scheme 3. Mechanisms of the branched PVAc in *ms* CRP (a) and alcoholysis of the branched PVAc (b). Mechanisms of the PVAc without branching in *ms* ITP (c) and alcoholysis of the PVAc without branching (d).

Table 4. The different chain transfer constants to the different positions of polymer.

Position of PVAc	T (°C)	C_{tr}
Methine group [a]	60	3.03×10^{-4}
Methyl group of acetoxy substituents [a]	60	1.27×10^{-4}
Iodine end group [b]	30	32.98

[a] S.-I. Nozakura, Y. Morishima, S. Murahashi, *J. Polym. Sci.*, **1972**, *10*, 2853.

[b] Experimental value: using Ethyl iodoacetate as CTA, calculated by the equation in chapter 1.

3.4 Conclusions

The synthesis of PVAc through *ms* ITP was demonstrated for the first time. Micrometer-sized PVAc particles were successfully synthesized without submicrometer-sized byproduct particles by conveniently applying *ms* ITP with V-70 as the initiator at 30°C. The polymerization proceeded in a controlled manner and with better colloid stability. The synthesis at high temperature failed because of the degradation of iodine-terminated PVAc chains and the generation of crosslinking points through aldol reactions, which is further promoted by the presence of PVA as a dispersant. The synergistic effect between the temperature and iodine facilitated the occurrence of side reactions. Besides the degradation of iodine chain ends, the increase in M_w/M_n with the monomer conversion also arises from the side reaction between water and iodine species. After considering the hydrolysis of iodine, the mechanism of ITP in an aqueous system was clarified, which paves the way for the application of ITP for other unconjugated monomers in aqueous systems. Moreover, a well-defined PVA was obtained from the controlled PVAc prepared through *ms* ITP, which offers a new route to synthesize PVA-based materials with desired M_n and narrow M_w/M_n.

3.5 References

1. J. C. Smith, *J. Phys. Chem.*, **46** (2), 229-232 (1942)

2. Y. Li, S. Li, J. Sun, *Adv. Mater. (Weinheim, Ger.)*, **33** (13), 2007371 (2021)

3. L. Zhao, Z. Ren, X. Liu, Q. Ling, Z. Li, H. Gu, *ACS Appl. Mater. Interfaces*, **13** (9), 11344-11355 (2021)

4. H. Tang, M. Radosz, Y. Shen, Controlled/"Living" Radical Polymerization of Vinyl Acetate. In *Controlled/Living Radical Polymerization: Progress in ATRP*, American Chemical Society: 2009; Vol. 1023, pp 139-157.

5. P. Lacroix-Desmazes, J. Tonnar, Degenerative Transfer with Alkyl Iodide. In *Polymer Science: A Comprehensive Reference*, 2012; pp 159-180.

6. O. L. Wheeler, S. L. Ernst, R. N. Crozier, *J. Polym. Sci.*, **8** (4), 409-423 (1952)

7. M. Abdollahi, P. Bigdeli, M. Hemmati, M. Ghahramani, M. Barari, *Polym. Int.*, **64** (12), 1808-1819 (2015)

8. S. Harrisson, X. Liu, J. N. Ollagnier, O. Coutelier, J. D. Marty, M. Destarac, *Polymers*, **6** (5), 1437-1488 (2014)

9. D. Britton, F. Heatley, P. A. Lovell, *Macromolecules*, **31** (9), 2828-2837 (1998)

10. S. I. Nozakura, Y. Morishima, S. Murahashi, *J. Polym. Sci., Part A: Polym. Chem.*, **10** (10), 2853-2866 (1972)

11. D. Boschmann, P. Vana, *Polym. Bull. (Heidelberg, Ger.)*, **53** (4), 231-242 (2005)

12. S. Sugihara, R. Kawakami, S. Irie, Y. Maeda, *Polym. J. (Tokyo, Jpn.)*, **53** (2), 309-321 (2021)

13. A. Wolpers, P. Vana, *Macromolecules*, **47** (3), 954-963 (2014)

14. M. Farrokhi, M. Abdollahi, *J. Polym. Res.*, **23** (6), (2016)

15. B. S. Casey, B. R. Morrison, R. G. Gilbert, *Prog. Polym. Sci.*, **18**, 1041-1096 (1993)

16. I. A. Maxwell, B. R. Morrison, D. H. Napper, R. G. Gilbert, *Macromolecules*, **24** (7), 1629-1640 (1991)

17. M. Okubo, Y. Kitayama, N. Yamashita, X. Liu, C. Huang, *Macromol. Theory Simul.*, **27** (5), 1800029 (2018)

18. Y. Ni, C. Tian, L. Zhang, Z. Cheng, X. Zhu, *ACS Macro Lett.*, **8** (11), 1419-1425 (2019)

19. C. Huang, H. Minami, M. Okubo, *Langmuir*, **37** (10), 3158-3165 (2021)

20. R. McHale, F. Aldabbagh, P. B. Zetterlund, H. Minami, M. Okubo, *Macromolecules*, **39** (20), 6853-6860 (2006)

21. C. Huang, N. Yamashita, A. Chaiyasat, X. Liu, M. Okubo, *Polymer*, **154**, 128-134 (2018)

22. J. C. Salamone, Concise polymeric materials encyclopedia. CRC Press, Boca Raton, FL (US): 1999; p 85.

23. S. L. Soni, D. Kumar, S. Jain, R. K. Ancheria, *AJPRD*, **7** (4), 49-55 (1970)

24. S. Barbon, E. Stocco, D. Dalzoppo, S. Todros, A. Canale, R. Boscolo-Berto, P. Pavan, V. Macchi, C. Grandi, R. De Caro, A. Porzionato, *Int. J. Mol. Sci.*, **21** (3), (2020)

25. D. Mawad, L. A. Poole-Warren, P. Martens, L. H. Koole, T. L. B. Slots, and C. S. J. van Hooy-Corstjens, *Biomacromolecules*, **9**, 263-268 (2008)

26. S. Aruldass, V. Mathivanan, A. R. Mohamed, C. T. Tye, *J. Environ. Chem. Eng.*, **7** (5), 103238-103245 (2019)

27. J. A. LaVerne, L. Wojnarovitsf, *J. phys. Chem.* , **98** (48), 12635-12640 (1994)

28. L. Wojnarovitsf, J. A. LaVerne, *Radiat. Phys. Chem.*, **47** (1), 99-101 (1996)

29. F. C. Kracek, *J. phys. Chem.*, **34**, 417-422 (1930)

30. I. R. E. stván Lengyel, and Kenneth Kustin, *Inorg. Chem*, **32**, 5880-5882 (1993)

31. Y. Mao, M. E. Cates, H. N. W. Lekkerkerker, *Phys. A: Stat. Mech. Appl.*, **222** (1), 10-24 (1995)

Chapter 4

Preparation of micrometer-sized poly(methyl methacrylate)-*block-poly(vinyl acetate) particles by two-step iodine transfer polymerization*

4.1 Introduction

Poly(vinyl acetate) (PVAc) is one of the important polymers, which has a wide range of industrial uses and acts,[1-3] especially acting as the precursor for poly(vinyl alcohol) (PVA). The alluring properties of low toxicity, high hydrophilicity, biodegradation, and biocompatibility possessed by PVA make it fascinating in the field of both chemistry and biology.[4, 5] Significantly, during the hydrolysis from PVAc to PVA, the water-insoluble polymer gradually becomes water-soluble. Hence, it is attractive to prepare the PVAc-based block copolymer to obtain an amphiphilic PVA-based block copolymer.

In manufacturing process, conventional radical polymerization (CRP) is typically employed to synthesize PVAc. However, the shortages of branched structures, high molecular weight (M_n), and broadened molecular weight distribution (M_w/M_n)[6, 7] could influence the performance of PVA after the degradation of PVAc.[8, 9] Therefore, the synthesis of PVAc with controlled M_n and M_w/M_n is of great importance for the development of its derivatives. In Chapter 3,[10] the controlled PVAc was successfully synthesized by microsuspension iodine transfer polymerization (*ms* ITP) using iodoform (CHI$_3$) as the chain transfer agent to not only

meet the above demands but also obtain micrometer-sized particles. The latter aim is usually

regarded as the difficulty of hydrophilic monomers in a conventional suspension or

microsuspension system, which is accompanied by submicrometer-sized particles since the

homogenous nucleation in the aqueous phase is difficult to be restrained.[11-14]

The success of the *ms* ITP of hydrophilic monomers relies on the radical exit depression

effect, according to which the escaping monomer and oligomer radicals can be captured by the

highly hydrophobic diiodomethyl group and iodine group from CHI_3 in the monomer droplet,

as described detailly in Chapter 1, 2.[15, 16] The *ms* ITP of methyl methacrylate (MMA) (solubility

in water: 1.5 g/100 mL, at 20°C)[17] resulted in micrometer-sized particles, as revealed in

Chaiyasat's work.[18] In this chapter, two-step ITP in a microsuspension system was used to

obtain micrometer-sized poly(methyl methacrylate)-*block*-poly(vinyl acetate) (PMMA-*b*-

PVAc) particles using only hydrophilic monomers as an attempt, which are able to dissolve in

water at a certain amount.

4.2 Experimental

4.2.1 Materials

Vinyl acetate (VAc) (Nacalai Tesque, Inc. Kyoto, Japan; stabilizer: hydroquinone, 5 ppm) and

MMA (Nacalai Tesque, Inc. Kyoto, Japan; stabilizer: hydroquinone monomethyl ether) were

purified using a column packed with basic aluminum oxide (Alumina Activated 200, Nacalai

Tesque, Inc. Kyoto, Japan). CHI_3 (Nacalai Tesque, Inc., Kyoto, Japan; purity, 99%), PVA (GH-

17, Nippon Synthetic Chemical Industry Co., Ltd, Osaka, Japan; degree of saponification,

86.5%–89%; molecular weight, 7×10^4), 2,2'-Azobis(2,4-dimethylvaleronitrile) (V-65; Nacalai

Tesque, Inc., Kyoto, Japan; purity ≥95.0%), 2,2'-azobis(4-methoxy-2,4-dimethylvaleronitrile)

(V-70; Fujifilm Wako Pure Chemical Co., Ltd, Osaka, Japan; purity ≥95.0%), *N, N*-

dimethylformamide (DMF; Nacalai Tesque, Inc., Kyoto, Japan; purity ≥99.0%), toluene (Junsei

Chemical Co., Ltd, Tokyo, Japan; purity ≥99.5%), and ruthenium tetroxide (RuO_4, Filgen, Inc.,

Nagoya, Japan) were used as received. Deionized water, which was obtained using a water

purification machine (Elix UV, Millipore Co., Ltd., Japan) and had a resistivity of 15 MΩ cm,

was used in all experiments.

4.2.2 Synthesis of micrometer-sized PMMA particles

Micrometer-sized PMMA particles were synthesized by *ms* ITP. V-65 (0.0362 g) and CHI_3

(0.072 g) were dissolved in MMA (3 g) in a molar ratio of [MMA]:[V-65]:[CHI_3] = 163:0.8:1,

and the monomer solution was poured into an aqueous phase consisting of 1 wt% PVA aqueous

solution (27 g). After homogenization at 4,000 rpm for 5 min using a homogenizer (ABM-2,

Nihonseiki Kaisha, Ltd, Japan), a monomer dispersion was obtained. Subsequently, the

monomer dispersion was evenly divided into four glass tubes, which were sealed off after being

degassed five times with vacuum/N_2 gas cycles and covered with aluminum foil. Finally, *ms*

ITP was conducted at 40°C for 24 h. In all the polymerizations, the sealed tubes were placed in

a water bath (BW101, Yamato Scientific Co., Ltd, Japan) with a horizontal shaking rate of 120

rpm. PMMA particles were collected by centrifugation at 8000 rpm for 10 min at 5°C, which

was repeated in triplicate.

4.2.3 Synthesis of micrometer-sized PMMA-b-PVAc particles

Micrometer-sized PMMA-*b*-PVAc particles were synthesized by seeded microsuspension ITP (*sms* ITP). An oil phase of V-70 (1 mg, 1 wt% relative to monomer), toluene (5 mg, 2 wt% relative to PMMA seeds), and VAc (0.1 g) were mixed with 1 wt% PVA aqueous solution (0.6 g), which was homogenized by a biomixer (NS-52K, Nihonseiki Kaisha, Ltd.) at 6500 rpm afterward. Next, the VAc emulsion, which was extracted one-tenth from the above emulsion, was added to the suspension of PMMA particles. As the *ms* ITP-obtained PMMA has an iodine end group, it was used as the macrochain transfer agent in this step and expressed as PMMA-I. The suspension of PMMA seeds was prepared in a molar ratio of [VAc]:[V-70]:[PMMA-I] = 200:0.56:1, and the water was adjusted to control the solid content of the total mixture to 10 wt%. Then, the mixture was immersed in an ice bath and stirred by a magnetic stirrer at 150 rpm for 2 h to proceed with the swelling of VAc. Following the swelling, the mixture was evenly divided using four glass tubes and sealed off after being degassed five times with vacuum/N_2 gas cycles. The sealed tubes were placed in a water bath at 30°C for 24 h or 48 h with a horizontal shaking rate of 80 rpm after covering them with aluminum foil (to prevent the light-induced side reaction of the iodine end group). PMMA-*b*-PVAc particles were collected by centrifugation conducted in triplicate in water at 8000 rpm for 10 min at 5°C.

4.2.4 Synthesis of PMMA/PVAc composite particles

PMMA and PVAc were synthesized by dispersion polymerization[19] and microsuspension conventional radical polymerization[10], respectively. The obtained PMMA (1 g) and PVAc (0.1

g) were dissolved in toluene (1 g), in which the weight ratio of PMMA and PVAc was controlled

at 10:1 similar to the ratio of ITP-obtained PMMA-*b*-PVAc. Next, the mixture was poured into

an aqueous phase consisting of a 1 wt% PVA aqueous solution (10 g). After homogenizing for

5 min using a homogenizer (ABM-2, Nihonseiki Kaisha, Ltd., Japan) at 4,000 rpm, a suspension

of composite particl was obtained. The polymers were collected after being centrifuged three

times with water at 8000 rpm, 5°C, and 10 min.

4.2.5 Characterization

The conversions and solid contents were measured by gravimetry. The percentage of

submicrometer-sized byproduct particles was calculated using the equation

$$\left(\frac{\text{Weight of water} \times \text{Solid content of supernatant after centrifugation}}{\text{monomer content in the weighted amount} \times \text{Convesion}} \right)$$ after the measurement of the solid

content of the supernatant using gravimetry. The overall morphologies of PMMA particles, and

PMMA-*b*-PVAc particles were observed using an optical microscope (OM, ECLIPSE 80i,

Nikon, Tokyo, Japan), and a scanning electron microscope (SEM, S-2460, Hitachi Science

Systems Ltd., Ibaraki, Japan) after coating the particles with platinum using a sputter coater.

The number-average diameter ($\overline{D}_n$) and the coefficient of variation (C_v) were determined by

counting all particles in the optical and SEM images (about 300 particles) using the image

analysis software WinROOF (Mitani Co., Fukui, Japan). The inner morphologies of PMMA-*b*-

PVAc particles were observed by a transmission electron microscope (TEM, JEM-1230, JEOL,

Tokyo, Japan) after staining the freeze-dried particles with RuO_4 and slicing them into cross-

sections (170 nm-thick). The weight-average and number-average molecular weights (M_w and

M_n, respectively), and molecular weight distribution (M_w/M_n) were determined by gel permeation chromatography using two methacrylate gel columns (TOSOH Corporation, TSK gel α 5000, 7.8 mm i.d $\times$ 30 cm, separation range per column: approximately $50–7 \times 10^6$ g/mol (exclusion limit) using DMF as an eluent at 40°C, and a flow rate of 1.0 mL/min) employing a refractive index (RI) detector (TOSOH RI-8020/21). The columns were calibrated with twelve standard PMMA samples for DMF ($730–1.65 \times 10^6$).

4.3 Results and discussion

4.3.1 Comparison of the rate of deactivation and the rate of hydrolysis of iodine

In the previous chapter, it has been displayed that the chain transfer constant (C_{tr}) could be calculated experimentally in the form of conversion by equation (1).[20]

$$C_{tr} = \ln(1-p)/\ln(1-q) \qquad \text{eq (1)}$$

The p and q represent the conversion of macrochain transfer agent (i.e., PMMA-I) and monomer, respectively. However, this time because of the extremely strict condition requested to obtain the direct data from GC, the C_{tr} of 2.6 was selected, which was given in the work of P. Lacroix-Desmazes et al.[21] By utilizing this equation, the remained concentration of the macro chain transfer agent (1-p) could be calculated easily.

The main chain transfer appeared in the early stage of *sms* ITP showed as below:

$$\text{P} \bullet + \text{PMMA-I} \xrightarrow{k_{tr}} \text{P-I} + \text{PMMA} \bullet \qquad \text{Reaction (1)}$$
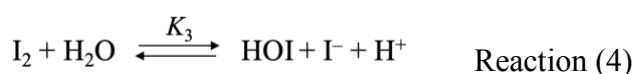
As revealed, the consumption of the PMMA-I within the period (t) based on reaction (1) can be calculated by equation (2) through the following mathematical procedures.

After taking the original and remained concentrations of PMMA-I into the mathematical model, it is possible to get the theoretical concentration of the polymer radicals.

$$\text{Consumption of [PMMA-I]} \quad -\frac{d[\text{PMMA}-\text{I}]}{dt} = k_{tr}\,[\text{P}\cdot][\text{PMMA-I}] \implies -\frac{d[\text{PMMA}-\text{I}]}{[\text{PMMA}-\text{I}]} = k_{tr}\,[\text{P}\cdot]\,dt$$

$$\text{Integration} \quad -\int_{[\text{PMMA}-\text{I}]_0}^{[\text{PMMA}-\text{I}]_t} \frac{d[\text{PMMA}-\text{I}]}{[\text{PMMA}-\text{I}]} = \int_0^t k_{tr}\,[\text{P}\cdot]\,dt \implies \ln\left(\frac{[\text{PMMA}-\text{I}]_0}{[\text{PMMA}-\text{I}]_t}\right) = k_{tr}\,[\text{P}\cdot]\,t$$

$$\text{eq (2)}$$

The free iodine radicals are probably to regenerate the dormant species with these polymer radicals. Meanwhile, these free iodine radicals could also combine with the other iodine radicals and react with water. The deactivation of a polymer radical with an iodine radical (I•) and the combination of the two iodine radicals are shown as reaction (2) and reaction (3), respectively. The generated iodine molecules undergo the hydrolysis steps, however in the situation of pH < 7, the general reaction is shown as the reaction (4). The rate constants for each reaction are $k_1 = 9.516 \times 10^9$, $k_2 = 5 \times 10^9$ M^{-1}S^{-1},[22] and $K_3 = 5.4 \times 10^{-13}$ M^2.[23]

$$\text{P}\cdot + \text{I}\cdot \xrightarrow{k_1} \text{P-I} \qquad\qquad \text{Reaction (2)}$$

$$\text{I}\cdot + \text{I}\cdot \xrightarrow{k_2} \text{I}_2 \qquad\qquad \text{Reaction (3)}$$

$$\text{I}_2 + \text{H}_2\text{O} \xrightleftharpoons{K_3} \text{HOI} + \text{I}^- + \text{H}^+ \qquad\qquad \text{Reaction (4)}$$

The reactions are second-order reactions, therefore, the generation of deactive polymer (P-I), iodine molecules (I_2), and iodine ions (I^-) within the period (t) based on reaction (2-4) can be calculated by equation (3-5), respectively.

$$[P-I]_t = k_1 [P \bullet][I\bullet]t \qquad \text{eq (3)}$$

$$[I_2]_t = k_2 [I\bullet]^2 t \qquad \text{eq (4)}$$

$$[I^-]_t = K_3 [I\bullet][H_2O]t \qquad \text{eq (5)}$$

To determine whether the regeneration of P-I or the hydrolysis of iodine dominates the procedure at an exact point in time, a comparison between the real-time concentration of P-I and I^- is represented through the following mathematical equation (6). The original input experimental data are given in Table 1.

$$\frac{[P-I]_t}{[I^-]_t} = \frac{k_1 [P\bullet]_t}{k_2 K_3 [I\bullet][H_2O]t} \qquad \text{eq (6)}$$

After inputting the data of the instantaneous conversion of monomer (6.9 and 11.4 % after 24-hour and 48-hour polymerization, respectively) and the concentration of water (55.55 M L^{-1}), the eq (6) can be simplified with numerical values in Table 1.

Meanwhile, the concentration of iodide ions ($[I^-]$) is calculated through the measurement of pH. It is under the assumption that all hydrogen cations (H^+) are derived from the hydrolysis of iodine. After 24-hour polymerization, the pH of the medium decreased to 3.085, while 2.755

of that after 48-hour polymerization was measured by a pH meter. At that time, the [I⁻]s in the media are about 8.222×10^{-4} M L⁻¹ after 24 hours and 17.4×10^{-4} M L⁻¹ after 48 hours. After substituting the values of [PMMA-I]$_t$ and [I⁻] into the eq (6), the number of [I•]$_t$ could be calculated. When the volume of water is known, the mole fractions of iodine species could be told through eq (7-10).

$$n_{[I, \, all]} = [PMMA\text{-}I]_0 \times V_{H2O} \qquad \text{eq (7)}$$

$$n_{[PMMA\text{-}I]t} = [PMMA\text{-}I]_t \times V_{H2O} \qquad \text{eq (8)}$$

$$n_{[I•, \, th]t} = [I•] \times V_{H2O} \qquad \text{eq (9)}$$

$$n_{[I⁻]} = [I⁻] \times V_{H2O} \qquad \text{eq (10)}$$

The $n_{[I, \, all]}$, $n_{[I•, \, th]t}$, $n_{[PMMA\text{-}I]t}$, and $n_{[I⁻]}$ represent the mole fraction of the total amount of iodine, the calculated I• in the polymerization, the iodine end group, and the I⁻, respectively.

If the regeneration of P-I is superior to the hydrolysis of iodine, the sum of $n_{[I•, \, th]t}$, $n_{[PMMA\text{-}I]t}$, and $n_{[I⁻]}$ should be less than or equal to the amount of $n_{[I, \, all]}$. But, the data shows that the present sum of $n_{[I•, \, th]t}$, $n_{[PMMA\text{-}I]t}$, and $n_{[I⁻]}$ is higher than $n_{[I, \, all]}$. Additionally, the number of dropped iodine end groups is much lower than the number of I⁻. Both indicate that the instantaneous [I•] leaving from PMMA-I is higher than the theoretic value and the hydrolysis of iodine occurs prior to the regeneration of P-I.

Table 1. Values of parameters for calculation of iodine species.

Coefficient	eq for polymn of 24h	eq for polymn of 48h
C_{tr}	2.6 [a]	2.6 [a]
q	0.069	0.114
p	0.1696	0.2670
$[\text{PMMA} - \text{I}]_0$ (mmol/L)	3.6714	4.6176
$[\text{PMMA} - \text{I}]_t$ (mmol/L)	$= [\text{PMMA} - \text{I}]_0 \times (1- p)$ $= 3.0486$	$= [\text{PMMA} - \text{I}]_0 \times (1- p)$ $=3.3709$
$k\,p$ $(\text{M}^{-1}\text{s}^{-1})$	$= 2.43\times10^8\exp(-30600/RT)$ [b] $R=8.314\text{J K}^{-1}\text{mol}^{-1}$	$= 2.43\times10^8\exp(-30600/RT)$ [b] $R=8.314\text{J K}^{-1}\text{mol}^{-1}$
$k\,\text{tr,PMMA-I}$ $(\text{M}^{-1}\text{s}^{-1})$	$= C_{tr}\times kp = 3371$	$= C_{tr}\times kp =3371$
$[\text{P} \bullet]$ $(\times 10^{-7}$ mmol/L)	6.3824	5.4024
$[\text{P}- \text{I}]/[\text{I}^-]$	$1/\,2.134 \times 10^3 \times [\text{I}\bullet]$	$1/\,0.903 \times 10^3 \times [\text{I}\bullet]$
$[\text{I}\bullet]$ $(\times 10^{-1}$ mmol/L)	1.264	5.716
$n_{[\text{I, all}]}$ $(\times 10^{-4}$ mmol)	9.413	9.711
$n_{[\text{PMMA-I}]t}$ $(\times 10^{-4}$ mmol)	7.816	7.089
$n_{[\text{I}\bullet,\, th]}$ $(\times 10^{-4}$ mmol)	0.324	1.211
$n_{[\text{I}^-]}$ $(\times 10^{-4}$ mmol)	2.108	3.659
$[\text{I}^-]$ $(\times 10^{-1}$ mmol/L)	8.222	17.40
V_{H2O} $(\times 10^{-4}$ L)	2.564	2.103
$[\text{H}_2\text{O}]$ (mol/L)	55.55	55.55

a) C. Boyer, P. Lacroix-Desmazes, J.-J. Robin, B. Boutevin, *Macromolecules*, **2006**, *39*, 4044

b) M. S. Matheson, E. E. Auer, Ellen B. Bevilacqua, *et al.*, *J. Am. Chem. Soc.*, **1949**, *71*, 2610

4.3.2 Micrometer-sized PMMA-*b*-PVAc particles

Previously, micrometer-sized PVAc and PMMA particles were separately synthesized without

the generation of submicrometer-sized particles using *ms* ITP by us [12] and Chaiyasat et

al.,[20] respectively. It shows the high feasibility of the synthesis of micrometer-sized PMMA-

b-PVAc particles by ITP in a microsuspension system. Micrometer-sized PMMA-*b*-PVAc particles were synthesized by *sms* ITP. Firstly, PMMA micrometer-sized particles were prepared by *ms* ITP as reported previously, where the content of submicrometer-sized byproducts was only 7% (Figure 1 and Table 2), and the obtained PMMA had an iodine end group, which was used as the macrochain transfer agent afterward. In the second step, to facilitate the absorption of VAc into the PMMA seeds, the VAc emulsion containing a small amount of toluene was added to the PMMA particles. After *sms* ITP, the obtained particles maintained colloidal stability, and no byproducts were obtained (Figure 1 and Table 2).
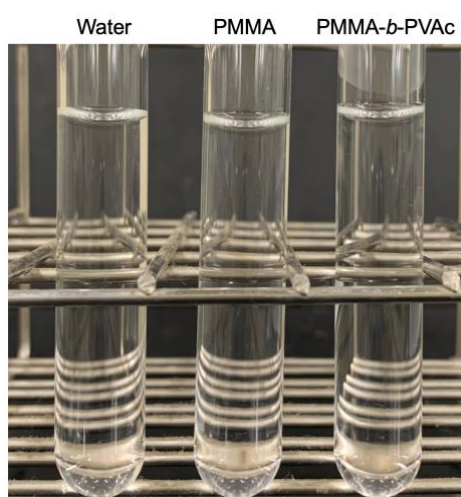

Figure 1. Supernatant appearance of the ITP-obtained PMMA and PMMA-*b*-PVAc after centrifugation once at 8000 rpm for 10 min.

Table 2. The percentage of submicrometer-sized byproduct particles of ITP-obtained PMMA and PMMA-*b*-PVAc.

	PMMA	PMMA-b-PVAc
The percentage of byproduct (%)	7.17	0

The particle sizes after each step are displayed in Figure 2(a, a', b, b'). The average diameter of the obtained particles after *sms* ITP was 7.40 μm, determined from optical micrographs, which was about 0.5 μm higher than that of PMMA seeds. Although the particle size gauged from the SEM image was lower than that from the optical micrograph (because some tiny particles were omitted during the manual measurement of particle diameters), it showed the equivalent difference in the particle size before and after *sms* ITP.
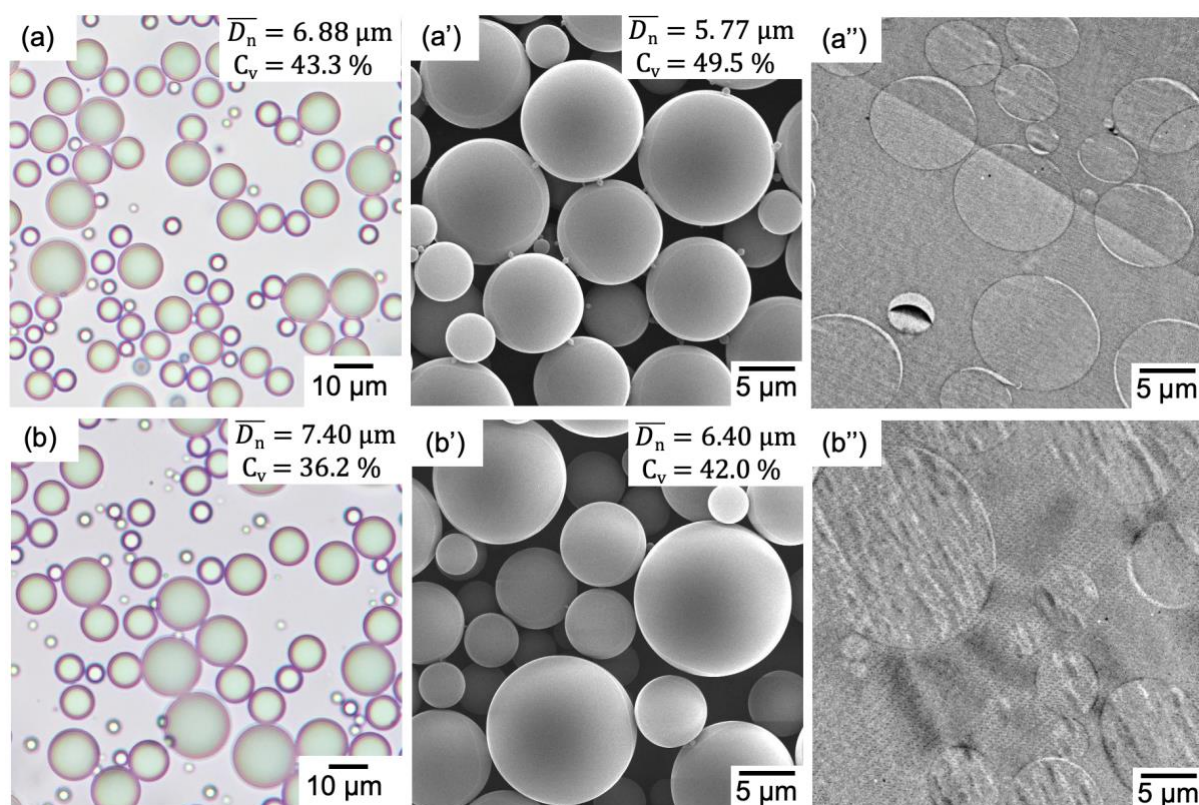

Figure 2. Optical (a, b), SEM (a', b'), and cross-sectional (a'', b'') images of PMMA and PMMA-*b*-PVAc particles synthesized by ITP. (The particle size was confirmed after measuring about 300 particles.)

From the above findings, the increased diameter indicated that PVAc was smoothly polymerized in *sms* ITP. However, further verification was required to determine whether PVAc

formed a block copolymer with PMMA homogenously. To confirm this, PMMA particles and

the particles obtained by *sms* ITP were stained with RuO₄, which lightly stained PVAc but not

PMMA.[24, 25] Comparing the inner morphologies of PMMA particles and the particles obtained

by *sms* ITP, the water wave-like structure appeared in the particles obtained by *sms* ITP (Figure

2b" and Figure 3(b, b')), which was not observed in PMMA particles (Figure 2a" and Figure

3(a, a')) and PMMA/PVAc composite particles (Figure 3(c, c')), indicating that PMMA-*b*-

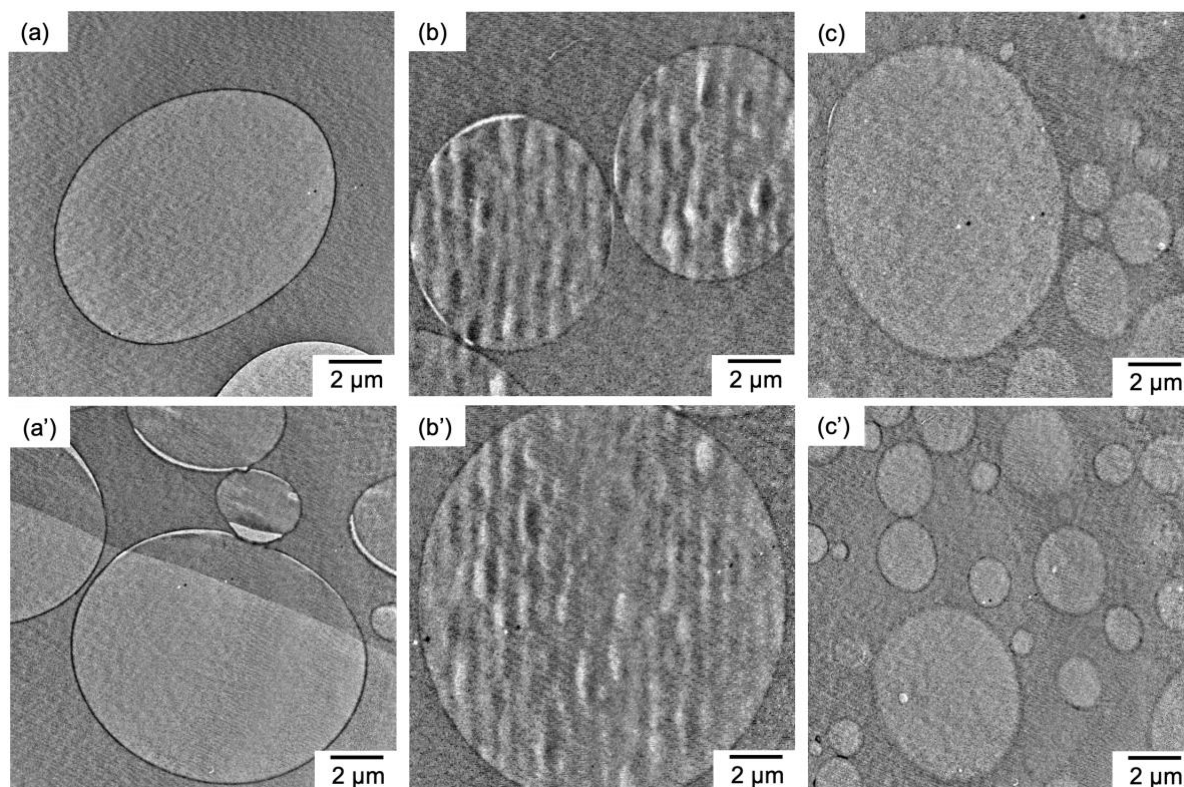PVAc particles were homogeneously prepared.

Figure 3. Cross-sections images of the PMMA particles (a, a'), PMMA-*b*-PVAc particles (b, b'), and PMMA/PVAc composite particles (c, c') at high magnification.

Table 3. The molecular weight, the theoretical molecular weight, and the molecular weight distribution before and after sms ITP of PMMA-I.

Sample	*sms* IP	Conv. (%)	M_n (g/mol)	$M_{n,th}$ (g/mol)	Top M_n (g/mol)	M_w/M_n
1	Before	85.5	14,600	14,300	15,900	1.33
	After	5.9	15,200	15,500	16,300	1.30
2	Before	80.5	17,700	13,100	23,600	1.60
	After	6.9	19,000	19,200	24,700	1.57
3	Before	80.5	17,700	13,100	23,600	1.60
	After	11.4	19,200	20,200	24,700	1.53

Nevertheless, low conversion and an increase in M_n were gained after *sms* ITP (Table 3), which can be attributed to inherent defects formed by ITP. As reported by Abdollahi et al., PVAc with an iodine end group (PVAc-I) is very sensitive to humidity.[26] The side reaction (Scheme 1a, Chapter 3), which occurs between the iodine end and the last unit of the PVAc block, easily leads to a dead end of the polymer chain. Additionally, as the macrochain transfer agent, PMMA-I is armed with low chain transfer activity, as revealed in C. Boyer's work.[21] Hence, partial PMMA-I would go through the drop of iodine end groups and meet the end with other oligomers rather than the regeneration of polymer with an iodine end (P-I) during *sms* ITP, which was also proved by the above calculation of instant concentrations of PMMA-I and iodide ions (I^-) (Table 1). Furthermore, following the generation of iodine molecules (I_2), the polymerization was inhibited.[22, 27, 28] For the emerging I_2 that was not consumed thoroughly, there existed a long induction period in this step. Consequently, the degradation of iodine end groups and the emergence of I_2 led to low conversion and low degree of polymerization of

PVAc (DP_{VAc}). Unfortunately, the determination of the polymer constituent, as well as the structure, was not possible using nuclear magnetic resonance spectroscopy (NMR). To ensure the preservation of iodine end groups, careful treatment is required in each step.

Based on the characterization of the PMMA-*b*-PVAc particles synthesized by *sms* ITP, the polymer chains in the particles are depicted in the scheme in Scheme 1.
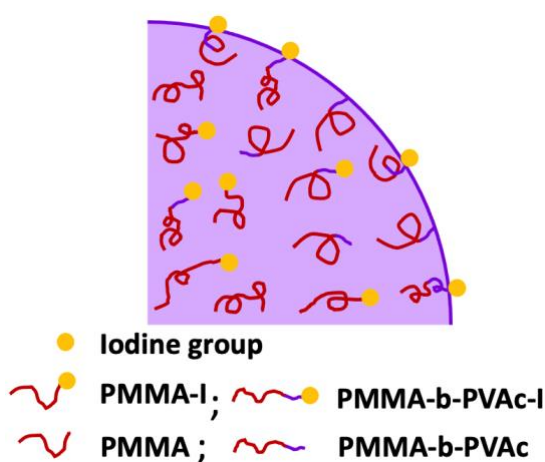
Scheme 1. Scheme of the polymer chains in the obtained particles after *sms* ITP.

4.4 Conclusion

The synthesis of micrometer-sized block copolymer particles using two hydrophilic monomers, MMA and Vac, was demonstrated through ITP. Micrometer-sized PMMA-*b*-PVAc particles were successfully synthesized by applying two-step ITP in a microsuspension system under mild conditions to maintain iodine end groups. The obtained PMMA-*b*-PVAc particles possessed low DP_{VAc} but maintained the desired M_n and narrow M_w/M_n.

4.5 References

1. A. C. S. dos Santos, H. M. Henrique, V. L. Cardoso, M. H. M. Reis, *Int. J. Biol. Macromol.*, **185**, 543-550 (2021)

2. D. S. Macedo, M. Vepsäläinen, D. Acharya, C. D. Wood, D. Wen, L. Thomson, S. Peacock, T. Rodopoulos, C. F. Hogan, *Electrochim. Acta*, **368**, 137636 (2021)

3. N. Zhang, P. Liu, Y. Yi, M. E. Gibril, S. Wang, F. Kong, *Coatings*, **11** (2), 192 (2021)

4. Y. Li, S. Li, J. Sun, *Adv. Mater. (Weinheim, Ger.)*, **33** (13), 2007371 (2021)

5. L. Zhao, Z. Ren, X. Liu, Q. Ling, Z. Li, H. Gu, *ACS Appl. Mater. Interfaces*, **13** (9), 11344-11355 (2021)

6. D. Britton, F. Heatley, P. A. Lovell, *Macromolecules*, **31** (9), 2828-2837 (1998)

7. S. I. Nozakura, Y. Morishima, S. Murahashi, *J. Polym. Sci., Part A-1: Polym. Chem.*, **10** (10), 2853-2866 (1972)

8. J. S. Lee, K. H. Choi, H. D. Ghim, S. S. Kim, D. H. Chun, H. Y. Kim, W. S. Lyoo, *J. Appl. Polym. Sci.*, **93** (4), 1638-1646 (2004)

9. N. Limpan, T. Prodpran, S. Benjakul, S. Prasarpran, *Food Hydrocoll.*, **29** (1), 226-233 (2012)

10. C. Huang, T. Suzuki, H. Minami, *Polym. Chem.*, **13** (5), 640-648 (2022)

11. B. S. Casey, B. R. Morrison, R. G. Gilbert, *Prog. Polym. Sci.*, **18**, 1041-1096 (1993)

12. I. A. Maxwell, B. R. Morrison, D. H. Napper, R. G. Gilbert, *Macromolecules*, **24** (7), 1629-1640 (1991)

13. M. Okubo, Y. Kitayama, N. Yamashita, X. Liu, C. Huang, *Macromol. Theory Simul.*, **27** (5), 1800029 (2018)

14. Y. Ni, C. Tian, L. Zhang, Z. Cheng, X. Zhu, *ACS Macro Lett.*, **8** (11), 1419-1425 (2019)

15. C. Huang, H. Minami, M. Okubo, *Langmuir*, **37** (10), 3158-3165 (2021)

16. C. Huang, N. Yamashita, A. Chaiyasat, X. Liu, M. Okubo, *Polymer*, **154**, 128-134 (2018)

17. J. K. Guillory, *J. Med. Chem.*, **46** (19), 4213-4213 (2003)

18. P. Chaiyasat, S. Namwong, M. Okubo, A. Chaiyasat, *RSC Adv.*, **6** (97), 95062-95066 (2016)

19. M. Okubo, J. Izumi, T. Hosotani, T. Yamashita, *Colloid Polym. Sci.*, **275** (8), 797-801 (1997)

20. P. Lacroix-Desmazes, J. Tonnar, Degenerative Transfer with Alkyl Iodide. In *Polymer Science: A Comprehensive Reference*, 2012; pp 159-180.

21. C. Boyer, P. Lacroix-Desmazes, J.J. Robin, B. Boutevin, *Macromolecules*, **39** (12), 4044-4053 (2006)

22. L.Wojnarovits, J. A. LaVerne, *Radiat. Phys. Chem.*, **47** (1), 99-101 (1996)

23. I. R. E. stván Lengyel, K. Kustin, *Inorg. Chem*, **32**, 5880-5882 (1993)

24. I. C. Engineers, *SPI/CI 52nd Annual Conference and Exposition 1997*. CRC Press: 2022.

25. J. S. Trent, J. I. Scheinbeim, P. R. Couchman, *Macromolecules*, **16** (4), 589-598 (1983)

26. M. Abdollahi, P. Bigdeli, M. Hemmati, M. Ghahramani, M. Barari, *Polym. Int.*, **64** (12), 1808-1819 (2015)

27. C. A. Barson, J. C. Bevington, B. J. Hunt, *Polymer*, **37** (25), 5699-5702 (1996)

28. P. Lacroix-Desmazes, R. Severac, B. Boutevin, *Macromolecules*, **38** (15), 6299-6309 (2005)

- 100 -

Chapter 5

Iodine-influenced morphological change of micrometer-sized poly(methyl methacrylate)-*block*-poly(vinyl acetate) particles upon hydrolysis

5.1 Introduction

As mentioned in Chapter 4, the alluring properties of low toxicity, high hydrophilicity, biodegradation, and biocompatibility possessed by Poly(vinyl alcohol) (PVA) make it fascinating in the field of both chemistry and biology.[1, 2] It is promising to convert the water-insoluble Poly(vinyl acetate) (PVAc) block to the water-soluble PVA block through which the physical properties of the polymer are reversed. Owing to this unique character, the confined assembly of anisotropic block copolymers gives rise to block copolymer particles with well-defined shapes and internal morphologies.[3, 4] Armes et al. reported that morphological transition can easily occur attributed to the sufficient mobility of polymer chains at a treatment temperature higher than the glass transition temperature (T_g) of polymer.[5] D' Agosto et al. reported that the high flexibility of PVAc can provide the movement and fusion of polymer chains, resulting in the construction of a PVAc-based block copolymer with nonspherical morphologies.[6] Inspired from these studies, it seems feasible to hydrolysis the synthesized water-insoluble micrometer-sized poly(methyl methacrylate)-*block*-poly(vinyl acetate) (PMMA-*b*-PVAc) particles at high temperatures to introduce the water-soluble PVA block and

investigate their morphological transition at the same time.

In this Chapter, a series of micrometer-sized poly(methyl methacrylate)-*block*-poly(vinyl alcohol) (PMMA-*b*-PVA) particles were obtained with a desired molecular weight (M_n) and relatively narrow molecular weight distribution (M_w/M_n = 1.33–1.60) despite a low degree of polymerization of the PVAc block (DP_{VAc} < 20). Significantly, an effort was made to realize the straightforward morphological changes of amphiphilic micrometer-sized PMMA-*b*-PVA particles with controlled M_n and narrow M_w/M_n in an aqueous system.

5.2 Experimental

5.2.1 Materials

VAc (Nacalai Tesque, Inc. Kyoto, Japan; stabilizer: hydroquinone, 5 ppm) and MMA (Nacalai Tesque, Inc. Kyoto, Japan; stabilizer: hydroquinone monomethyl ether) were purified using a column packed with basic aluminum oxide (Alumina Activated 200, Nacalai Tesque, Inc. Kyoto, Japan). CHI_3 (Nacalai Tesque, Inc., Kyoto, Japan; purity, 99%), PVA (GH-17, Nippon Synthetic Chemical Industry Co., Ltd, Osaka, Japan; degree of saponification, 86.5%–89%; molecular weight, 7×10^4), 2,2'-Azobis(2,4-dimethylvaleronitrile) (V-65; Nacalai Tesque, Inc., Kyoto, Japan; purity ≥95.0%), 2,2'-azobis(4-methoxy-2,4-dimethylvaleronitrile) (V-70; Fujifilm Wako Pure Chemical Co., Ltd, Osaka, Japan; purity ≥95.0%), sodium hydroxide (NaOH; Nacalai Tesque, Inc., Kyoto, Japan; purity ≥97.0%), *N*, *N*-dimethylformamide (DMF; Nacalai Tesque, Inc., Kyoto, Japan; purity ≥99.0%), toluene (Junsei Chemical Co., Ltd, Tokyo, Japan; purity ≥99.5%), and ruthenium tetroxide (RuO_4, Filgen, Inc., Nagoya, Japan) were used as received.

Deionized water, which was obtained using a water purification machine (Elix UV, Millipore Co., Ltd., Japan) and had a resistivity of 15 MΩ cm, was used in all experiments.

5.2.2 Synthesis of micrometer-sized PMMA particles

Micrometer-sized PMMA particles were synthesized by *ms* ITP. V-65 (0.0362 g) and CHI_3 (0.072 g) were dissolved in MMA (3 g) in a molar ratio of $[MMA]:[V-65]:[CHI_3] = 163:0.8:1$, and the monomer solution was poured into an aqueous phase consisting of 1 wt% PVA aqueous solution (27 g). After homogenization at 4,000 rpm for 5 min using a homogenizer (ABM-2, Nihonseiki Kaisha, Ltd, Japan), a monomer dispersion was obtained. Subsequently, the monomer dispersion was evenly divided into four glass tubes, which were sealed off after being degassed five times with vacuum/N_2 gas cycles and covered with aluminum foil. Finally, *ms* ITP was conducted at 40°C for 24 h. In all the polymerizations, the sealed tubes were placed in a water bath (BW101, Yamato Scientific Co., Ltd, Japan) with a horizontal shaking rate of 120 rpm. PMMA particles were collected by centrifugation at 8000 rpm for 10 min at 5°C, which was repeated in triplicate.

5.2.3 Synthesis of micrometer-sized PMMA-b-PVAc particles

Micrometer-sized PMMA-*b*-PVAc particles were synthesized by seeded microsuspension ITP (*sms* ITP). An oil phase of V-70 (1 mg, 1 wt% relative to monomer), toluene (5 mg, 2 wt% relative to PMMA seeds), and VAc (0.1 g) were mixed with 1 wt% PVA aqueous solution (0.6 g), which was homogenized by a biomixer (NS-52K, Nihonseiki Kaisha, Ltd.) at 6500 rpm

afterward. Next, the VAc emulsion, which was extracted one-tenth from the above emulsion, was added to the suspension of PMMA particles. As the *ms* ITP-obtained PMMA has an iodine end group, it was used as the macrochain transfer agent in this step and expressed as PMMA-I. The suspension of PMMA seeds was prepared in a molar ratio of [VAc]:[V-70]:[PMMA-I] = 200:0.56:1, and the water was adjusted to control the solid content of the total mixture to 10 wt%. Then, the mixture was immersed in an ice bath and stirred by a magnetic stirrer at 150 rpm for 2 h to proceed with the swelling of VAc. Following the swelling, the mixture was evenly divided using four glass tubes and sealed off after being degassed five times with vacuum/N_2 gas cycles. The sealed tubes were placed in a water bath at 30°C for 24 h or 48 h with a horizontal shaking rate of 80 rpm after covering them with aluminum foil (to prevent the light-induced side reaction of the iodine end group). PMMA-*b*-PVAc particles were collected by centrifugation conducted in triplicate in water at 8000 rpm for 10 min at 5°C.

5.2.4 Hydrolysis of micrometer-sized PMMA-*b*-PVAc particles

The suspension of PMMA-*b*-PVAc particles (0.015 g) was prepared at a solid content of 7.5 wt%. Then, NaOH was dissolved in the suspension, whose weight was calculated from the equation (the mole number of VAc units × the molecular weight of NaOH). Subsequently, the mixture was sealed in a glass tube after degassing and covered with aluminum foil. The hydrolysis was conducted in an oil bath (Personal H-10, Taitec Corporation, Japan) at 125°C for 1 h with a horizontal shaking rate of 120 rpm. After hydrolysis, PMMA-*b*-PVAc particles were collected by centrifugation in water at 8000 rpm, 5°C, and 15 min.

5.2.5 Calculation of carrying rate of iodine end groups

The UV-Vis was used to calculate the carrying rate of the iodine end group of polymers after each step. Since the dipole-dipole bond between DMF and the iodine group could be generated by reaction (1), through which the iodine group could drop from the polymer chain.[7, 8] The probable fate of the free iodine groups is the generation of iodine molecules. To make the iodine group drop from the polymer chain completely, the solution of polymer in DMF was treated under UV light for 4 hours and stood for one night.
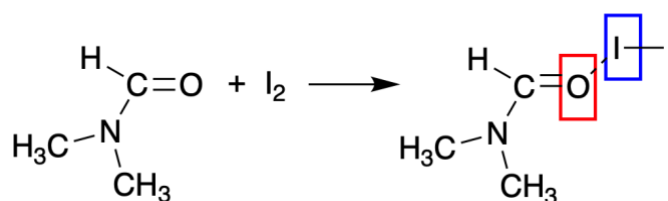
Reaction (1)

For the data of the measured absorbance intensity of polymer with iodine end (polymer-I) (A_{exp}), the measured absorbance intensity of iodine molecules (A_I), and the concentration of iodine molecules (C_I) are known, it is possible to calculate the concentration of polymer-I ($C_{polymer-I, exp}$) by equation (1).

$$C_{polymer-I,exp} = \frac{A_{exp}}{A_I} \times C_I \times 2$$

eq (1)

Then, the ratio of the $C_{polymer-I, exp}$ to the concentration of the weighted polymer ($C_{polymer-I,theo}$) is defined as the carrying rate of the iodine end group ($R_{iodine\ end\ group}$, equation(2)).

$$\text{Carrying rate of Iodine end group} = \frac{C_{polymer-I,exp}}{C_{polymer-I,theo}}$$

$$\text{eq (2)}$$

The characteristic peak of I_2 in DMF at 262 nm, which shifted a little due to the influence of the polymer chain, was used to calculate the carrying rate of the iodine end group. It is assumed that the PMMA-*b*-PVAc were hydrolyzed thoroughly to PMMA-*b*-PVA, since the low DP_{VAc}. So, the polymer after hydrolysis is expressed as PMMA-*b*-PVA.

5.2.6 Characterization

All of the conversions and solid contents were measured by gravimetry. The appearance of the suspension after hydrolysis was observed with the naked eye. The overall morphologies PMMA-*b*-PVAc particles after hydrolysis were observed using an optical microscope (OM, ECLIPSE 80i, Nikon, Tokyo, Japan), and a scanning electron microscope (SEM, S-2460, Hitachi Science Systems Ltd., Ibaraki, Japan). The inner morphologies of PMMA-*b*-PVAc particles after hydrolysis were observed by a transmission electron microscope (TEM, JEM-1230, JEOL, Tokyo, Japan) after staining the freeze-dried particles with RuO_4 and slicing them into cross-sections (170 nm-thick). The weight-average and number-average molecular weights (M_w and M_n, respectively), and molecular weight distribution (M_w/M_n) were determined by gel permeation chromatography (GPC, TOSOH Corporation, TSK gel α 5000, 7.8 mm i.d × 30 cm, separation range per column: approximately $50–7 \times 10^6$ g/mol (exclusion limit) using DMF as

an eluent at 40°C, and a flow rate of 1.0 mL/min) employing a refractive index (RI) detector

(TOSOH RI-8020/21). The columns were calibrated with twelve standard PMMA samples for

DMF (730–1.65 × 10^6). The carrying rate of iodine was determined by an ultraviolet-visible

spectrophotometer (UV-Vis, UV-2700, Shimadzu Corporation, Kyoto, Japan), to the theoretical

value of the polymer with iodine ends ($C_{polymer-I,exp}/C_{polymer-I,theo}$). The particle stability after

hydrolysis was confirmed through observation and zeta (ζ) potential measurements (ELSZ-1M,

Otsuka Electronics Co., Ltd, Osaka, Japan) using water as the dispersion medium. For

micrometer-sized particles, the ζ potential data obtained after the first run was adopted in this

work. The glass transition temperature (T_g) was determined by differential scanning calorimetry

(DSC, DSC7000X, Hitachi, Ltd, Tokyo, Japan).

5.3 Results and discussion

5.3.1 Morphologies after hydrolysis

Basing on the same recipe as dicussed in Chapter 3, a series of PMMA-*b*-PVAcs was

synthesized with an acceptable control/livingness, as shown in Table 1. We also confirmed the

M_n and M_w/M_n of these PMMA-*b*-PVAcs after hydrolysis, which results of the soluble part were

consistence with the theoretical molecular weight ($M_{n,th}$) (Table 1).

During the hydrolysis of PMMA-*b*-PVAc which the affinities of the PVAc block and the

PMMA block to water were altered and microphase separation occurred. To provide polymers

with flexibility and make hydrolysis happen smoothly, a temperature of 125°C, which was

higher than the maximum T_g ($T_{g,max} = 120.8°C$) of the synthesized PMMA-*b*-PVAc, was applied

to these particles with the assistance of the residual toluene in the process of hydrolysis. As in the case of the *ms* ITP-obtained PMMA, the remaining toluene influenced the particle morphology by promoting chain movements during hydrolysis. The unswollen PMMA particles after hydrolysis showed spherical particles (Figure 1a), whereas the swollen PMMA particles showed a converged structure (Figure 1b). Regarding PMMA-*b*-PVAc particles, three morphologies were observed after hydrolysis, which transited with the increase in the degree of polymerization ratios of PVAc to PMMA (DP_{VAc}/DP_{MMA}) (Table 2 and Figure 2). Basing on their morphologies, these particles were named as spherical particles with hollows in the particle (SHP), multipods with hollows (MH), and spherical particles with hollows near the surface (SHS), respectively.
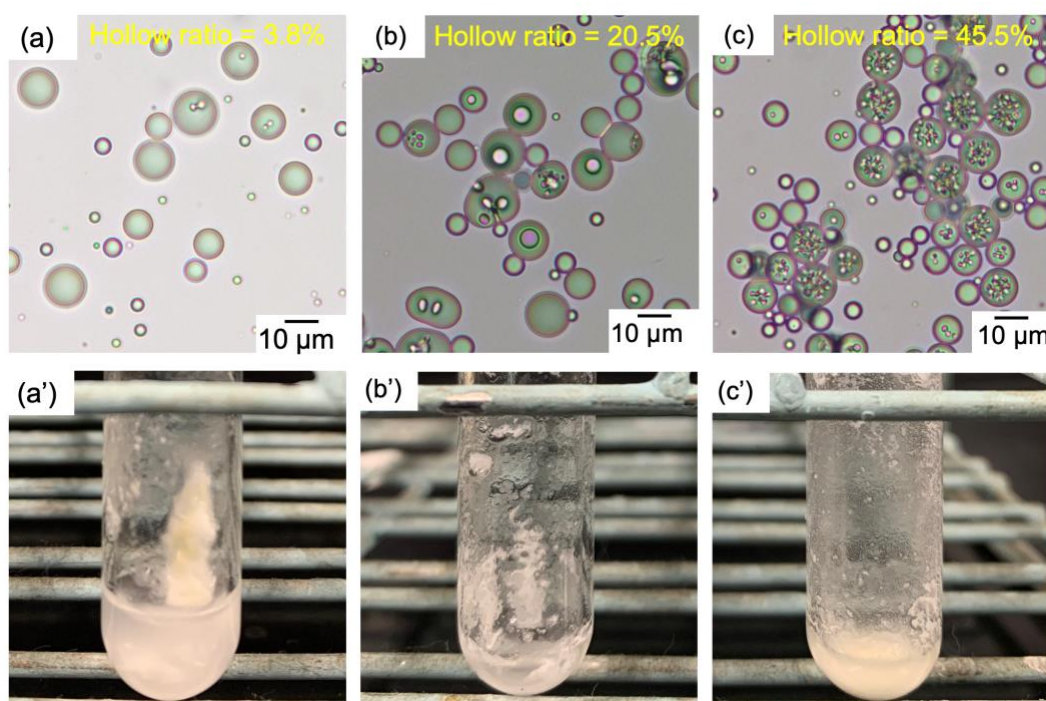

Figure 1. Optical images (a-c) and appearances (a'-c') of PMMA particles (a, a', b, b'), which before hydrolysis were treated without (a, a') and with (b, b') the swelling process of toluene, and swollen PMMA-*b*-PVAc (c, c') particles after hydrolysis. (Hollow ratio (%) = the number of particles with hollow structures/the number of particles in an optical micrograph $\times$ 100)

Table 1. The molecular weight, the theoretical molecular weight, and the molecular weight distribution before and after sms ITP of the series of PMMA-I.

Sample	*sms* IP	Conv. (%)	M_n (g/mol)	$M_{n,th}$ (g/mol)	Top M_n (g/mol)	M_w/M_n
1	Before	85.5	14,600	14,300	15,900	1.33
	After	5.9	15,200	15,500	16,300	1.30
	Hydrolyzed		14,900	14,900	16,300	1.20
2	Before	82.0	15,200	13,900	19,200	1.45
	After	3.1	16,000	15,700	19,700	1.43
	Hydrolyzed		15,700	15,600	19,200	1.35
3	Before	82.0	15,200	13,900	19,200	1.45
	After	1.5	16,200	15,500	19,700	1.37
	Hydrolyzed		15,700	15,700	20,100	1.44
4	Before	81.7	13,700	13,400	16,200	1.41
	After	4.1	14,700	14,400	17,800	1.43
	Hydrolyzed		14,600	14,200	17,300	1.34
5	Before	80.5	17,700	13,100	23,600	1.60
	After	6.9	19,000	19,200	24,700	1.57
	Hydrolyzed		18,900	18,400	24,700	1.73
6	Before	81.7	13,700	13,400	16,200	1.41
	After	8.1	14,900	15,000	17,700	1.45
	Hydrolyzed		14,400	14,300	17,700	1.48
7	Before	80.5	17,700	13,100	23,600	1.60
	After	11.4	19,200	20,200	24,700	1.53
	Hydrolyzed		18,500	18,500	24,700	1.47

Table 2. Polymerization degrees of PVAc and PMMA calculated from molecular weight, the ratios of the degree of polymerization of PVAc to that of PMMA, and the morphologies of the prepared PMMA-*b*-PVAc particles after hydrolysis.

No.	DP_{VAc}	DP_{MMA}	DP_{VAc}/DP_{MMA}	Morphology [a]
1	6	143	0.042	SHP
2	9	149	0.060	SHP
3	11	149	0.074	SHP
4	11	136	0.081	MH
5	15	175	0.086	MH
6	13	136	0.096	SHS
7	17	175	0.097	SHS

[a] SHP: spherical particles with hollows in the particle, MH: multipods with hollows, SHS: spherical particles with hollows near the surface
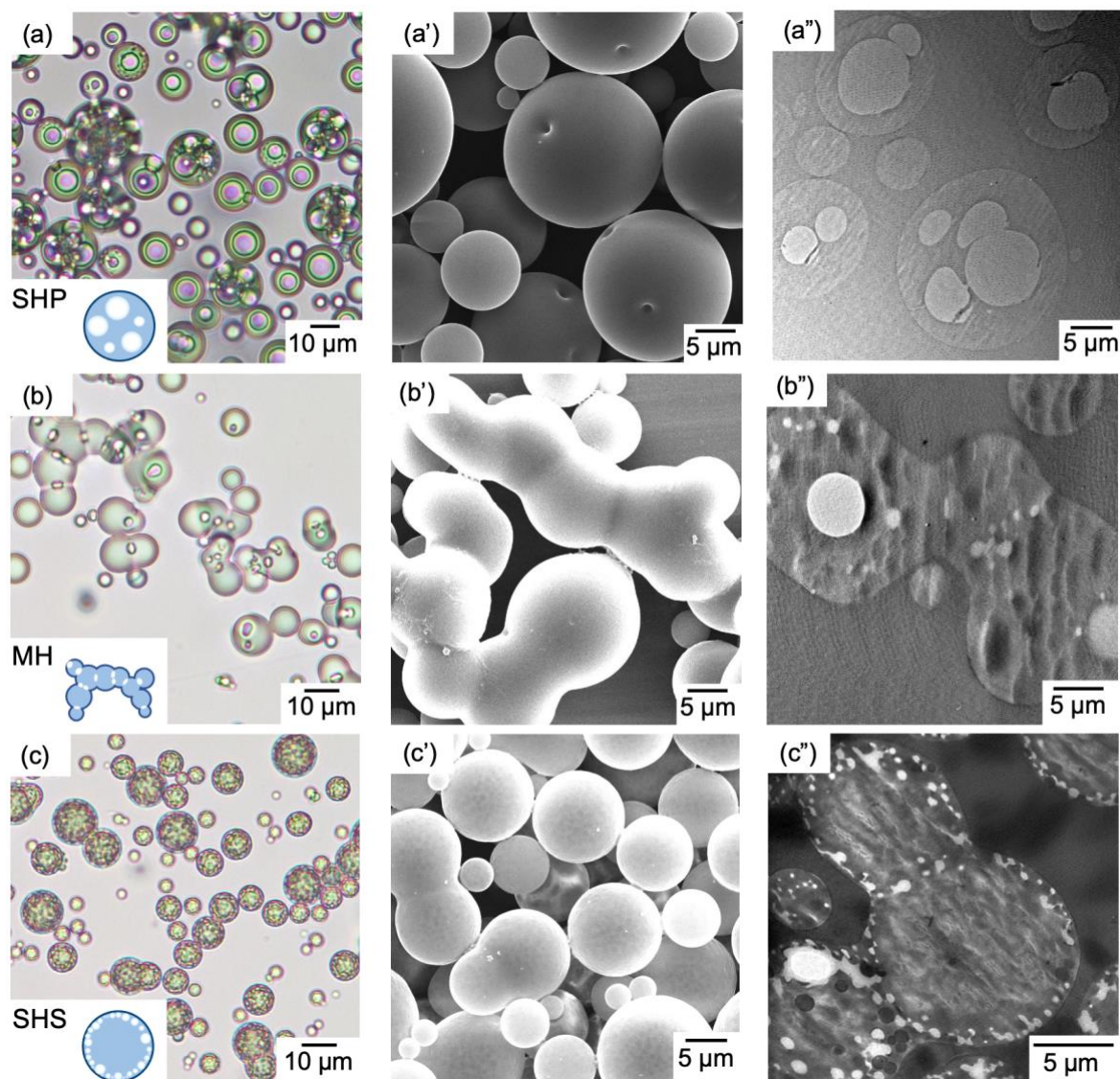
Figure 2. Optical (a-c), SEM (a'-c'), and cross-sectional (a"-c") images of the washed PMMA-*b*-PVAc particles with different morphologies after hydrolysis: spherical particles with hollows in the particle (SHP) (a-a"), multipods with hollows (MH) (b-b"), and spherical particles with hollows near the surface (SHS) (c-c").

5.3.2 Spherical particles with hollows in the particles (SHP)

When DP_{VAc}/DP_{MMA} was lower than 0.074, the morphology of SHP was obtained (Figure 2(a-a")). This morphology was mainly caused by the cooperation between osmotic pressure and the increased water solubility, which was proposed in the previous work as an easy method of the formation of hydrophobic (multi-)hollow particles.[9, 10] Iodic ions generated from the dropped

iodine ends (Figure 3) were the source of osmotic pressure. Once the heat was supplied, the

iodine ends dropped easily, ascribed to the unstable C–I bond (Figure 3a).[11] Due to the improved

chain mobility after heating, small amounts of water penetrated the particles and led to the

hydrolysis of iodine (Figure 3(b-c)), which further resulted in the adsorption of water by

osmosis (Scheme 1(b, c)). This phenomenon was also observed in the case of pure PMMA-I

particles (Figure 1(a, b)) synthesized by *ms* ITP. However, in the presence of the PVAc block,

the increasing affinity of particles with water during hydrolysis promoted water penetration

(Scheme 1(d, e)), resulting in the higher hollow ratio of hydrolyzed PMMA-*b*-PVAc particles

(Figure 1c). Indeed, the hollow generation mechanism is appropriate for the other two
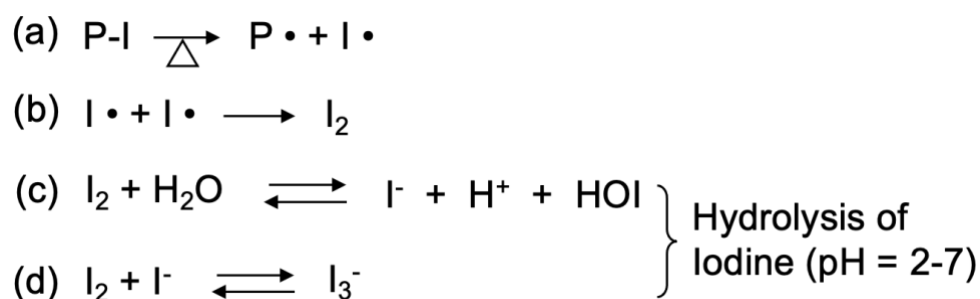
morphologies, which will be discussed later.

(a) $P\text{-}I \xrightarrow{\triangle} P\cdot + I\cdot$

(b) $I\cdot + I\cdot \longrightarrow I_2$

(c) $I_2 + H_2O \rightleftharpoons I^- + H^+ + HOI$

(d) $I_2 + I^- \rightleftharpoons I_3^-$

$\left.\begin{array}{c} \\ \\ \end{array}\right\}$ Hydrolysis of Iodine (pH = 2-7)

Figure 3. Side reactions of the generation of iodic ions.

Notably, the PMMA-*b*-PVAc particles maintained better colloidal stability compared to

PMMA particles after hydrolysis (Figure 1(a'-c')). This is a consequence of the electrostatic

force offered by iodic ions. As revealed in Chapter 3,[12] the PVAc particles prepared by *ms* ITP

had a higher absolute ζ potential (−14.02 mV) than the PVAc particles prepared by *ms* CRP (−

4.67 mV), leading to high colloidal stability. In this work, although the direct proof of iodic

ions could not be given after *sms* ITP, the comparison of pH before and after *sms* ITP can show

the difference since the hydrogen ions in this step primarily stem from the side reaction (Scheme

1a, Chapter 3). It was confirmed that the suspension had lower pH after the *sms* ITP of VAc

than that of PMMA after the same treatment (Figure 4 and Figure 5), accounting for the higher

concentration of iodic ions in the PMMA-*b*-PVAc particles than that in the PMMA particles.

So, far, the influence of iodic ions on the morphology of PMMA-*b*-PVAc particles after

hydrolysis cannot be neglected.
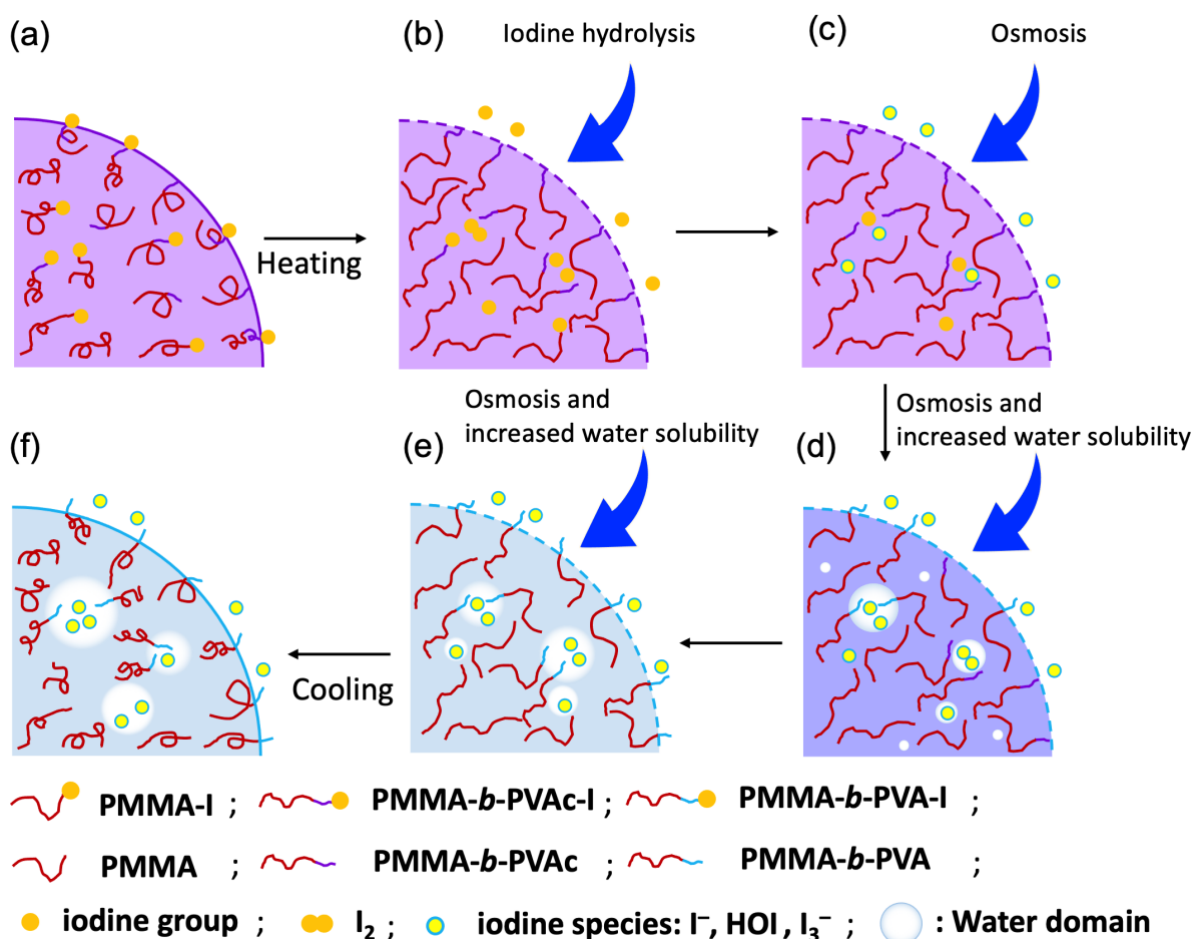
Scheme 1. Schematic depicting the formation mechanism of spherical particles with hollows in the particle (SHP).
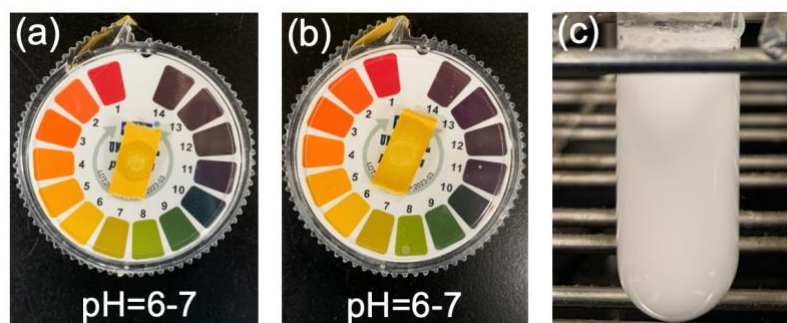
Figure 4. pH tested by pH paper before (a) and after (b) the same treatment of PMMA-I as *sms* ITP but without VAc, and appearance of suspension (c) after treatment.
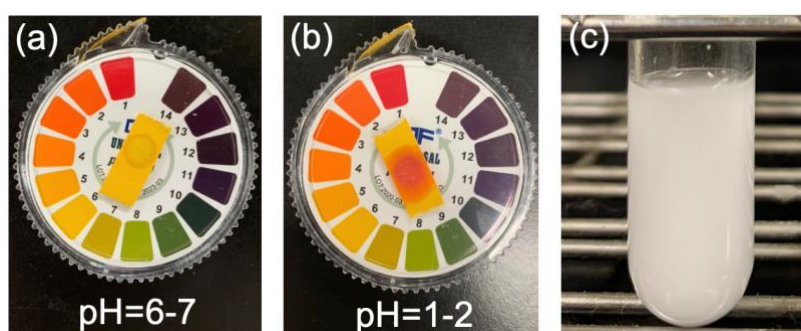

Figure 5. pH tested by pH paper before (a) and after (b) *sms* ITP of VAc, and appearance of suspension (c) after *sms* ITP.

5.3.3 Multipods with hollows (MH)

As DP_{VAc}/DP_{MMA} increased, the morphology of MH was observed (Figure 2(b-b")). However, the morphology only existed within a narrow window of DP_{VAc}/DP_{MMA} ranging from 0.081 to 0.086. Besides the relatively developed chain mobility, the decreased electrostatic force during hydrolysis also contributed to the formation of this morphology. To declare the impacts of the two factors on the morphology of MH, a series of PMMA-*b*-PVAc polymers with the same DP_{VAc} but different DP_{MMA} were hydrolyzed, and their ζ potential values were determined before and after hydrolysis. With the increase in DP_{VAc}/DP_{MMA}, the morphologies of PMMA-*b*-PVAc particles evolved from spherical particles to multipods after hydrolysis (Figure 6),

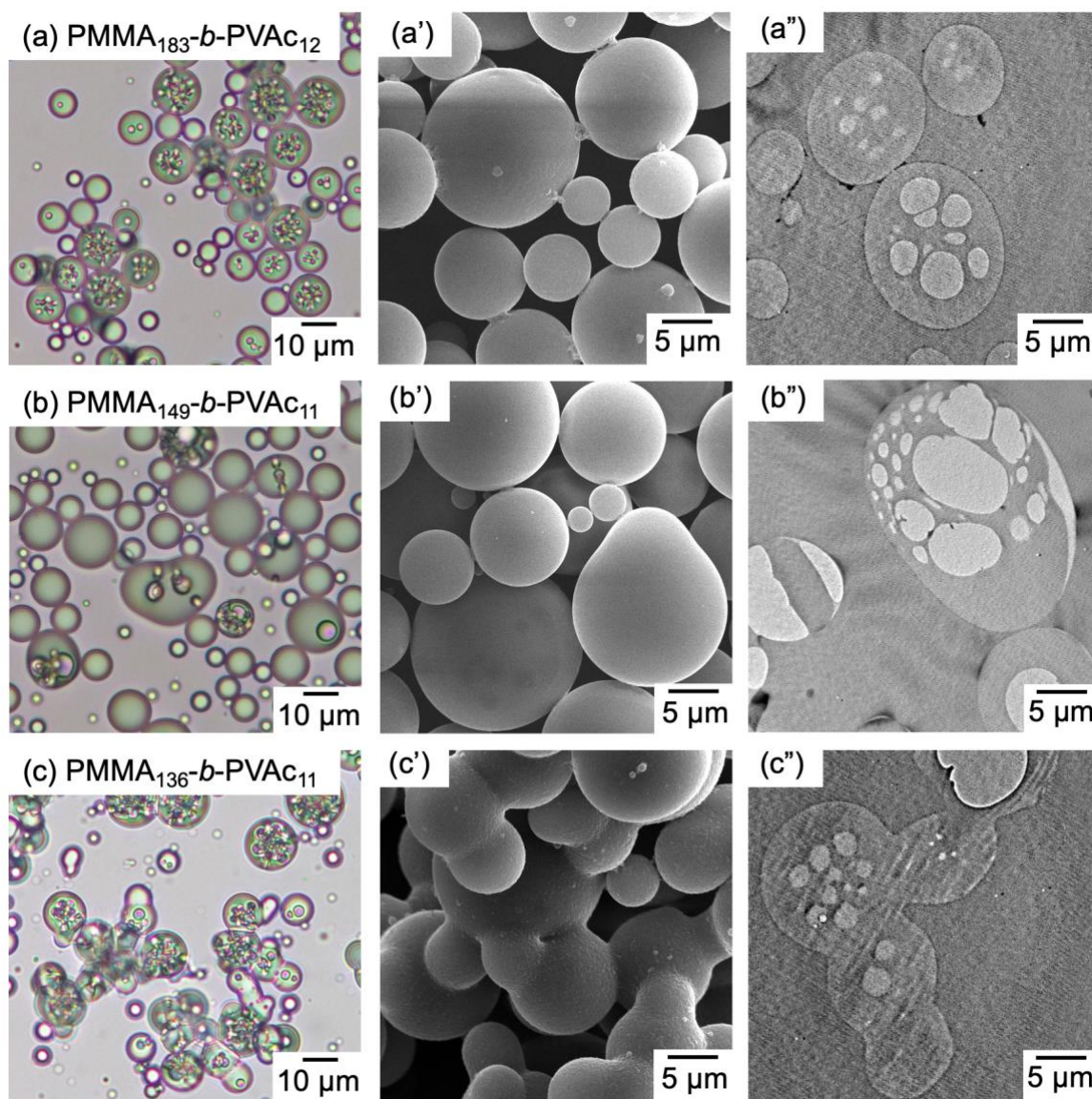proving the effectiveness of the developed flexibility of the polymer chains.

Figure 6. Optical (a-c), SEM (a'- c') and cross-sectional (a"-c") images of the PMMA-*b*-PVAc polymers with same DP_{VAc}, but different ratio of DP_{VAc}/DP_{MMA} after hydrolysis: $PMMA_{183}$-*b*-$PVAc_{12}$, $DP_{VAc}/DP_{MMA} = 0.066$ (a-a"), $PMMA_{149}$-*b*-$PVAc_{11}$, $DP_{VAc}/DP_{MMA} = 0.074$ (b-b"), and $PMMA_{136}$-*b*-$PVAc_{11}$, $DP_{VAc}/DP_{MMA} = 0.081$ (c-c").

When comparing the ζ potentials of PMMA-*b*-PVAc, in the case of MH, the PMMA-*b*-PVAc particles possessed a lower ζ potential (Table 3). Moreover, in the case of MH, the colloid

stability decreased following the weakened ζ potential after hydrolysis (Figure 7). As mentioned above, the ζ potential was mainly affected by iodic ions, so the relationship between the morphological transformation (from SHP to MH) and iodic ions was further studied. The calculated concentration of iodic ions generated during hydrolysis showed a lower value in the case of MH ($C_{iodic\ ions}$ = 0.168 mmol/L) than that of SHP ($C_{iodic\ ions}$ = 0.358 mmol/L), corresponding to the lower colloidal stability (Table 4 and Table 5).

Table 3. Zeta potentials of PMMA-*b*-PVAc particles before and after hydrolysis in the case of SHP and MH, respectively.

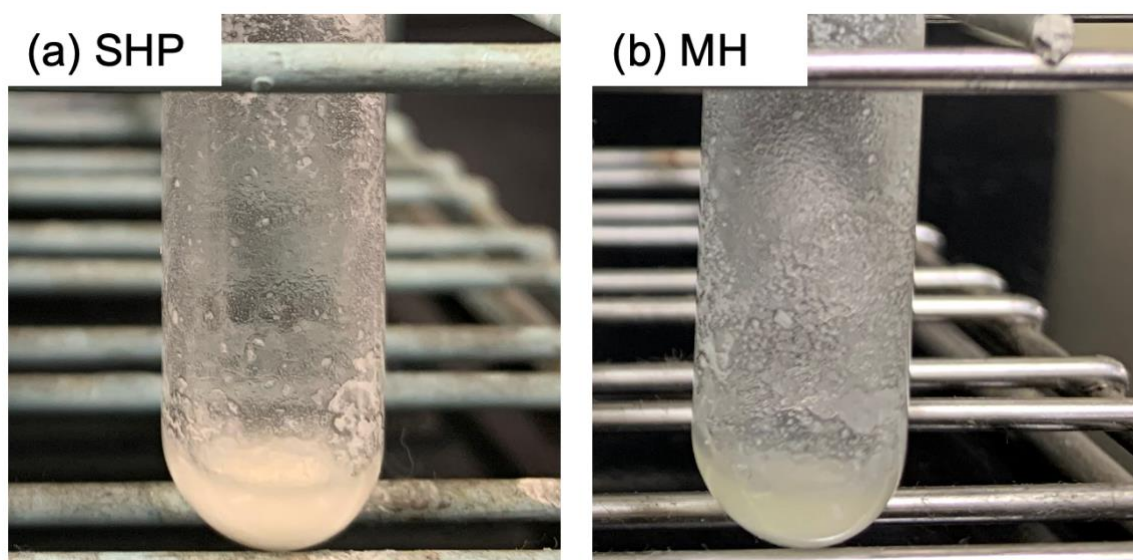|	Hydrolysis	ζ potential (mV)	Morphology
PMMA$_{183}$-b-PVAc$_{12}$	Before	−20.99	
	After	−19.35	SHP
PMMA$_{136}$-b-PVAc$_{11}$	Before	−12.02	
	After	−6.72	MH

Figure 7. Appearances (a, b) of particle stability of different PMMA-*b*-PVAcs after hydrolysis showing the morphology of SHP (a) and MH (b), respectively.

Table 4. The theoretical concentration of polymer with iodine end ($C_{polymer-I,theo}$), the measured concentration of polymer with iodine end ($C_{polymer-I,exp}$), and the calculated value of carrying rate of iodine end groups ($R_{iodine\ end\ group}$) in the case of SHP.

| Sample	$C_{polymer-I,theo}$ (mmol/L)	$C_{polymer-I,exp}$ (mmol/L)	Carrying rate of iodine end groups ($R_{iodine\ end\ group}$, %)
PMMA$_{183}$-I	0.145	0.2200	100.0
PMMA$_{183}$-*b*-PVAc$_{12}$-I	0.122	0.0354	29.0
PMMA$_{183}$-*b*-PVA$_{12}$	0.012	0.0089	74.2

Table 5. The theoretical concentration of polymer with iodine end ($C_{polymer-I,theo}$), the measured concentration of polymer with iodine end ($C_{polymer-I,exp}$), and the calculated value of carrying rate of iodine end groups ($R_{iodine\ end\ group}$) in the case of MH.

Sample	$C_{polymer-I,theo}$ (mmol/L)	$C_{polymer-I,exp}$ (mmol/L)	Carrying rate of iodine end groups ($R_{iodine\ end\ group}$, %)
PMMA$_{136}$-I	0.154	0.1000	65.0
PMMA$_{136}$-*b*-PVAc$_{11}$-I	0.090	0.0231	25.7
PMMA$_{136}$-*b*-PVA$_{11}$	0.006	0.005	88.3

Due to the synergistic effect of the relatively improved chain flexibility and deteriorated colloid stability of PMMA-*b*-PVAc particles, the coalescence between these particles was promoted under heat.[13] Furthermore, after coalescence, the hollow structures were also observed at the joints of the conjugates (Figure 2b"). The scenario of the trapped hollows is illustrated in Scheme 2. Indeed, accompanied by the generation of the PVA block and iodic ions within the hydrolysis, hydration also happened. Due to the poor colloidal stability, a few particles tended to aggregate into clusters containing interstitial water as a consequence of the hydrated PVA blocks and ions.[14] During coalescence, the interstitial water would exist in the region of PVA and iodic ions owing to the higher affinity of the PVA segment and iodic ions to

water. After that, the general chain mobility of polymers was poor, so the position of this interstitial water was restricted at the intersection of two particles.
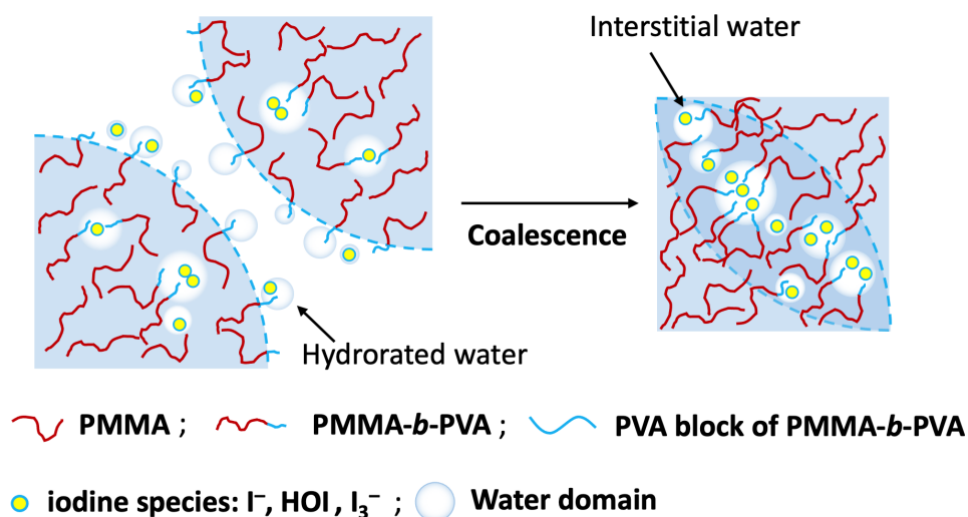
Scheme 2. Schematic mechanism of the formation of the hollow structures at the joint of two particles.

5.3.4 Spherical particles with hollows near the surface (SHS)

Based on the preconceived notion of the morphological evolution with the further increase in DP_{VAc}/DP_{MMA}, bigger aggregation with hollows could be expected. However, when the PMMA-*b*-PVAc particles were synthesized with DP_{MMA} of 175 and DP_{VAc} of 17, whose DP_{VAc}/DP_{MMA} was higher than 0.096, the morphology of SHS was observed (Figure 2(c-c")), owing to the further cooperation between longer PVA segments and iodic ions at a relatively high concentration. Once the PMMA-*b*-PVAc particles under hydrolysis meet the two requirements at a high temperature, it is probable to acquire the crosslinked structures. In the Chapter 3,[12] the crosslinking of PVA was discussed concretely. At a high temperature, the hydroxyl groups of PVA are oxidized by iodine radicals into ketone and aldehyde specimens

(Scheme 1b, Chapter 3).[15, 16] Afterward, the double bonds are formed through aldol condensation, which gives rise to the crosslinking reaction (Scheme 1(c, d), Chapter 3). To verify whether the crosslinked structures appeared in this case, the PMMA-*b*-PVAc particles with high DP_{VAc}/DP_{MMA} were added to DMF, which is a good solvent for both polymers, after hydrolysis. It was found that the polymers could not be dissolved completely even after 24 h (Figure 8), indicating the generation of the crosslinked polymer.
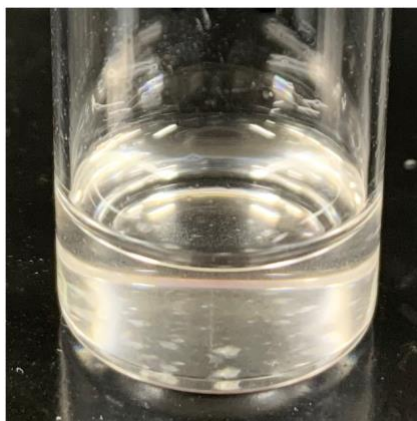

Figure 8. The unsolved polymer after hydrolysis stands in DMF for 24 hours when the DP_{VAc}/DP_{MMA} of PMMA-*b*-PVAc is higher than 0.096.

In addition, in the presence of the triiodide ion (I_3^-), PVA tends to form a complex, which enhances the regularity of PVA segments and helps water penetrate this locus.[17, 18] As magnified in Scheme 3, besides the ion-rich zone, the extra water can get caught in the region where the complexed I_3^- exists. However, this behavior leads to a reduction in the water that is bound to the loose PVA segments, resulting from the reinforced regularity of this PVA. Because of the reinforced regularity, the distance between the polymers at this position can be narrowed, which is in favor of the crosslinking reactions among them. For the hydrolysis happens easily at the

surface and the higher affinity between these iodic PVA segments and water, the morphology

of SHS is the result of a high degree of crosslinked structures at the surface.
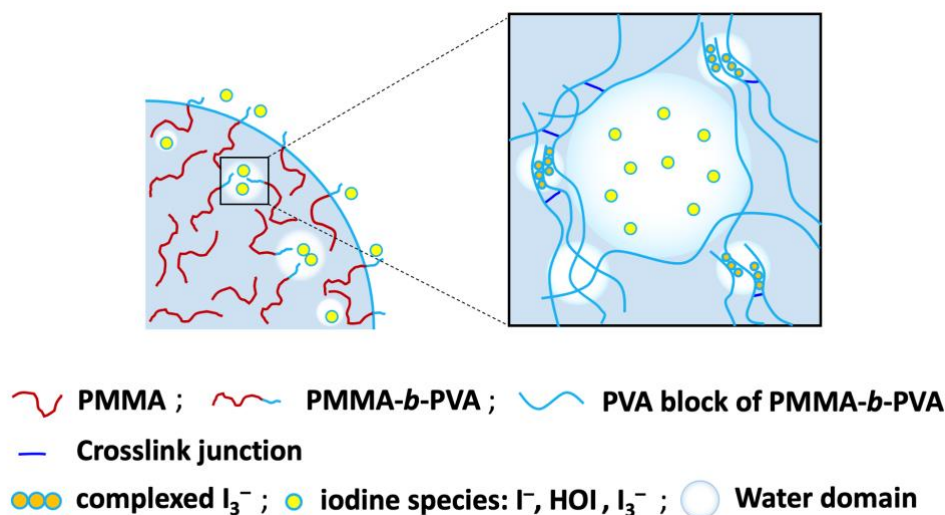
Scheme 3. Schematic mechanism of the formation of hollows on the surface of particles.

In contrast, when PMMA-*b*-PVAc particles were synthesized with the same DP_{MMA} and

DP_{VAc} at high DP_{VAc}/DP_{MMA} but with a lower number of iodine end groups (Table 6), the

morphology of SHS became difficult to achieve and was replaced by MH after hydrolysis

(Figure 9). The higher $R_{iodine\ end\ group}$ of PMMA-*b*-PVAc increased in the case of SHS ($R_{iodine\ end}$

$_{group}$ = 67.1%, Table 7) compared to that in the case of MH ($R_{iodine\ end\ group}$ = 47.0%, Table 6). In

other words, more crosslinking sites are introduced during hydrolysis as the iodine end groups

of PMMA-*b*-PVAc particles increase. Therefore, the morphology of SHS depends on the

remaining iodine end groups of PMMA-*b*-PVAc particles.

Besides the morphological evolution, the controlled amphiphilic iodic PVA-based block

copolymer could be obtained. It shows the potential to realize progress in the both chemical

delivery capacity and biocompatible antibacterial property, and may be applied as a performance iodine-based bactericide in the future.[19]
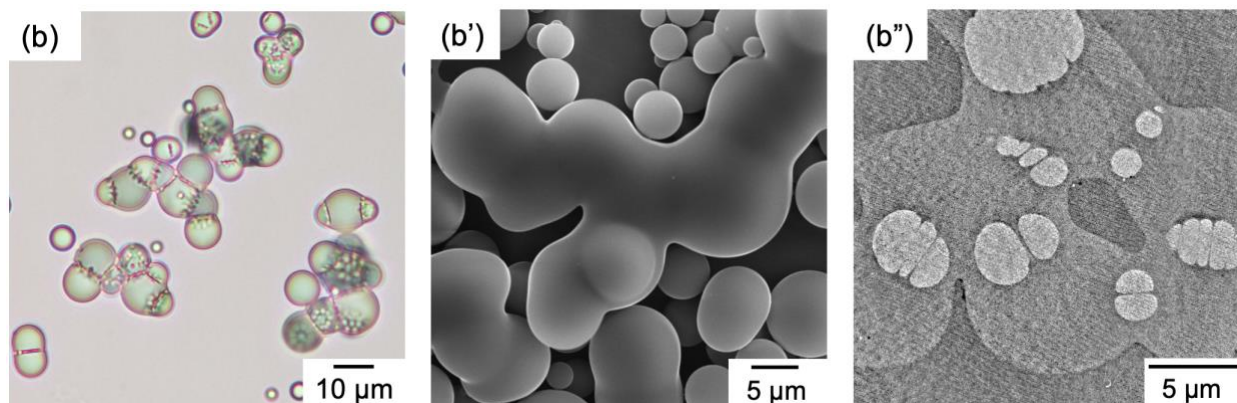

Figure 9. Optical (a), SEM (b), and cross-sectional (c) images of the washed PMMA$_{175}$-*b*-PVAc$_{18}$ particles after hydrolysis.

Table 6. The theoretical concentration of polymer with iodine end (C$_{polymer-I,theo}$), the measured concentration of polymer with iodine end (C$_{polymer-I,exp}$), and the calculated value of carrying rate of iodine end groups (R$_{iodine\ end\ group}$) in the case of MH, when the PMMA-*b*-PVAc prepared with a high ratio of DP$_{VAc}$/DP$_{MMA}$.

Sample	C$_{polymer-I,theo}$ (mmol/L)	C$_{polymer-I,exp}$ (mmol/L)	Carrying rate of iodine end groups (R$_{iodine\ end\ group}$, %)
PMMA$_{175}$-I	0.154	0.1060	68.9
PMMA$_{175}$-*b*-PVAc$_{18}$-I	0.086	0.0588	47.0
PMMA$_{175}$-*b*-PVA$_{18}$	0.052	0.0319	61.3

Table 7. The theoretical concentration of polymer with iodine end (C$_{polymer-I,theo}$), the measured concentration of polymer with iodine end (C$_{polymer-I,exp}$), and the calculated value of carrying rate of iodine end groups (R$_{iodine\ end\ group}$) in the case of SHS.

Sample	C$_{polymer-I,theo}$ (mmol/L)	C$_{polymer-I,exp}$ (mmol/L)	Carrying rate of iodine end groups (R$_{iodine\ end\ group}$, %)
PMMA$_{175}$-I	0.141	0.1302	92.2
PMMA$_{175}$-*b*-PVAc$_{17}$-I	0.042	0.0282	67.1
PMMA$_{175}$-*b*-PVA$_{17}$	0.077	0.0393	51.0

5.4 Conclusion

The convertible affinity of the PVAc block to water and microphase separation were achieved by hydrolyzing the micrometer-sized PMMA-*b*-PVAc particles. Three different morphologies were observed with the increase in DP_{VAc}/DP_{MMA}, and the formation mechanism of each morphology was clarified in detail. Overall, the morphological change of PMMA-*b*-PVAc particles after hydrolysis arises from the synergistic effect of the ionized iodine and hydrophilic PVA segments. Moreover, the presence of iodic ions stabilized the particles after hydrolysis. Above all, the morphological transition of amphiphilic particles in an aqueous phase, which resulted from the hydrolysis of the hydrophobic PMMA-*b*-PVAc particles with designed M_n and narrow M_w/M_n, offers a new strategy to realize environmentally friendly particle morphology transition.

5.5 References

1. Y. Li, S. Li, J. Sun, *Adv. Mater. (Weinheim, Ger.)*, **33** (13), 2007371 (2021)

2. L. Zhao, Z. Ren, X. Liu, Q. Ling, Z. Li, H. Gu, *ACS Appl. Mater. Interfaces*, **13** (9), 11344-11355 (2021)

3. O. Terreau, C. Bartels, A. Eisenberg, *Langmuir*, **20** (3), 637-645 (2004)

4. K. H. Ku, J. M. Shin, H. Yun, G. R. Yi, S. G. Jang, B. J. Kim, *Adv. Funct. Mater.*, **28** (42), 1802961 (2018)

5. C. György, T. J. Neal, T. Smith, D. J. Growney, S. P. Armes, *Macromolecules*, **55** (10), 4091-4101 (2022)

6. P. Galanopoulo, P. Y. Dugas, M. Lansalot, F. D'Agosto, *Polym. Chem.*, **11** (23), 3922-3930 (2020)

7. X. Liu, L. Zhang, Z. Cheng, X. Zhu, *Polym. Chem.*, **7** (21), 3576-3588 (2016)

8. C. Schmulbach, R. S. Drago, *J. Am. Chem. Soc.*, **82** (17), 4484-4487 (1960)

9. C. Huang, H. Kobayashi, M. Moritaka, M. Okubo, *Polym. Chem.*, **8** (45), 6972-6980 (2017)

10. H. K. C. H. M. Okubo, E. Miyanaga, T. Suzuki,, *Langmuir*, (2017)

11. Y.R. Luo, *Comprehensive handbook of Chemical Bond Energies*. first ed.; CRC Press: Boca Raton, 2007; p 1688.

12. C. Huang, T. Suzuki, H. Minami, *Polym. Chem.*, **13** (5), 640-648 (2022)

13. N. Visaveliya, J. M. Köhler, *ACS Appl. Mater. Interfaces.*, **6** (14), 11254-11264 (2014)

14. F. Brunel, J. Lesage de la Haye, M. Lansalot, F. D'Agosto, *J. Phys. Chem. B.*, **123** (30), 6609-6617 (2019)

15. S. Barbon, E. Stocco, D. Dalzoppo, S. Todros, A. Canale, R. Boscolo-Berto, P. Pavan, V. Macchi, C. Grandi, R. De Caro, A. Porzionato, *Int. J. Mol. Sci.*, **21** (3), (2020)

16. D. Mawad, L. A. Poole-Warren, P. Martens, L. H. Koole, T. L. B. Slots, and C. S. J. van Hooy-Corstjens, *Biomacromolecules*, **9**, 263-268 (2008)

17. Y. Song, S. Zhang, J. Kang, J. Chen, Y. Cao, *RSC Adv.*, **11** (46), 28785-28796 (2021)

18. K. Miyasaka, PVA-Iodine complexes: Formation, structure, and properties. In *Structure in Polymers with Special Properties*, H. G. Zachmann, Ed. Springer Berlin Heidelberg: Berlin, Heidelberg, 1993; pp 91-129.

19. Z. Miao, Y. Sun, Z. Tao, Y. Chen, Y. Ma, D. Zhu, X. Huang, Z. Zha, *Adv. Healthc. Mater.*, **10** (18), 2100722 (2021)

Conclusion

In this work, iodine transfer polymerization (ITP) in a microsuspension system was performed in the environmentally friendly media – water, and examined theoretically and experimentally. Application of ITP technique to synthesis of 100% micrometer-sized particles using monomers, which have a high-water solubility, in an aqueous system that had been well developed is considerably complex and difficult because of the side reactions between water and iodic species. The polymerization conditions on different monomers should be carefully established.

In **Chapter 1**, the kinetic model for ITP was proposed to predict the possibility of a certain polymerizing condition, in which the temperature and the concentrations of monomer, initiator and transfer agent were preset. The simulation comprised the following individual reaction steps: initiation, propagation, termination, and chain transfer reactions, including their kinetic coefficients. The comparison of the R_p^w of polymerization processes would be emphasized at a conversion of 20%, according to the calculation results of $P_{max}s$.

In **Chapter 2**, the micrometer-sized PMA particles were successfully synthesized without submicrometer-sized byproduct particles by conveniently applying *ms* I with a two-step temperature process at a threshold content of BPO for the maximum industrial efficiency. By varying the pretreatment temperature, the number of oligomer radicals in the preliminary stage was controlled and captured in the oil droplets effectively, which was performed under the instruction of the kinetic simulation.

In **Chapter 3**, The synthesis of PVAc through *ms* ITP was demonstrated for the first time. Micrometer-sized PVAc particles were successfully synthesized without submicrometer-sized byproduct particles by conveniently applying *ms* ITP with V-70 as the initiator at 30°C, which is consistent with the simulation result. The *ms* ITP proceeded in a controlled manner and with better colloid stability than *ms* CRP. The synergistic effect between the temperature, PVA dispersant, and iodine was found facilitating the occurrence of side reactions: the hydrolysis of iodine molecules, the degradation of iodine-terminated PVAc chains, and the generation of crosslinking points through aldol reactions. After considering the hydrolysis of iodine, the mechanism of ITP in an aqueous system of VAc was clarified, which paves the way for the application of ITP for other unconjugated monomers in aqueous systems. Moreover, a well-defined PVA was obtained from the controlled PVAc prepared through *ms* ITP, which offers a new route to synthesize PVA-based materials with desired M_n and narrow M_w/M_n.

In **Chapter 4**, the synthesis of micrometer-sized block copolymer particles using two hydrophilic monomers, MMA and Vac, was demonstrated through *ms* ITP for the first time. Micrometer-sized PMMA-*b*-PVAc particles were successfully synthesized with desired M_n and narrow M_w/M_n by applying two-step ITP in a microsuspension system under mild condition.

In **Chapter 5**, a series of PMMA-*b*-PVAc was synthesized with different DP_{VAc}/DP_{MMA}. The convertible affinity of the PVAc block to water and microphase separation were achieved by hydrolyzing the micrometer-sized PMMA-*b*-PVAc particles directly in an aqueous phase at high temperature. Three different morphologies were observed with the increase in DP_{VAc}/DP_{MMA}, and the formation mechanism of each morphology was clarified in detail.

Overall, the morphological change of PMMA-*b*-PVAc particles after hydrolysis arises from the synergistic effect of the ionized iodine and hydrophilic PVA segments.

From the results of the former four Chapters, the aim is to synthesize micrometer-sized polymer particles using hydrophilic monomers by *ms* ITP. Utilizing the idea of Radical Exiting Depression (RED) effect, the number of oligomer radicals in the preliminary stage was controlled and captured in the oil droplets effectively, by adjusting the polymerization conditions under the prediction of the kinetic simulation of R_p^w. These results show the probability of applying *ms* ITP to other hydrophilic monomers to obtain micrometer-sized particles without submicrometer-sized particles, even in the case of block copolymers. From the result of the last Chapter, it shows the high feasibility to realize environmentally friendly restrained particle morphology transition. Besides the morphological evolution, the controlled amphiphilic iodic PVA-based block copolymer could be obtained. It shows the potential to realize progress in the both chemical delivery capacity and biocompatible antibacterial property, and may be applied as a performance iodine-based bactericide in the future.

Publication List

Chapter 1

"The kinetic simulation model for the synthesis of micrometer-sized particles by microsuspension iodine transfer polymerization"

Chapter 2

"Synthesis of micrometer-sized poly(methyl acrylate) by temperature-step microsuspension polymerization with iodoform utilizing the concept of radical exiting depression"

<div align="right">

C. Huang, H. Minami, M. Okubo

Langmuir, **37**, 3158-3165 (2021)

</div>

Chapter 3

"Synthesis of micrometer-sized poly(vinyl acetate) particles through microsuspension iodine transfer polymerization: effect of iodine species in a water medium"

<div align="right">

C. Huang, T. Suzuki, H. Minami

Polym. Chem., **13**, 640-648 (2022)

</div>

Chapter 4

"Preparation of micrometer-sized poly(methyl methacrylate)-*block*-poly(vinyl acetate) particles by two-step iodine transfer polymerization"

Chapter 5

"Iodine-influenced morphological change of micrometer-sized poly(methyl methacrylate)-*block*-poly(vinyl acetate) particles upon hydrolysis"